KYUSHU INSTITUTE OF TECHNOLOGY

Department of Applied Sciences and Integrated System Engineering

Doctor of Philosophy

Study on ultra-light thermal systems for ultra-small deep space probes

A dissertation

submitted to the department of Applied Sciences and Integrated System Engineering

and the committee on graduate studies

of Kyushu Institute of Technology

in partial fulfillment of the requirements

for the degree of

Doctor of Philosophy

Bianca Adina Szász

Doctoral Advisor: Prof. Kei-ichi Okuyama

2013/2016

Abstract

Deep space exploration has one of its motivations in the human endeavor to explore the resources of the Solar System, while the space exploration programs motivate the young people to study in science and engineering. Recently, the size and cost of the satellites missions have been reduced and nowadays many universities have the capability to build small satellites and spacecraft. The continuous improvement in micro spacecraft technologies can increase the space travel reliability. Also, through the small deep space probes missions which aim in collecting space flight data and returning them to Earth, the thermal protection systems for the future human space missions can be validated.

Some of the biggest challenges related to these missions are the harsh thermal environment of deep space and the atmospheric re-entry. The aim of this research is to address the two aspects, the one related to the harsh thermal environment of outer space, for which the study case will be represented by Shinen2 deep space mission, and the one related to atmospheric re-entry, focused on the validation of the ablative materials called LATS (Light-weight Ablator Series for Transport Vehicle Systems). The both studies are contributing in enhancing the knowledge and in developing new technologies related to a future small spacecraft mission, led by universities.

To accomplish the objectives of the research, the following studies have been done:

- Development of a passive thermal control method for a deep space probe (Shinen2), having an outer structure made of CFRTP (Carbon Fiber Reinforced Thermoplastics) materials (first time used for a space vehicle);
- Development and validation of empirical and numerical methods to estimate the recession rate of LATS materials during re-entry;

The thesis include five chapters. First chapter is the Introduction Chapter, describing the motivation for ultra-small spacecraft missions led by universities, the harsh environment of deep space and during atmospheric reentry, the challenges in designing the thermal system, and also the objectives and the structure of the thesis.

Chapter two presents a description of the various methods to design a thermal control system, suitable for a deep space mission like Shinen2, about the thermomechanical properties of CFRTP and LATS materials and about the numerical and empirical methods used to test the efficiency of LATS materials.

Chapter three comprises the orbit analysis, the thermal design, analysis and validation of the ultra-small deep space probe, Shinen2, developed by Kyushu Institute of Technology in collaboration with Kagoshima University and launched on December 2014. For reasons of weight saving and power saving, Shinen2 did not carry a heater to warm itself. A passive

thermal control of a deep space probe is very difficult to be attained and the thermal design of Shinen2 didn't have a precedent model.

Chapter four focuses on the study of light thermal protection systems for re-entry spacecraft, using LATS materials. To study the thermal performances of LATS materials, numerical and empirical studies were performed using the flight data of USERS spacecraft and the results of high enthalpy heating tests, performed at Japan Aerospace Exploration Agency (JAXA, Japan).

The Conclusions chapter, Chapter five, summarizes the findings of the research and describes a conceptual design of the thermal system for a future ultra-small spacecraft mission, led by universities. Also, Chapter five describes the recommendations for future studies.

The main findings of the research are that the developed passive thermal control of Shinen2 was proven reliable in deep space and LATS ablative materials were proven to have high thermal efficiency and they can well function as heat shield materials even under a high-enthalpy flow, in spite of their low density.

List of Figures

List of Tables

List of Abbreviations

ABBREVIATIONS

AFRP = Aramid Fiber Reinforced Plastics
ARD = Aerospace Research and Development Directorate
AU = Astronomical Unit
CEV = Crew Exploration Vehicle
CF = Carbon Fiber
CFD = Computational Fluid Dynamics
CFRP = Carbon Fiber Reinforced Plastic
CFRTP = Carbon Fiber Thermoplastic
CFRTS = Carbon Fiber Reinforced Thermosetting Resins
CCU = Communication Control Unit
CPU = Central Processing Unit
DLR = Deutsches Zentrum für Luft- und Raumfahrt
DMSC = Direct Simulation Monte Carlo
DSC = Differential Scanning Calorimetry
EM = Engineering model
FM = Flight Model
GEI = Geocentric Equatorial Inertial System
GEO = Geocentric Coordinate System
GFRP = Glass Fiber Reinforced Plastics
GMAT = General Mission Analysis Tool
GSE = Geocentric Solar Ecliptic
HAE = Heliocentric Aries Ecliptic
HEE = Heliocentric Earth Ecliptic
IR = Infrared Radiation
ISAS = Institute of Space and Astronautical Science
ISS = International Space Station
JAXA = Japan Aerospace Exploration Agency
JD = Julian Day
JUTEM = Japan Ultra-High Temperature Materials Research Institute
LATS = Light-Weight Ablator Series for Transport Vehicle Systems
LCA = Light Weight Ceramic Ablator
MERS = Microgravity Experiment Recoverable Satellite
MJD = Modified Julian Day
MOM = Mars Orbiter Mission
MSL = Mars Science Laboratory
NASA = National Aeronautics and Space Administration
PAI = Polyamide Imide
PBT = Polybutylene Terephthalate
PC = Polycarbonate
PCB = Polychlorinated biphenyl
PEEK = Polyether ether ketone
PEI = Polyether Imide

PEKK = Polyether Ketone Ketone
PET = Polyethylene Terephthalate
PICA = Phenolic Impregnated Carbon Ablator
PCU = Power Control Unit
PP = Polypropylene
PPS = Polyphenylene Sulfide
REM = Return-entry Module
RX = Receiver
SCU = Shinen2 Control Unit
SRC = Stardust Sample Return Capsule
STM = Structural thermal model
TC = Thermocouple
TCS = Thermal Control Subsystem
TPS = Thermal Protection System
TPI = Thermoplastic Polyimide
TX = Transmitter
USERS REV = Unmanned Space Experiment Recovery System Recovery Vehicle
UT = Universal Time
WSJT = Weak Signal Communication

Contents

I. Introduction

1.1 Ultra-Light Deep Space Probes

1.1.1 Space Exploration Today

There are several motivational factors which push forward the space exploration endeavour. One of the factors is science, having as objectives the study of other planets and of space environment and the application of innovative technologies in space, in the attempt to increase the understanding of the origin and history of the Solar System. An another factor is the fundamental need of human species to explore. These factors are correlated, representing different facets of the human drive to understand and control their surroundings and also to extend their horizons [1-4].

After the first 20 years of the first space exploration missions which started with the launch of the Sputnik 1, on 4 October 1957, first satellite ever launched to space, the space programs started to focus on renewable hardware, like the Space Shuttle program, and also the space programs started to be based more on cooperation rather than on competition. One example of a successful international cooperation is the International Space Station (ISS).

Starting with the end of twentieth century, several private companies began promoting space tourism. One example is the competition for the Moon exploration, sponsored by Google: Google Lunar X Prize. Nowadays, a strong tendency of transferring the development of space technologies from the governmental agencies to the private sector can be seen.

From the beginning of the twentieth-first century, U.S., European Union and several countries like China, India, Russia, Japan began to be involved in planning future manned space missions to Moon or to Mars. After the ending of mission life of ISS after 2020, the space programs will focus on the development of space missions beyond the low Earth orbit.

Mars exploration has always been an important target of the space programs of the United States, Russia (previously Soviet Union), Europe, India or Japan. Starting with 1960s, several robotic spacecraft, like orbiters, landers, or rovers, have been launched toward Mars. The main missions of these space projects were to gather scientific data about the history of Mars and of its current conditions, providing answers to very old questions regarding the planet Mars.

A space mission to Mars implies a high degree of complexity and very high costs and, so far, about two-thirds of all Mars missions failed. However, one notable successful Mars mission is the India’s Mars Orbiter Mission (MOM) [1-5, 1-6, 1-7], which is considered one of the least expansive interplanetary space project ever developed. The total cost of the mission was estimated at about US$73 million [1-8].

1.1.2 The motivation for ultra-light deep space missions

There are several economic benefits like the NASA spin-offs, which can generate many times the revenues of the cost of a successful space mission. Also, there are other several future benefits from the space exploration programs like the mineral and metal resources which can be found on asteroids or on other planets. The value of these resources can be of several billions of dollars. Another positive of space exploration programs is that they can motivate young people to study in science and engineering.

According to [1-9], the micro spacecraft technologies will represent one of the bases on which the future complex human space missions to Moon or Mars will be developed. These technologies will make possible "sustained and affordable human and robotic missions," and "Micro spacecraft that can collect space flight data and return it to Earth will enhance space travel reliability through better designs," said G. Scott Hubbard, director of NASA Ames Research Center, located in California's Silicon Valley.

In the last years, the size and cost of the satellites missions have been reduced, and a larger number of satellites were launched to space. Due to the cost reduction, many universities around the world have now the capability to build small satellites and spacecraft for the purpose of students' education and technology demonstration [1-10], and several venture companies are pursuing the practical use of nano-satellites in the area of earth observation, space science, or space demonstration [1-11, 1-12].

However, in case of deep space missions, not Earth-orbiting mission, the deep space probes still remains large-scale and high-cost mission. In order to overcome such difficulty, small-scale and low-cost deep space missions should be realized, contributing to a high-frequent and challenging deep space exploration [1-13].

One of an ultra-small deep space probe mission, led by an university and recently launched (in December 2014), is Shinen2 (Fig.1-1), which is one of the first ultra-small deep space probes in the world which uses an amateur radio communication system in deep space. It was developed by Kyushu Institute of Technology (Japan) in collaboration with Kagoshima University (Japan) .There are 3 main objectives for Shinen2 space mission:

1) Demonstration of communication system based on ham radio in deep space;

2) Demonstration in deep space of a structure made of CFRTP (Carbon Fiber Reinforced Thermoplastics) composite materials.

3) Measuring radiation using Radiation Sensor.

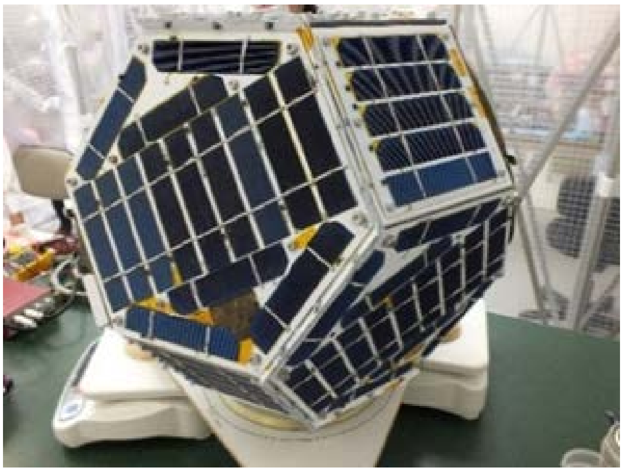

Fig. 1-1. Flight model of Shinen2 [1-1]

Shinen2 represents an experimental-shaped probe, its quasi-spherical shape allowing a more uniform heat transfer compared to a cubic shape [1-1]. Thermal design and analysis of Shinen2 is a very important part of the system design as the probe will pass through very different thermal environments while travelling in outer space.

The harsh environment of the outer space is not the only challenge for designing a thermal system in case of a deep space probe. Another challenge is the atmospheric re-entry phase. According to [1-9], by a micro spacecraft mission, a heatshield can be tested and used later in more complex future missions to protect the spacecraft and the passengers from the very high temperatures encountered during the atmospheric re-entry. The collected data from the re-entry phase can help engineers to validate the respective heat shield and to improve the design for the future missions.

Several missions to Mars and Venus are planned in the future. To reduce the risk and the costs, several micro probes could be sent to Mars, Venus or other places in the Solar System, to collect data and to test new technologies. Some particular cases are Jupiter, Saturn, Uranus or Neptune which have a gaseous atmosphere and from where the micro space probes can collect volatiles gases in order to study the atmospheres of these planets. Another aspect of the micro space probes missions is the development and flight-testing of the nanosensors, useful for future complex robotic exploration missions, which can reduce the costs of these future missions [1-9].

1.2 Ultra-Light Thermal Systems

1.2.1 The role of a Thermal System

Designing a thermal system for a deep space is one of the most fundamental parts of a deep space mission design. Two aspects of a thermal system are analysed in the present research: one is the thermal control suitable for a deep space mission like Shinen2 and an another is the design of an efficient thermal shield for the atmospheric re-entry phase.

According to [1-14], the Thermal Control Subsystem (TCS) is the hardware used to control temperatures of all vehicle components and the typical TCS elements include surface finishes, insulation blankets, heaters, and refrigerators. There are three ways through which heat is transferred: conduction, convection and radiation and, in space, only conduction and radiation are considered, due to the lack of atmosphere in space.

The thermal control of a spacecraft is based on energy management and the environmental heating plays an important role. The environmental heating on orbit consists of sunlight, direct and reflected off of the Earth, and the infrared energy coming from Earth. From all the environmental factors, sunlight is the most important source of environmental heating for a space mission. Besides these factors, there are other temperature constraints related to the environment conditions for the transportation, prelaunch, launch and ascent phases. The engineers must make sure that the temperature will not exceed the limits during these phases of the mission.

Also, for the re-entry study, aerodynamic heating plays a very important role in the vehicle design. Using an efficient thermal protection system (TPS) is important not only for maintaining the structural integrity, but also for preserving the payload and on-board devices. As pointed out in [1-15], the TPS design is a critical aspect of the spacecraft design, since its under dimensioning may result in the loss of the payload and the over dimensioning implies an increasing in weight and cost [1-2].

1.2.2 Challenges in designing a Thermal System for an ultra-light space probe

Thermal design plays a very important role due to the fact that it must assure the survival of electric components including the communication system through which the ground stations are kept in contact with the space probe.

According to [1-1], the most important challenges in thermal design of Shinen2 are the fact that the deep space probe will pass through very different thermal environments (between 0.9 and 1.1 AU), its size is only 500 mm in diameter, its weight is about only 17.9 kilograms and an active thermal control is difficult to implement because it requires large equipment. For these reasons, instead of an active thermal control, a passive thermal control is used for temperature management.

Regarding the challenges in designing a Thermal Protection System for a re-entry probe, the study of the effects of the aerothermodynamics environment over the re-entry spacecraft has a crucial importance. The ablative materials are commonly used as thermal shield for the re-entry spacecraft. In particular, as remarked in [1-16], an ablator made of phenolic carbon fiber-reinforced plastics (CFRP) is known to possess superior resistance against aerodynamic heating.

Carbon fiber reinforced plastic (CFRP), is a composite material made of carbon fiber and resin, and it is frequently used as a heat shield material. According to [1-17], carbon-based ablators were used for several planetary entry missions, like Mars Science Laboratory (MSL), Crew Exploration Vehicle (CEV), or Venus missions.

The maximum heat flux ever encountered in a space mission was the case of the Galileo probe deceleration module of NASA's Jupiter explorer. The probe was designed to withstand a maximum heat flux of about 300 MW/m^2, and the measured heat flux was of 134 MW/m^2 . The external surface of the probe was made by high-density CFRP (with a virgin material density of 1,448 kg/m^3). As noted in [1-17], the same material, high-density CFRP, was used for the return-entry module (REM) capsule of Japan's unmanned space experiment recovery system (USERS).

In case of a TPS made of ablative materials, the kinetic energy is converted into heat, which consumes the TPS through ablation [1-17]. Ablation is a very complex phenomenon related with diverse simultaneous physical processes [1-17], which makes it extremely difficult to analyse and predict. Also, because the shape of the surface changes due to ablation, a small deviation in the prediction of the ablation can lead to an increase in the re-entry trajectory uncertainty.

Recently, lightweight ablators started to be used more frequently as their thermal performances often equals the performance of heavyweight ablators. According to [1-17], if a lightweight ablator with a density of ~300 kg/m^3 and a CFRP-based ablator 1,500 kg/m^3 are heated under a heat flux of 2.0 MW/m^2, the surface and in-depth temperatures of the two ablators are almost identical. The use of lightweight ablator can lead to a reduction in the mass of the spacecraft, and ultimately of the cost of that spacecraft. In the last years, a new lightweight ablator called the Lightweight Ablator Series for Transfer Vehicle Systems (LATS) have been developed [1-3].

1.3 Purpose and Structure of the Thesis

1.3.1 Purpose of the Thesis

The advancements in the micro spacecraft programs can improve space travel reliability by testing new technologies, materials and designs. Also, through the small deep space probes missions which collect space flight data and return them to Earth, the thermal protection systems for human missions can be validated.

Some of the biggest challenges related to these missions are the harsh thermal environment of deep space and the atmospheric re-entry. The aim of this research is to address the two aspects, the one related to the harsh thermal environment of outer space, for which the study case will be represented by Shinen2 deep space mission, and the one related to atmospheric re-entry, focused on the validation of the ablative materials called LATS (Light-weight Ablator Series for Transport Vehicle Systems). The both studies are contributing in enhancing the knowledge and in developing new technologies related to a future small spacecraft mission, led by universities.

To accomplish the purpose of the research, the following studies have been done:

1. Development of a passive thermal control method for a deep space probe (Shinen2), having an outer structure made of CFRTP (Carbon Fiber Reinforced Thermoplastics) and CFRP (Carbon Fiber Reinforced Plastics) materials. The CFRTP material is used for the first time as the outer structure of a space vehicle;
2. Development of empirical and numerical methods to estimate the recession rate of LATS materials during re-entry;

The studies will represent the first steps in designing a thermal system for a future small spacecraft mission, having a similar structure with Shinen2 and a thermal shield made of LATS materials.

1.3.2 Structure of the thesis

The thesis was organized in five chapters. Chapter one is the Introduction Chapter, describing the motivation for ultra-small spacecraft missions led by universities, the harsh environment of deep space and during atmospheric re-entry, the challenges in designing the thermal system, and also the objectives and the structure of the thesis.

Chapter two presents a description of the various methods to design a thermal control system, suitable for a deep space mission like Shinen2, about the thermomechanical properties of CFRP-based materials and about the numerical and empirical methods used to test the efficiency of LATS materials.

Chapter three comprises the orbit analysis, the thermal design, analysis and validation of the ultra-small deep space probe, Shinen2, developed by Kyushu Institute of Technology in collaboration with Kagoshima University and launched on December 2014. For reasons of weight saving and power saving, Shinen2 did not carry a heater to warm itself. A passive thermal control of a deep space probe is very difficult to be attained and the thermal design of Shinen2 didn’t have a precedent model.

Chapter four focuses on the study of light thermal protection systems for re-entry spacecraft, using LATS materials. To study the thermal performances of LATS materials, numerical and empirical studies were performed using the flight data of USERS spacecraft and the results of high enthalpy heating tests, performed at Japan Aerospace Exploration Agency (JAXA, Japan), at Japan Ultra-High Temperature Materials Research Institute (JUTEM, Japan) and also at German Aerospace Centre (DLR, Germany).

The Conclusions chapter, Chapter five, summarizes the findings of the research, the contributions to a thermal system design of a future ultra-small spacecraft mission, led by universities. Chapter five describes also the recommendations for future studies.

References

[1-1] Bianca Szasz and Keiichi Okuyama, *Thermal Design and Analysis of SHINEN2, an Ultra-Small Deep Space Probe*, Proceedings of The 58th Space Sciences and Technology Conference, Nagasaki, Japan, 2014.

[1-2] Bianca Szasz, Kei-ichi Okuyama, Sumio Kato, Takayuki Shimoda, *Empirical Study of the Lightweight Ablator Series for Transfer Vehicle Systems (LATS)*, Transaction of JSASS, Aerospace Technology Japan, accepted for publication.

[1-3] Bianca Szasz, Kei-ichi Okuyama, *A New Method for Estimating the Mass Recession Rate for Ablator Systems*, Proceedings of The XII International Conference on Thermophysics and Heat Transfer (ICTHT 2014), London, United Kingdom.

[1-4] E. Brian Pritchard, *Mars: Past, Present, and Future*, Progress in Astronautics and Aeronautics, Volume 145, American Institute of Aeronautics and Astronautics, Washington, U.S.A., 1992.

[1-5] *India becomes first Asian nation to reach Mars orbit, joins elite global space club*, The Washington Post. 24 September 2014. Retrieved 24 September 2014.

[1-6] *India's spacecraft reaches Mars orbit ... and history*, CNN. 24 September 2014. Retrieved 24 September 2014.

[1-7] Harris, Gardiner (24 September 2014), *On a Shoestring, India Sends Orbiter to Mars on Its First Try,* New York Times. Retrieved 25 September 2014.

[1-8] Bhatt, Abhinav (5 November 2013), *India's 450-crore mission to Mars to begin today: 10 facts*, NDTV. Retrieved 13 October 2014.

[1-9] NASA Website, *Micro Spacecraft to Pave the Way for Future Space Exploration*, URL: http://www.nasa.gov/centers/ames/research/exploringtheuniverse/blackbox.html (2016).

[1-10] Funase, R., Nakamura, Y. and et al., *Development of COTS-based Pico-Satellite Bus and Its Application to Quick and Low Cost On-orbit Demonstration of Novel Space Technology*, Transactions of the Japan Society for Aeronautical and Space Sciences, Space Technology Japan, Vol.6, pp.1-9, 2008.

[1-11] Nakasuka, S., *From Education to Practical Use of Nano-satellites – Japanese University Challenge towards Low Cost Space Utilization*, 8th IAA Symposium on Small Satellite for Earth Observation, Berlin, Germany, 2011.

[1-12] Boshuizen, C., Mason, J. and et al., *Results from the Planet Labs Flock Constellation*, 28th Annual AIAA/USU Conference on Small Satellites, SSC14-I-1, Logan, Utah, USA, 2014.

[1-13] Ryu Funase, Hiroyuki Koizumi, Shinichi Nakasuka, Yasuhiro Kawakatsu, Yosuke Fukushima, Atsushi Tomiki, Yuta Kobayashi, Junichi Nakatsuka, Makoto Mita, Daisuke

Kobayashi, Taku Nonomura, *50kg-class Deep Space Exploration Technology Demonstration Micro-spacecraft PROCYON*, SSC14-VI-3.

[1-14] Delft University of Technology website, URL: http://lr.tudelft.nl (2016).

[1-15] Silva, D.V.F.M.R., 2001, *Estimative of Thermal Properties of Ablative Materials*, M.Sc. Dissertation, Federal University of Rio de Janeiro – UFRJ, Rio de Janeiro, Brazil, 108 p.

[1-16] Kei-ichi Okuyama, Sumio Kato, Tetsuya Yamada, *Thermo-chemical recession characteristics of CFRP in an earth atmospheric re-entry environment*, TANSO, Vol.2005 (2005), No.219, P 232-237.

[1-17] Keiichi Okuyama, Sumio Kato and Hiroaki Ohya, *Thermochemical Performance of a Lightweight Charring Carbon Fiber Reinforced Plastic*, Trans. Japan Soc. Aero. Space Sci., Vol.56, No.3, pp. 159-169, 2013.

II. Theoretical Background

2.1 Passive thermal control methods

2.1.1 Common passive thermal control methods

As noted in [2-3], big space vehicles have some advantages in comparison with small space vehicles in the thermal field, first their large mass allowing the use of different thermal systems but at the same time the bigger thermal inertia helps to control the temperature inside the desire range. The thermal design must consider that the heat flux coming from the radiation of the sun together with the heat generated by the electrical components inside the satellite must keep the temperatures inside the established limits. Table 2-1 shows some typical limits for the internal components.

Table 2-1 Typical temperatures limits for inside satellites components [2-4]

Component	Tmin (ºC)	Tmax (ºC)
Battery (Charge)	0	45
Battery (Discharge)	-20	60
CPU	-40	85
Micro-Spectrometer	-20	40
Magnetometer	-40	85

The hostile conditions of extreme variations of the temperature and the radiation environment must be analysed to select the most convenient method (passive or active) to avoid a failure or damage on the payload and structure [2-5]. Passive thermal control are commonly used, like painting and insulators due to the small heat generated inside.

According to [2-6], the radiative properties of the external surfaces (emittance and solar absorptance) must be properly selected in order to achieve the thermal balance at the desired temperatures. The thermal balance for the external surfaces is achieved between the sunlight, the Earth-emitted IR, other external sources of heat, re-radiation to space and internal dissipation.

Some examples of wavelength-dependent thermal control coatings are solar reflectors (second-surface mirrors), white and black paints, silver- or aluminium-backed Teflon. If it is desired to minimize the absorbed solar energy and also infrared emission, it is recommended to use polished metal (aluminium foil or gold plating). On the interior of the vehicle, to enhance the heat transfer between different compartments, black paint is recommended [2-6]. The coating materials, before being used in space, must be proven reliable in aspects regarding in-space stability, outgassing, or mechanical adhesion to the substrate [2-6].

2.1.2 Advantages of using CFRP and CFRTP

Another issue that must be addressed is represented by the materials which are used for manufacturing the space vehicle. According to [2-7], Carbon Fibers are a 21st century high technology material, having high specific tensile strength, high specific elastic module, low thermal expansion coefficient, chemical stability, high heat resistant and low specific gravity.

Carbon Fibers are fibrous carbon materials having a micro graphite crystal structure made by fibrillation of Acrylic resin, or from oil/coal pitch and then by being given a certain heat treatment. They are manufactured by using different raw materials and applying divergent production processes, wide diversity of the fibers having different specifications [2-7].

Commonly, carbon fibers are applied for reinforcement of composite materials, made with a ceramic or metal matrix, filled with resin. As mentioned in [2-7], Carbon Fiber Reinforced Plastics (CFRP) is superior to steel or glass fiber reinforced plastics (GFRP), especially in properties like the specific elastic modulus and tensile strength. A comparison in thermal properties between Glass Fiber Reinforced Plastics, Carbon Fiber Reinforced Plastics, Aramid Fiber Reinforced Plastics, High Tension Steel and Aluminium Allow is given in Fig.2-1. Carbon fiber composite materials are widely used in industries like aerospace, for civil and military aircrafts, rockets for space development and artificial satellites etc. [2-7].

According to [2-8], Carbon fiber reinforced plastics (CFRP) can be divided into two kinds, Carbon Fiber Reinforced Thermosetting Resins (CFRTS) and Carbon Fiber Reinforced Thermoplastics (CFRTP), depending on polymers used as matrixes for carbon fiber reinforced plastics (CFRP). Shinen2, an ultra-small deep space probe recently launched to space, was the first space mission which has an outer structure made by CFRTP materials and it is the first time when CFRTP are used in a space mission. CFRTP materials (Carbon Fiber Reinforced Thermoplastics) are different than CFRP (Carbon Fiber Reinforced Plastics).

The primary physical difference between thermosetting polymers and thermoplastic polymers is that thermoplastic polymers, which are solid state at room temperature, can be melted into a liquid above certain temperatures and cooled back into solid state repeatedly as required, whereas thermosetting polymers always remain in a permanent solid state after once cured [2-8].

GFRP – Glass Fiber Reinforced Plastics;

CFRP – Carbon Fiber Reinforced Plastics;

AFRP – Aramid Fiber Reinforced Plastics

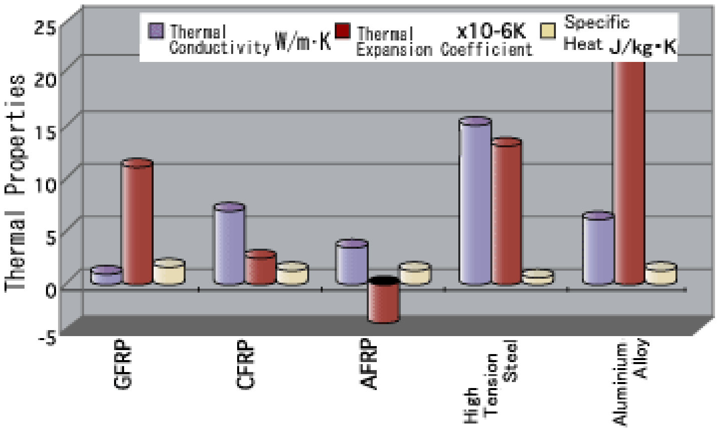

Fig. 2-1 Comparison of Thermal Characteristics of various compounds [2-7]

CFRTS has an advantage of resisting against high temperature and chemical substance. On the other hand, CFRTP is said to be easier for rapid processing and recycling since it can melt when the temperature is higher than the matrix melting temperature. Currently, more and more CF (carbon fibers) companies have been applied into CFRTP, because CFRTS comparatively lose much more economical and ecological benefits [2-9].

CFRTP forming is usually divided into two processes: one is the impregnation process of the resin to reinforcing fibers to produce prepreg sheet and the other is molding process by using the prepreg sheet. In the method of supplying the resin in producing prepreg, non-woven fabric of matrix resin has been expected to shorten the manufacturing time and reduce cost. For the process of producing prepreg, roll forming method has advantages of a continuous process compared to a compression press molding process [2-10].

Even though CFRTP can be recycled, its extensive usage is still under development because currently it is risky to apply r-CF (recycled carbon fiber) in vital structures, because of mechanical performance degradation due to fiber breakage during the recycling process ([2-11], [2-12]). CFRTP have weak adhesive force at interface between thermoplastic polymer matrix and the fibers [2-13]. The principles of manufacturing is represented in Fig.2-2, Fig.2-3 and Fig. 2-4.

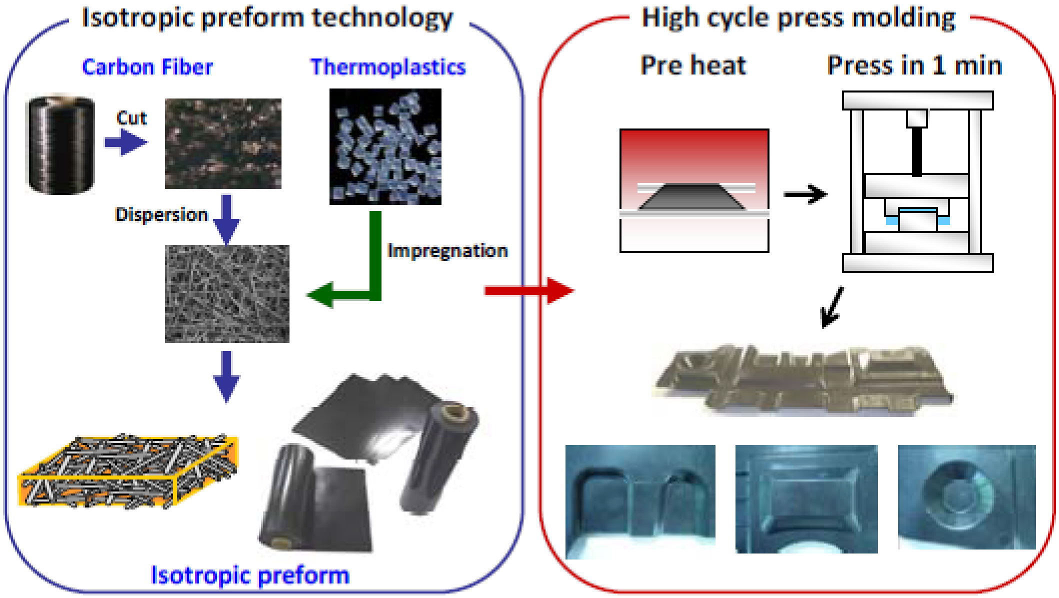

Fig.2-2 Discontinuous CF reinforced thermoplastics prepreg sheet [2-14]

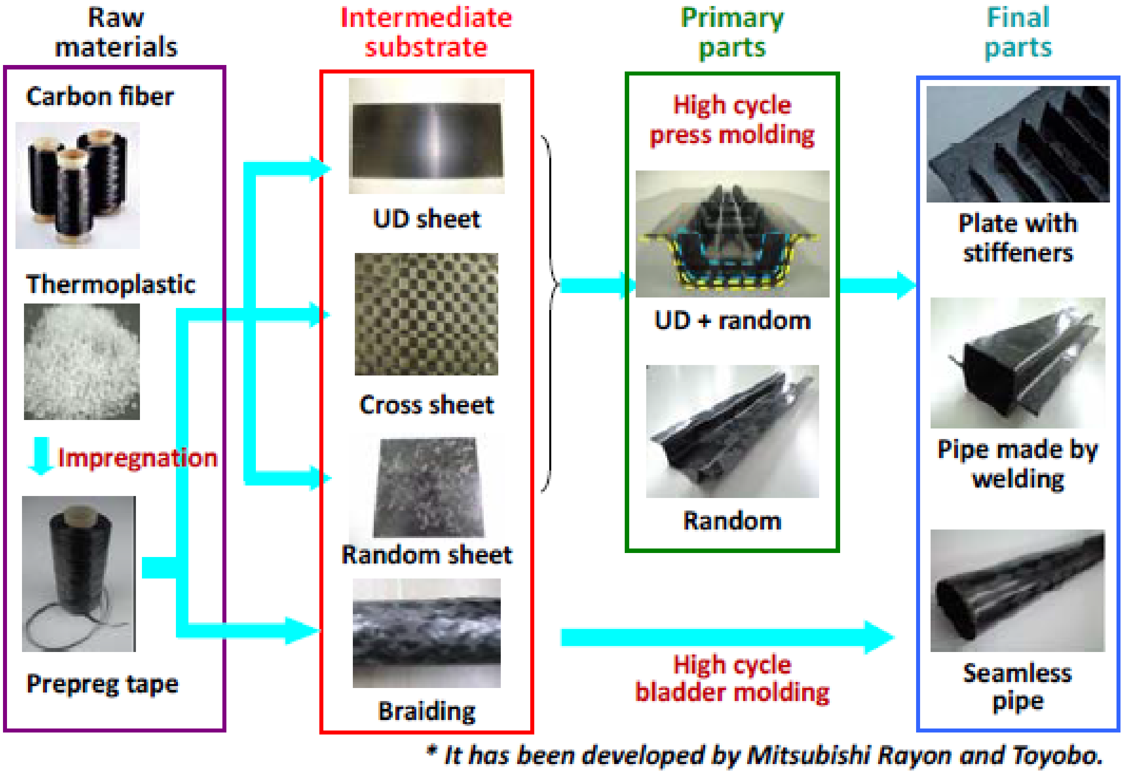

Fig.2-3 Continuous CF reinforced UD-tape and its various applications [2-14]

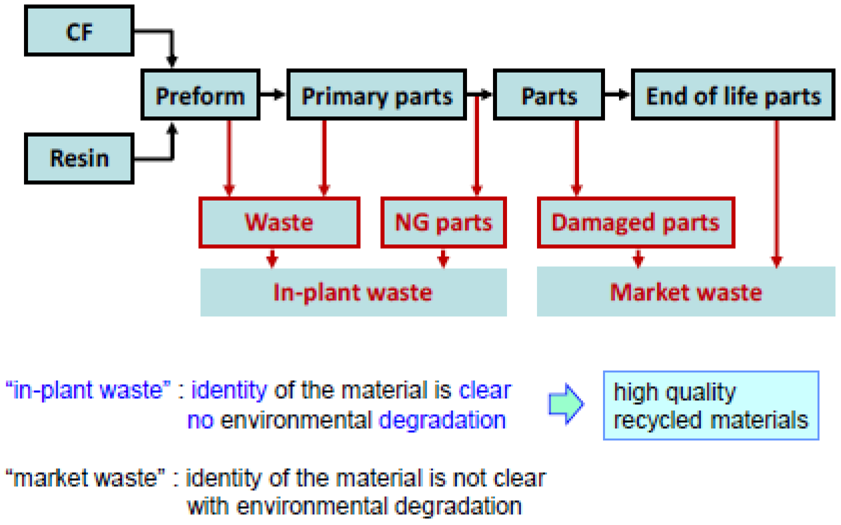

Fig.2-4 Difference between "in-plant waste" and "market waste" [2-14]

CFRTP, made by welding joints, has the same mechanical strength or bigger than the base materials, which is not the case of CFRTS, Carbon Fiber Reinforced Thermosetting Resins [2-15]. The difference in adhesion between CFRTS and CFRTP is shown in Fig. 2-5.

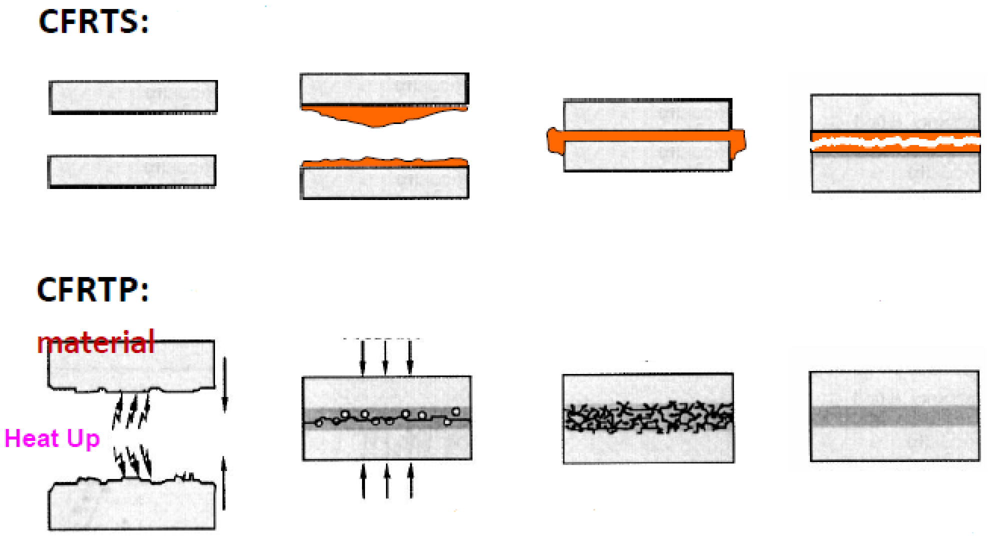

Fig.2-5 Difference in adhesion between CFRTS and CFRTP

CFRTS, made by bolting or with adhesive joints, is weaker than the base material. In case of CFRTP, the fibers tangles and fiber volume fraction becomes higher at the welded section, making the final product stronger than the base material [2-15]. Also, the fracture mechanism of CFRTP can be ductile in comparison to that of CFRTS [2-15]. The differences in jointed and curved section between CFRTS and CFRTP can be seen in Table 2-2.

Table 2-2 Differences in jointed and curved section between CFRTS and CFRTP [2-14]

	Thermosetting CFRP	**Thermoplastic CFRP**
Bonding joints	**Adhesive joint** × disassembly ○ workability △ reliability → facility become larger due to the integrated molding	**Welding joint** △ disassembly ○ affordable, easy, fast (a few seconds) ○ joint section is stronger than base material → mold small parts affordably, and assembly by welding joint technique !!
Bolted joints	○ disassembly × delamination when drilling × fiber cut, stress concentration → measures like metal insert → increase in weight, manufacturing time, and cost	○ disassembly ○ no delamination when drilling △ fiber is cut, stress is concentrated, but fracture is ductile → measures like insert are not necessary → reduction in weight, manufacturing time, and cost → applicable to joints with metal, and reliable parts
Curved section	× measures for stress concentration and delamination are necessary → structure becomes thick, complex and heavy	○ design is similar to metal ○ possibility of new high cycle molding methods utilizing the high workability → structure becomes simpler, lighter-weight, and affordable !!

The specific bending stiffness and tensile strength of CFRTP comparing to other materials are shown in the Fig.2-6.

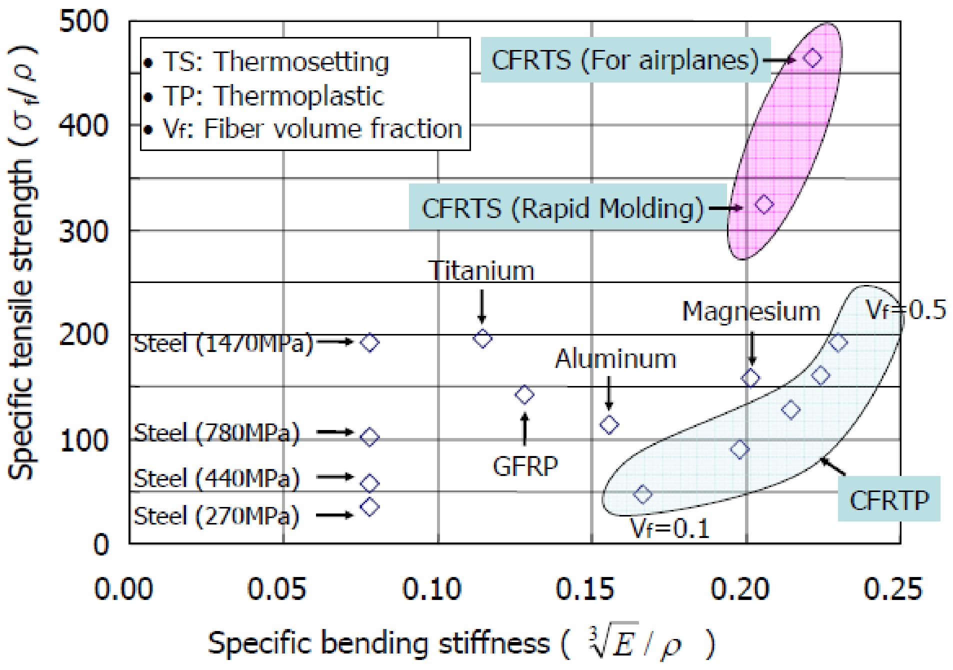

Fig.2-6 Specific Bending Stiffness and Tensile Strength [2-15]

Fig.2-7 illustrates the rational formula of polyetheretherketone (PEEK). Due to the fact that PEEK materials have high heat and corrosion resistance [2-16], they are usually used for the interiors and upholsteries of the cabin and parts in airplanes and automobiles [2-13].

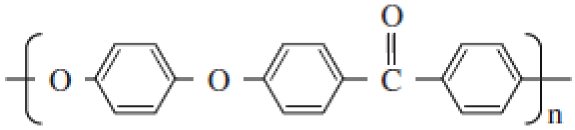

Fig.2-7 Rational formula of polyetheretherketone (PEEK) [2-13]

There have been only few applications of CFRTPs for structural parts in the Aerospace sector yet [2-17]. One reason for this are probably the higher material costs of high temperature thermoplastics compared to their thermoset relatives. At the DLR Center for Lightweight Production Technology in Augsburg research is focused on the automation of high volume production, in order to reduce the process costs of such parts significantly [2-17].

The University of Tokyo has organized Japanese national project to develop CFRTP for mass production automobile from 2008 to 2012 fiscal year. Meanwhile, a lot of groups which are interested in CFRP have been appeared and among them research centers for composite materials, especially for CFRTP, have been established in the past few years [2-14].

The background of this bubbly investment is sure to be the awareness of automotive manufacturers. They have applied ultra-lightweight technology only to the special automobile to supply extreme driving performance, but nowadays they have faced to the social demand for developing mass production electric vehicle and ultra-lightweight vehicle to mitigate the global oil consumption and CO_2 emission (Table 2-3) [2-14].

Table 2-3 Expectations for CFRTP (similarities and differences between airplane and automotive application) [2-14]

		Airplane	Automobile
Motivation		high oil price → tight national budget (including military budget) → low-cost CFRP (<50€/kg) and maintenance	high oil prices and CO$_2$ measures → weight lightening & early spread of EV (by battery reduction) → low-cost CFRP (<10€) and recycling
Direction of technology development	**Material & Preform**	low-cost engineering plastics	low-cost & productive CF low-cost general-purpose resin low-cost impregnation
	Molding	low-cost manufacturing →from hours to minutes →thermoforming/welding yield improvement →automatic tape placement measures for labor costs and intellectual property → automation	low-cost manufacturing →less than one minute →thermoforming/welding yield improvement →recycling of in-plant waste measures for labor costs and intellectual property → automation
	Operation	repairability impact resistance simplification of NDI	repairability recyclability of market waste new design for dynamic social demand

CFRTP and CFRTS can have a weight reduction of 1/3 comparing to a steel panel, the elastic strain range is 4 times more than the steel panel (the frequency of repair is decreased in this way) [2-15].

Examples of thermoplastic polymers used as matrixes of carbon fiber reinforced thermoplastics (CFRTP) are given below [2-8]:

- Polyether Ether Ketone (PEEK)
- Polyether Ketone Ketone (PEKK)
- Polyphenylene Sulfide (PPS)
- Polyether Imide (PEI)
- Polybutylene Terephthalate (PBT)
- Polyethylene Terephthalate (PET)
- Polycarbonate (PC)
- Polyamide Imide (PAI)
- Polypropylene (PP)
- Thermoplastic Polyimide (TPI)
- Nylon6
- Nylon66

In case of Shinen2, the matrix for CFRTP outer structure, was made by Polyether Ether Ketone (PEEK) and it can be seen in the Fig.2-8.

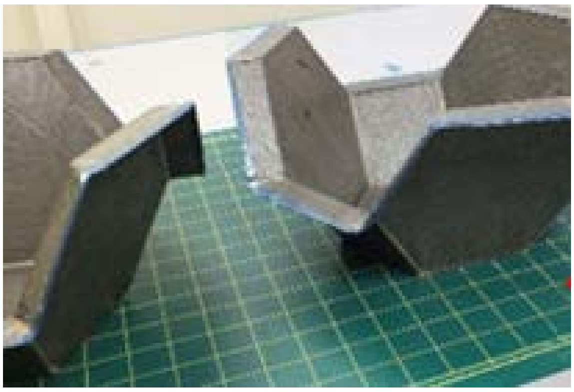

Fig.2-8 Outer structure of Shinen2, made by CFRTP

2.2 Thermal characteristics of CFRP-based ablators for space use

2.2.1 Common ablator materials for re-entry probes

According to [2-18], there are four principal material categories:

- high-temperature, chemically homogeneous materials which are consumed as a combined results of chemical attack and sublimation at the exposed surface (e.g. graphite);
- composite ablation materials which decompose in depth to form a high-temperature char layer;

- inorganic glassy materials, such as quartz and silica, which ablate due to the combined effect of vaporization, chemical reactions, and liquid removal;
- low-temperature organic ablators such as Teflon.

Since the first two material types (non-charring and charring ablators), can resist to higher temperatures, they are the primary point of interest in space projects which involve re-entry studies [2-18]. In the present research, the charring materials will be used as study subject.

Charring materials are composed by a filler (commonly a resin) and a reinforcing material (like carbon). The resin, when heated, undergoes a series of chemical reactions that release gaseous by products (a phenomenon called pyrolysis) leaving a layer of char or residue [2-18]. According to [2-19], a charring ablator made of phenolic carbon fiber-reinforced plastics (CFRP) is known to possess superior resistance against aerodynamic heating, having excellent thermos-physical properties and low densities.

Heat shield material must satisfy the requirement of excellent performance such as high specific strength as well as high specific stiffness: it must have high resistance to the shear load generated by the high-speed air current [2-19]. The rate of aerodynamic heating of the re-entry vehicle which returns to the ground from space is high; in the case of return from the low earth orbit as a velocity of 7.8 *km/s*, the value is several MW/m^2, and in the case of return from the moon orbit at a velocity of about 12 *km/s*, the value is 10 MW/m^2 or even more.

2.2.2 CFRP-based ablators

The re-entry vehicle fitted with ablator is pyrolyzed and carbonized by aerodynamic heating. The vehicle surface is cooled by endothermic reaction, such as dissolution of the ablator. Moreover, the pyrolysis gas, which is generated from the ablator surface, reduces the aerodynamic heating by being diffused on the vehicle surface.

Charring ablator is usually used for the heat shield system. Among charring ablators, phenolic carbon ablator is often used for the heat shield system. The phenolic carbon ablator has been applied to the earth re-entry capsules such as USERS REV capsule (Unmanned Space Experiment Recovery System Recovery Vehicle) and Hayabusa Re-entry capsule or the planetary entry probe “Gallileo” of NASA. Each of these capsules used a high density ablator with the value of about 1500 kg/m^3 and were CFRP-based ablators [2-20]. USERS spacecraft mission was launched in 2002. The maximum heat flux used when designing the REM capsule was approximately 3.1 MW/m^2, whereas the real heat flux at re-entry was approximately 1.5 MW/m^2 [2-19]. In the USERS mission, the ablative materials had a high density of about 1.5 *g/cc*.

CFRP (carbon-fiber-reinforced plastic) and GFRP (glass-fiber-reinforced plastic) are typical ablators, which have had good track records in the re-entry vehicles used. Compared with GFRP, CFRP has a great advantage that it can be used in a wide range of heating conditions including severe heating environment: the thermal reaction of CFRP on the surface material is simple compared with that of GFRP and it is easier to predict both CFRP surface temperature and CFRP recession. According to [2-19], CFRP has been applied to the heat shield system of the re-entry capsule and the fairings of the rockets, the engine nozzles, etc.

2.3 Properties of Lightweight Carbon-based Ablators

2.3.1 Advantages of using Lightweight Ablators

The weight ratio of the TPS for the re-entry capsules launched before Hayabusa and USERS were very high, more than 50%. In United States and Russia, scientists have recently studied innovative ideas to manufacture lightweight ablators. In case of the porous carbon, the density and porosity can be controlled, because porous carbon has a uniform structure with mechanical stability.

There are many kinds of lightweight ablators which are made of fiber reinforced plastics with a porous structure [2-19]. Typical materials are the Acusil series for the Comets program, the AVCORT5026 for the Apollo program, the SLRCA series for the Mars Pathfinder program, the SPA for the MIRKA program, the AQ60 for the Huygens program, the PICA for the Stardust program and so on. PICA materials, made of NASA, were, at the beginning, the only lightweight ablators which had carbon fiber (with the density values of about 300 kg/m^3) [2-2].

The most successful lightweight ablator was PICA. PICA is made of pre-form carbon fiber coupled with a small amount of carbon, on which phenol resin is impregnated. The density of virgin PICA is between 0.22 and 1.04 g/cm^3 and it was used for the Stardust mission [2-21].

Also, recently, Okuyama *et al.* manufactured a lightweight ablator called LATS (Lightweight Ablators for Transfer Vehicle Systems), with a virgin density between 0.2 and 1.5 g/cm^3, made of laminar layers of carbon fibers felt impregnated with phenol resin. The new lightweight CFRP is made of a carbon fiber felt and resin and the manufacturing method is different from that of PICA. The density of the LATS can be chosen between 200 and 1,500 kg/m^3. According to [2-19], LATS materials are considered to function as a heat shield material in a severe environment of high-enthalpy flow.

The main difference between LATS and conventional ablators is the density and the fact that LATS is a porous material at the surface. In Fig.2-9 and Fig.2-10, thermal conductivity, respectively the specific heat for LATS, PICA and conventional ablators are shown. The measured values are taken from [2-21] and [2-22]. The thermal conductivity and specific heat of conventional ablators are significantly higher than the thermal conductivity and specific heat of low-density ablators. One important thing to notice is also that the value of thermal conductivity for 0.3 *g/cc* LATS materials are similar to the thermal conductivity of PICA (0.22 to 0.3 *g/cc* density).

2.3.2 Phenolic Impregnated Carbon Ablators (PICA)

The phenolic impregnated carbon ablator (PICA) is a ceramic composite that have been used for the heat shields of several spacecraft and is a Light Weight Ceramic Ablators (LCAs). According to [2-23], the ceramic composites are being used for the thermal protection of structures due to their very high melting point of about 3200 °C, high oxidation resistance up to 2000 °C and their low ablation rates at high temperatures.

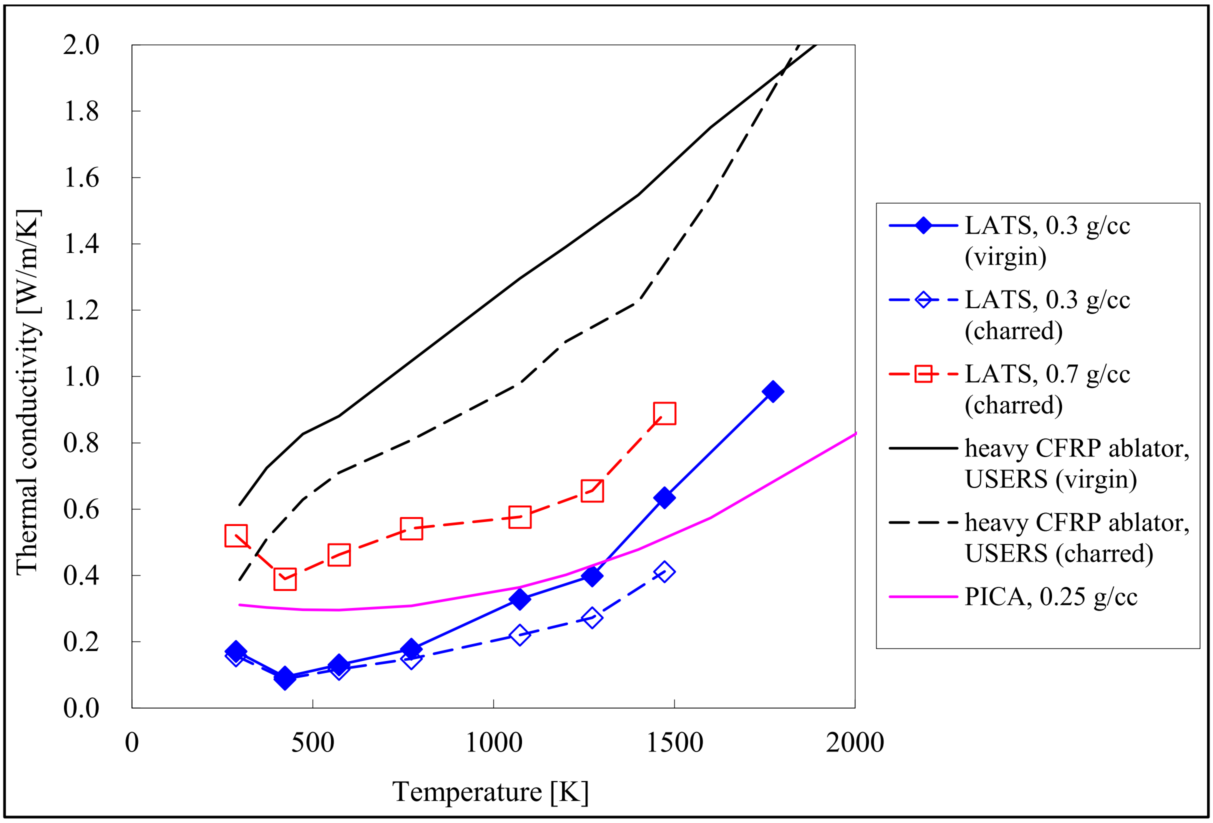

Fig.2-9 Dependency of the thermal conductivity with the temperature (for LATS, USERS, PICA)

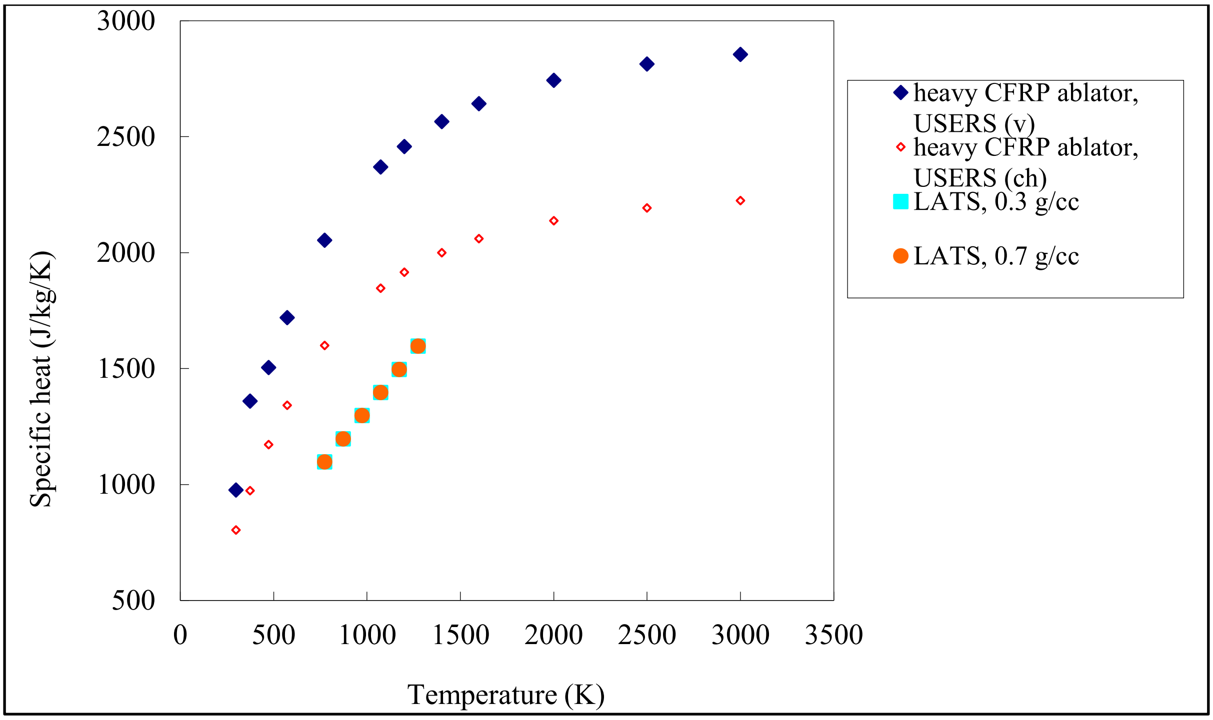

Fig.2-10 Dependency of the specific heat with the temperature (for LATS and USERS)

PICA was developed at NASA's Ames Research Center in the 1990s. According to [2-23], PICA has a very low density (weighting about 20% of conventional heat shields), and can withstand temperatures as high as 1930 °C. The PICA materials consist of carbon fibers coated with a thin layer of phenolic polymer resin. Resin provides bonding and it also creates a light heat- resistant shield.

PICA was first used for a space mission on the NASA's Stardust Sample Return Capsule (SRC), on January 2006, and it entered the Earth's atmosphere at the fastest recorded entry speed. Also, PICA was used for the heat shield of the Mars Science Lab (MSL) that landed on Mars in August 2012 (Fig.2-11). According to [2-23], due to the large size of the Curiosity Rover of the Mars Science Laboratory mission, a total of 113 tiles (3.2 cm thick) were employed with. The heat shield made by PICA tiles was capable of sustaining thermal loading of 197 W/cm^2. [2-23]

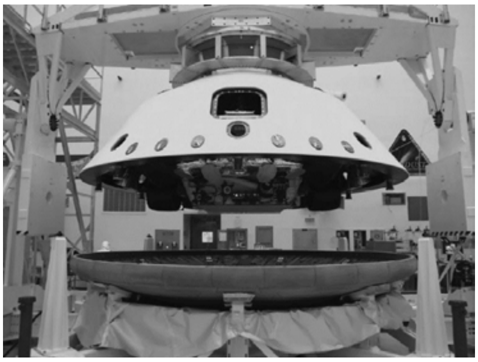

Fig.2-11 PICA tiles for the MSL mission that landed on Mars in Aug. 2012 (Courtesy of JPL/NASA, Reference Figure No. MSL-2011-05-26-143545-img_0959.JPG)

The outline of the thermal capabilities of PICA materials is given in the Fig.2-12-Fig.2-15.

2.3.3 Lightweight Ablator Series for Transfer Vehicle Systems (LATS)

Scientists, searching for new ways of improving the CFRP materials, developed a new class of lightweight carbon fiber reinforced plastics. Its name was chosen as LATS – the lightweight ablator series for transfer vehicle systems. One main reason for developing LATS materials was to assure a low mass for the thermal shield and to find a different manufacturing solution method instead of PICA (developed by NASA).

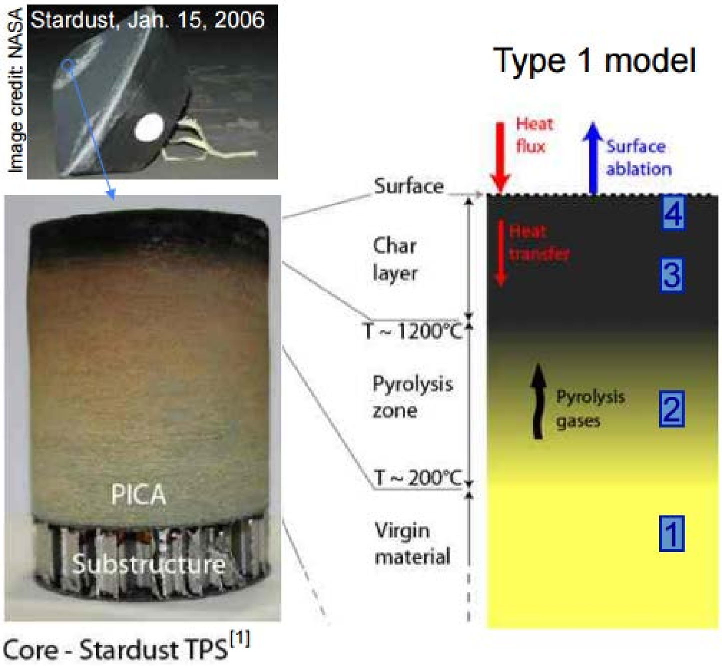

Fig.2-12 Outline of PICA material [2-24]

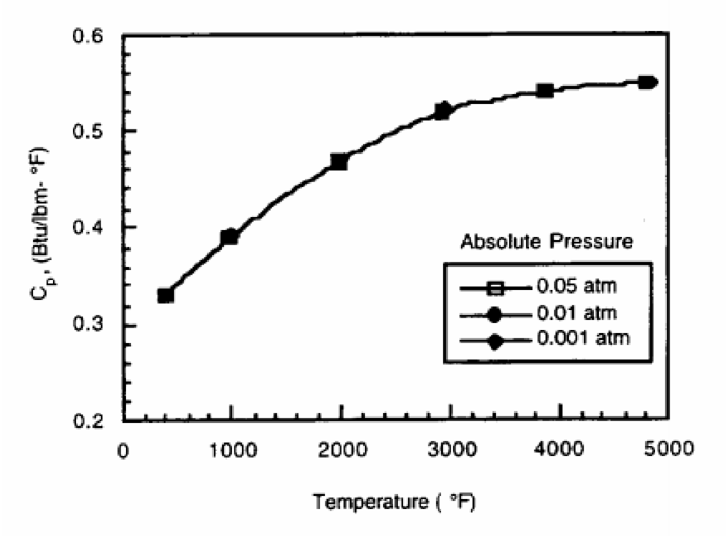

Fig.2-13 Heat Capacity of PICA-15 [2-25]

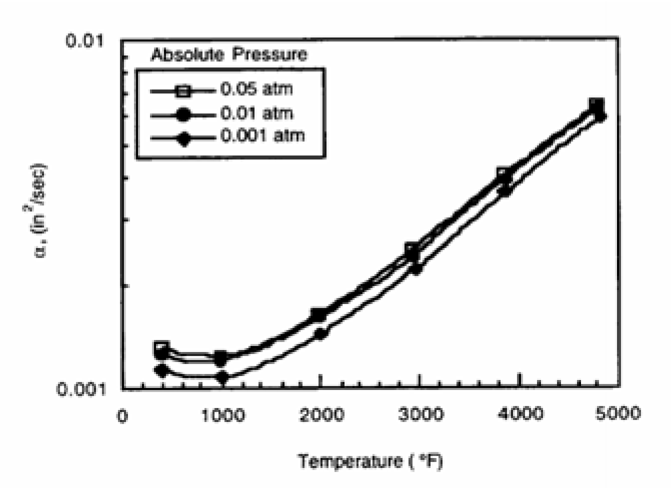

Fig.2-14 Thermal Diffusivity of PICA-15 [2-25]

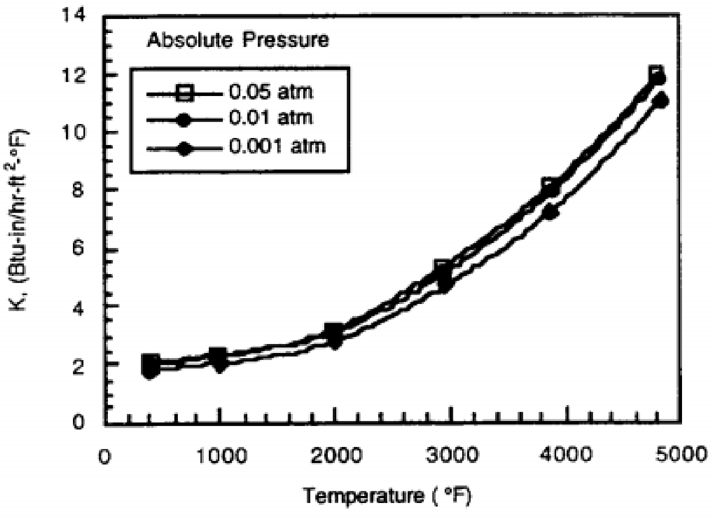

Fig.2-15 Thermal Conductivity of PICA-15 [2-25]

According to [2-22], the difference between PICA materials and LATS materials is that, for obtaining PICA material, a sheet of thick carbon is made, on which a phenolic resin is impregnated, while the LATS material is made by the accumulation of thin carbon felts that are impregnated with resin. The manufacturing process of LATS is based on heating and pressurizing a material in which resin is impregnated in the laminated carbon fiber felt and one of the advantages of using LATS materials is the simplicity of the resin impregnation process, because the dried bulk density can be easily controlled.

A relationship between the virgin and char density has been already established by previous research [2-22]. The density of virgin LATS materials is between 200 and 1500 kg/m^3, and the carbonized LATS density ρ_{ch} is a function of this virgin LATS density ρ_m in (2-1) [2-22]:

$$\rho_{ch} = 0.716\rho_m \tag{2-1}$$

As pointed out in [2-22], when heated, LATS material has excellent thermal performance characteristics.

Also, in the last years, several measurements of the thermal properties for LATS materials have been done. One of them was the measurement of heat capacity and a Differential Scanning Calorimetry, or DSC, was used. DSC is a thermal analysis technique that analyzes how the heat capacity (Cp) of a material is changing with the temperature. When a sample of known mass is heated or cooled, the changes in the heat capacity are considered as changes in the heat flow. According to [2-26], based on these techniques, the transitions such as melts, glass transitions, phase changes, and curing can be studied. Due to its advantages, DSC is used in many industries, including polymers, food, paper, pharmaceuticals, printing, manufacturing, agriculture, electronics, semiconductors.

DSC is a very common thermal analysis technique due to its ease and speed of detecting the transitions in materials and it is used in many process control, analytical, quality assurance, R&D laboratories [2-26].

To measure the heat capacitance (the amount of energy a unit of matter can hold [2-26]) of LATS materials, the differential scanning calorimeter has been used. The measurements made by the Differential Scanning Calorimetry (DSC) provide quantitative and qualitative information about physical and chemical changes involving endothermic or exothermic processes, or changes in heat capacity, by measuring the temperatures and heat flows associated with transitions in materials as a function of time and temperature in a controlled atmosphere [2-27], detecting any change that alters the heat flow in and out of a sample [2-26].

The reference material for the measurements with the differential calorimeter is Iridium. The heating follows a linear temperature ramp. An endothermic heat flows into the sample (Fig.2-16,2-17,2-18) and the exothermic heat flows out of the sample [2-27]. The Differential Scanning Calorimeter is presented in Fig.2-19.

Assuming work and mass loss are zero, the following equations can be used [2-27]:

$$\Delta H = Cp * \Delta T \tag{2-2}$$

Or in differential form:

$$\frac{dH}{dt} = Cp * \frac{dT}{dt} + thermal\ events \tag{2-3}$$

Cp=specific heat (J/g°C)

T=temperature (°C)

H=heat (J)

dH/dt=heat flow (J/min)

$mW = mJ/sec$

dT/dt=heating rate (°C$/min$)

The moment an exothermic or endothermic change take place in the sample, power (energy) is applied or removed from the furnace to compensate for the energy change occurring in the sample. The system is always kept in "Thermal Null" and the amount of power required to maintain the system in equilibrium is directly proportional to the energy changes [2-27].

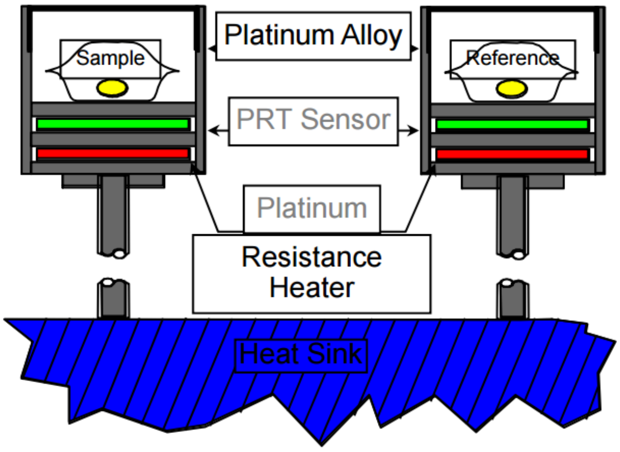

Fig.2-16 Principle of Differential Scanning Calorimeter [2-27]

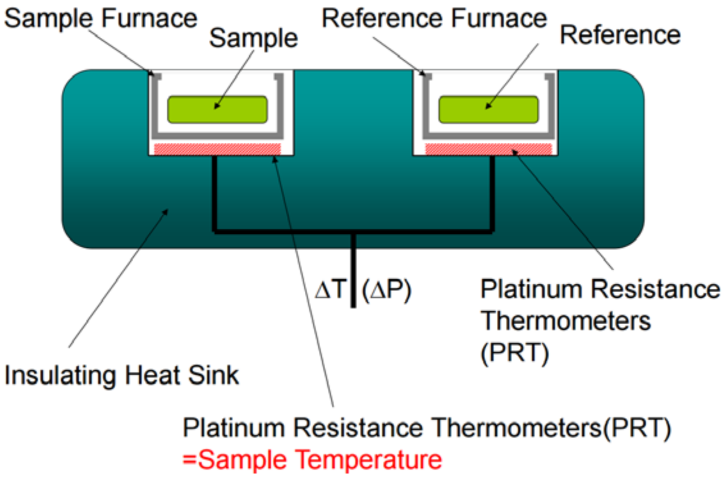

Fig.2-17 Typical Power Compensation DSC Cell [2-27]

To measure the latent heat of LATS ablator, Q2000 DSC was used. 6 samples of 500 kg/m^3 density LATS material and 6 samples of 700 kg/m^3 density LATS material were tested (Fig.2-20 and Fig.2-21). They were heated until 500 degrees Celsius. Measuring the temperature slope with time and the heat flow, the latent heat can be calculated.

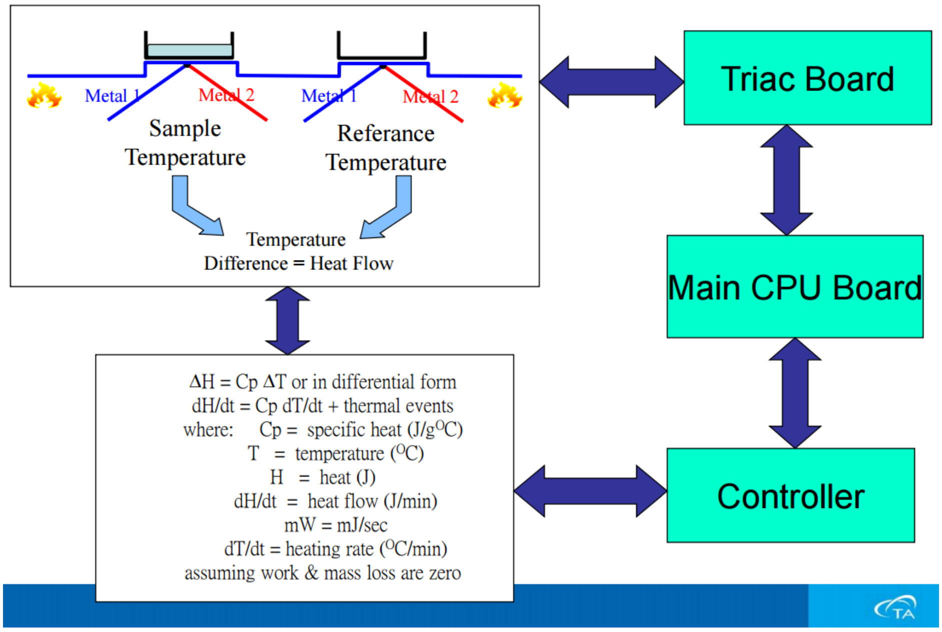

ΔH = Cp ΔT or in differential form
dH/dt = Cp dT/dt + thermal events
where: Cp = specific heat (J/g^{O}C)
T = temperature (^{O}C)
H = heat (J)
dH/dt = heat flow (J/min)
mW = mJ/sec
dT/dt = heating rate (^{O}C/min)
assuming work & mass loss are zero

Fig.2-18 DSC Measurements [2-27]

In calculating the latent heat, the first part of the curve was ignored (because of the presence of water vaporization and other phenomena) and only the part from the highest peak to the lowest value of heat flow (between about 240 to 440 degrees Celsius) was taken into consideration. The latent heat was calculated for each step of the measurement and it is the area beneath the curve representing the dependency of heat flow with the temperature, area given by the following formula:

$$L = -(\sum_{i=1}^{N} \frac{dq_i}{dt} - N * \frac{dq_1}{dt}) * (T_N - T_1)) \tag{2-4}$$

where L is the latent heat, dq/dt is the heat flow (in watt) and N represents the number of measurement points. The results should be multiplied by 60 as the initial time is given in minutes and, also, the negative sign should be added because the heat flow should be taken in its absolute value. Table 2-4 shows the results in latent heat.

Fig.2-19 Q2000 DSC

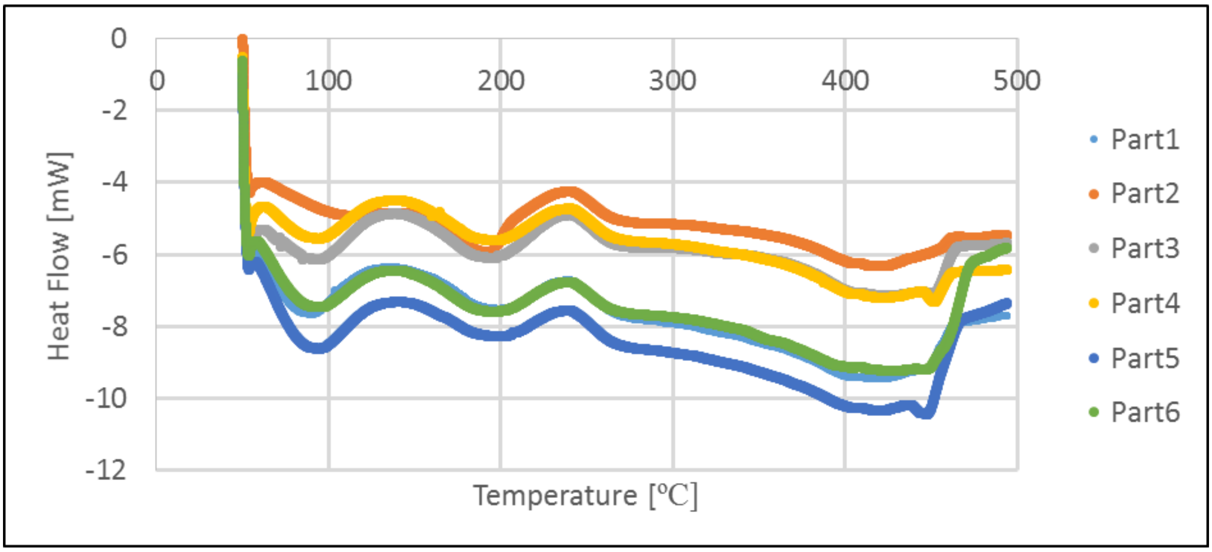

Fig.2-20 DSC measurement of heat flow versus temperature for 500 kg/m^3 LATS ablator

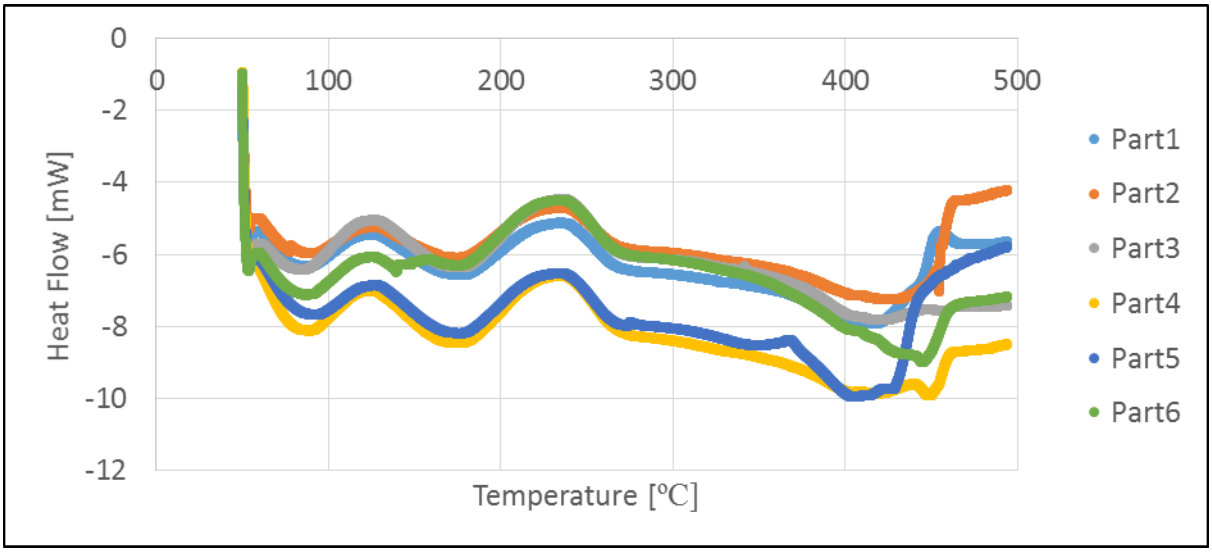

Fig.2-21 DSC measurement of heat flow versus temperature for 700 kg/m^3 LATS ablator

In 2016, the company AGUNE measured the specific heat and thermal conductivity of LATS materials using TC-9000 instrument and latent heat using 404 F1 Pegasus instrument. Two types of ablators were tested: 2D and 3D ablators. There were 5 samples of 2D ablator and 5 samples of 3D ablator, being tested at 20, 300, 500, 700, respectively 1000 degrees Celsius. The results can be seen in the following Table 2-5.

Table 2-4 Average values of the Latent Heat for 500 and 700 kg/m^3 density ablators

	RUN No.	Density (kg/m^3)	Latent heat [*kJ/10mg*]	Latent heat [*kJ/g*]	Average Latent heat [*kJ/g*]
Sample 1	084	500	6.816	681.568	340.145
Sample 2	087		1.657	165.678	
Sample 3	090		2.733	273.255	
Sample 4	091		2.986	298.636	
Sample 5	096		3.323	332.319	
Sample 6	097		2.894	289.416	
Sample 7	082	700	4.777	477.713	417.765
Sample 8	083		4.896	489.637	
Sample 9	088		3.028	302.757	
Sample 10	089		4.492	449.210	
Sample 11	094		3.281	328.118	
Sample 12	095		4.592	459.152	

Table 2-5 Thermal properties of 2D and 3D ablator

Type of ablator	Temperature (ºC)	Thermal diffusivity (cm^2/sec)	Density (kg/m^3)	Specific heat $(J/(g*K)$	Thermal conductivity $(W/(m*K)$
2D	20	0.00385	840	1.3	0.420
	300	0.00283		2.1	0.499
	500	0.00407		2.2	0.752
	700	0.00555		1.5	0.699
	1000	0.00798		0.8	0.536
3D	20	0.00646	770	1.2	0.597
	300	0.00551		1.9	0.806
	500	0.00611		2.0	0.941
	700	0.00744		1.5	0.859
	1000	0.00986		1.0	0.759

As can be seen from the Fig.2-22, the specific heat is higher for 2D ablator for temperature below 700 degrees Celsius and higher for 3D ablator above this value.

Besides the above mentioned measurements, others were performed in the past. The results are summarized in the Fig.2-23, Fig.2-24 and Fig.2-25.

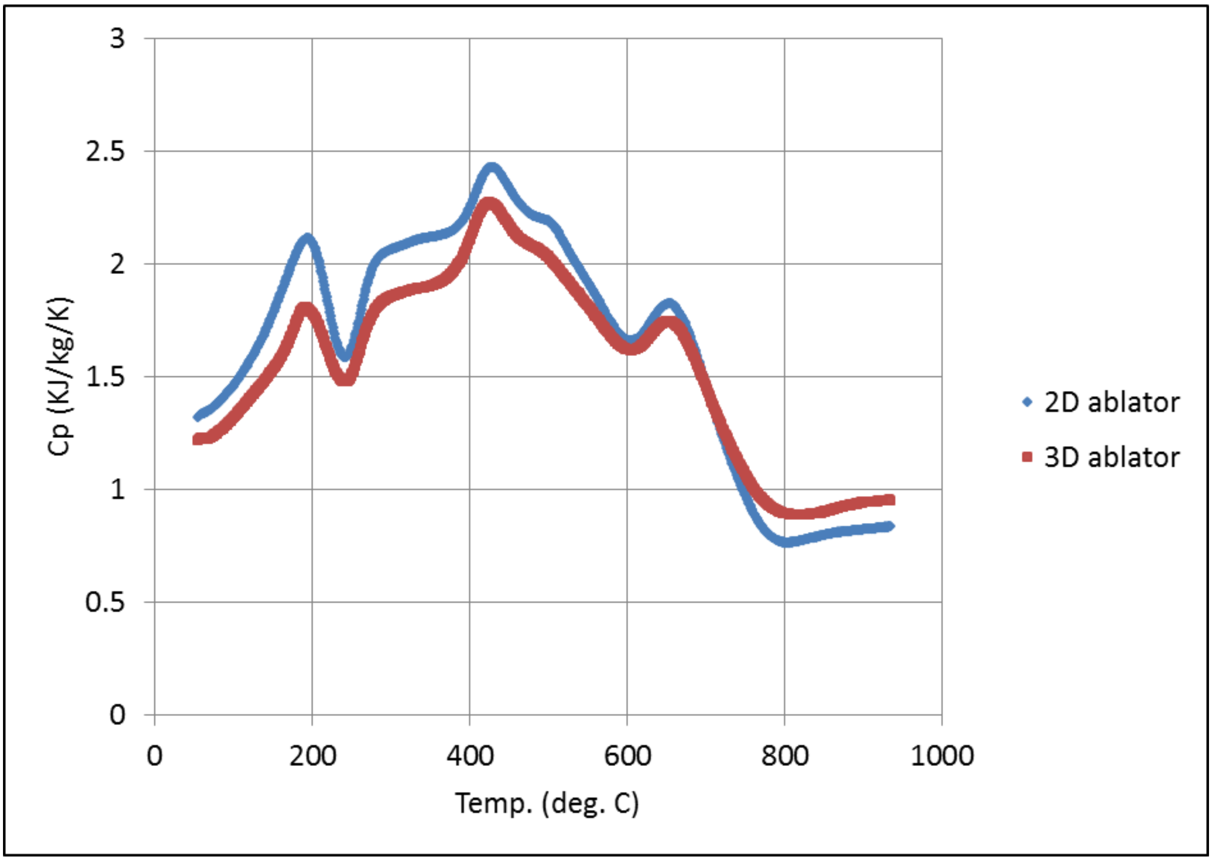

Fig.2-22 Specific heat for 2D and 3D ablator

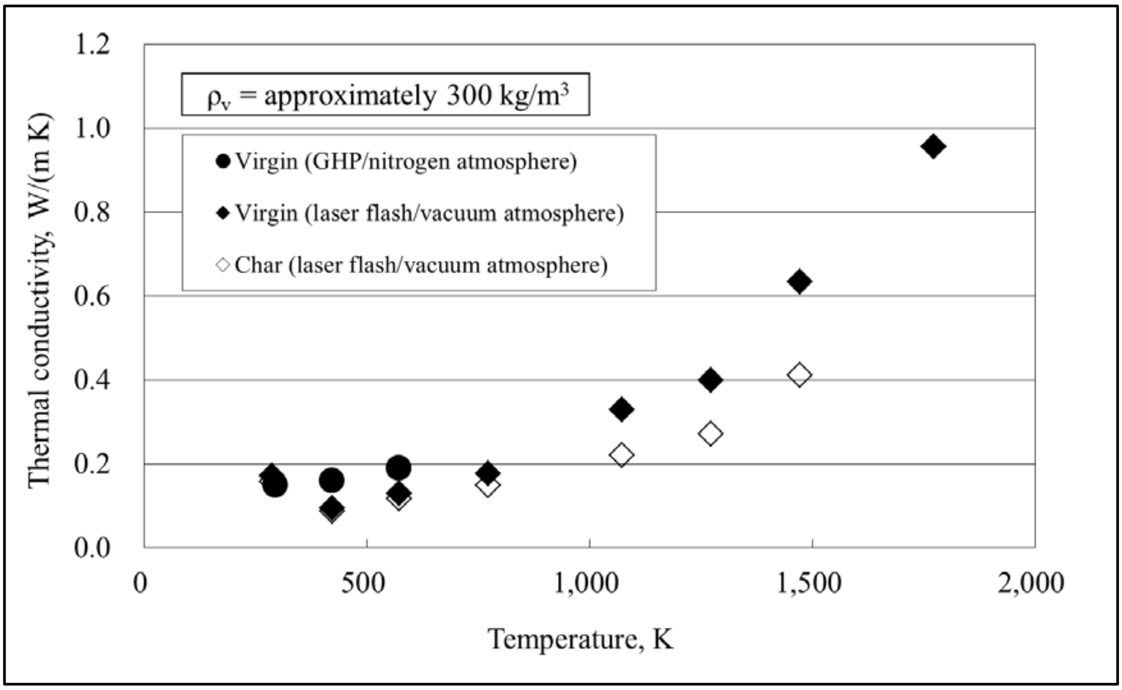

Fig.2-23 Relationship between measured thermal conductivity and temperature [2-21]

The main advantages of LATS and PICA materials, comparing to conventional ablators, are their very low density (low as 200 kg/m^3). According to [2-28], there are the following challenges concerning manufacturing of the PICA block:

- Deflection limits and PICA strengths indicate PICA flight panels may be limited to a maximum dimension of < 0.5 m, with current limits set around 0.25 m;
- Initial Boeing/FMI design features joined PICA panels --- however, NASA analysis indicates serious problems with resulting stresses in PICA.

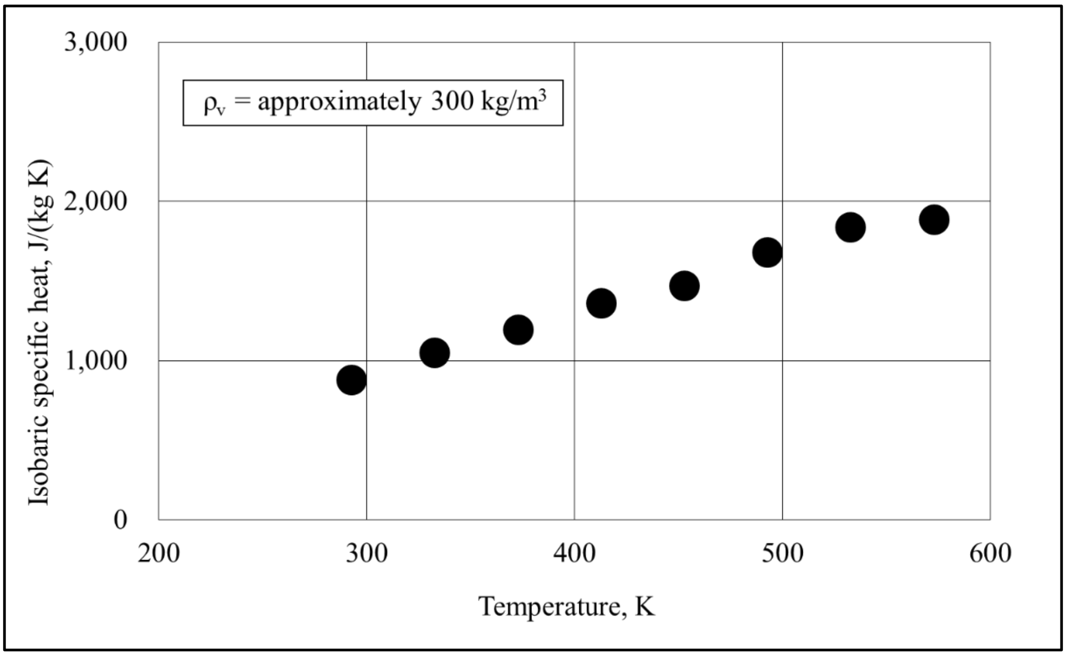

Fig.2-24 Relationship between measured isobaric specific heat and temperature [2-21]

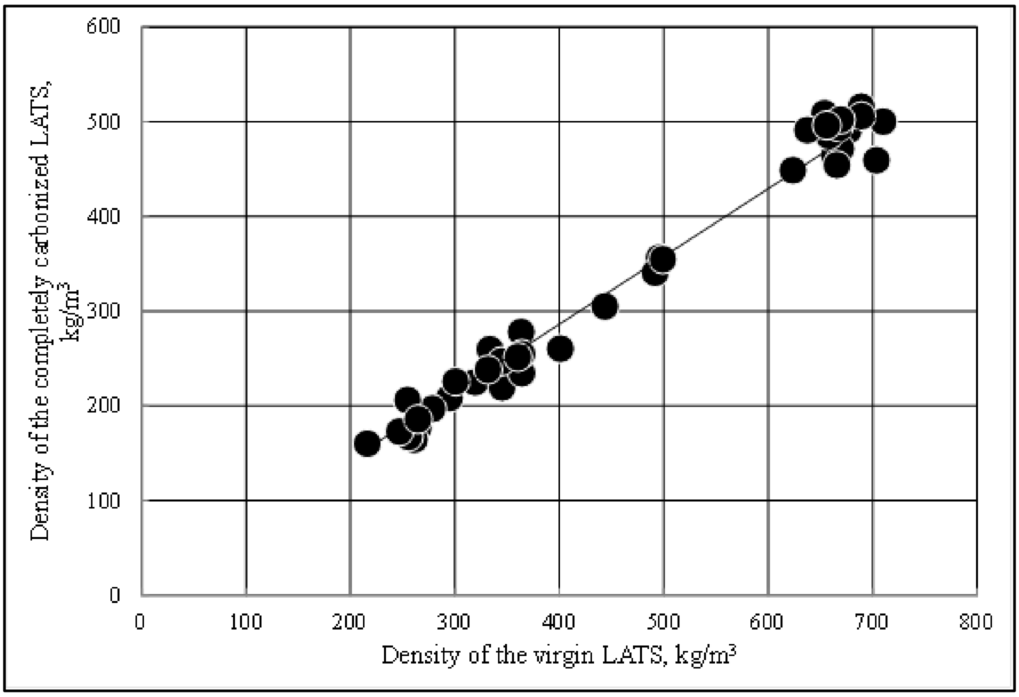

Fig.2-25 Relationship between density of virgin LATS and carbonized LATS [2-21]

Comparing to PICA, LATS materials have the following advantages:

- The density can be controlled more easily;
- They can adapt easier to any shape of the spacecraft, being composed by laminar and flexible layers of carbon felt (comparing to PICA, seen in Fig.2-26, which has significant deflection limits).

The disadvantage is that LATS materials don’t have the same thermal properties in all directions like PICA (the thermomechanical properties, like thermal conductivity, are different on normal direction than those on the tangential direction).

In the Fig.2-27 below, the manufacturing method of LATS materials is compared to that of PICA. PICA can be produced monolithically for a small vehicle or in large tiles (“modules”) in case of a larger vehicle. The carbon block is inserted in a container with resin and heat and pressure are applied to it. In comparison, LATS materials are built by many layers of carbon felt in which resin is impregnated and then the heat and pressure are applied from 2 normal directions.

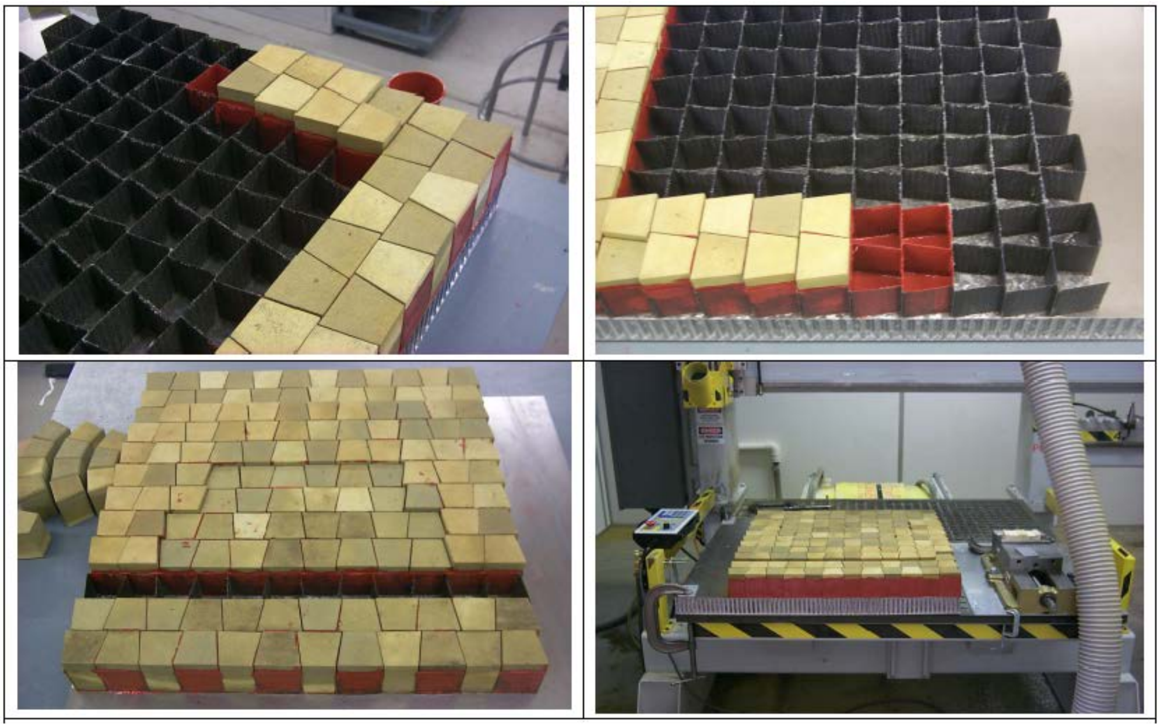

Fig.2-26 Production of the Flat Manufacturing Demonstration Panel Using PICA Blocks [2-29]

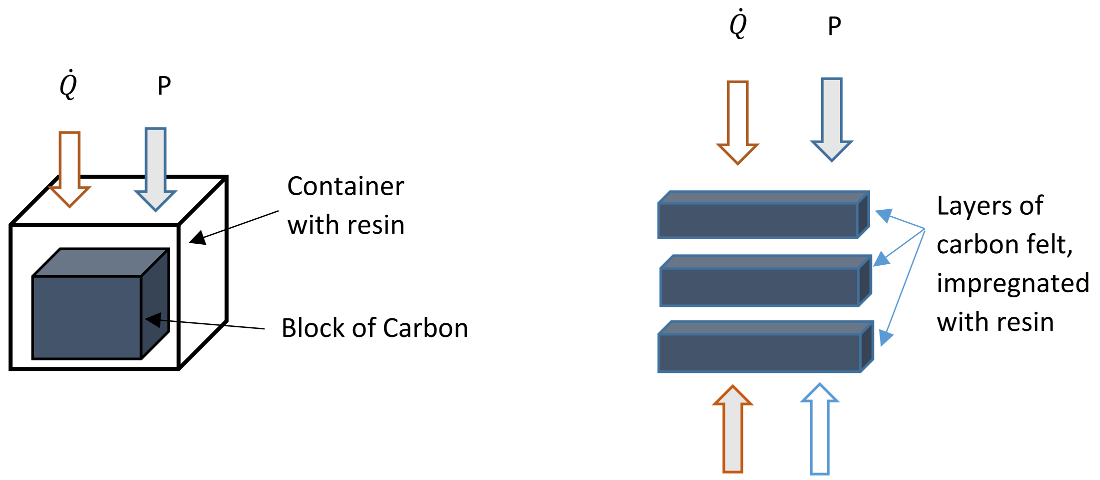

a) PICA b) LATS

Fig.2-27 Schematic comparison of the manufacturing method of PICA and LATS materials

Although LATS has low density comparing to conventional ablators, the thermal diffusivity is similar with the one of a conventional ablators. Thermal diffusivity is defined as follows:

$$\alpha = \frac{k}{\rho \cdot C_p} \tag{2-5}$$

Where k is thermal conductivity (W/m/K), ρ is the char density (kg/m^3) and C_p is the specific heat at constant pressure (*J/kg/K*). The thermal diffusivity plays a very important role in the heat transfer phenomenon. The heat transfer inside the ablator, for the unidimensional case, is based on the one-dimensional heat conduction equation:

$$\frac{\partial T}{\partial t} = \alpha \frac{\partial^2 y}{\partial x^2} \tag{2-6}$$

where T is the temperature, t is the time and the heat transfer is along the x axis and α is thermal diffusivity (m^2/s).

The thermal conductivity is significant smaller in case of LATS material comparative to the conventional ablators like heavy-CFRP ablator of USERS, but also their density and specific heat. A comparison between the value of thermal diffusivity for LATS and conventional ablator can be seen in Fig.2-28.

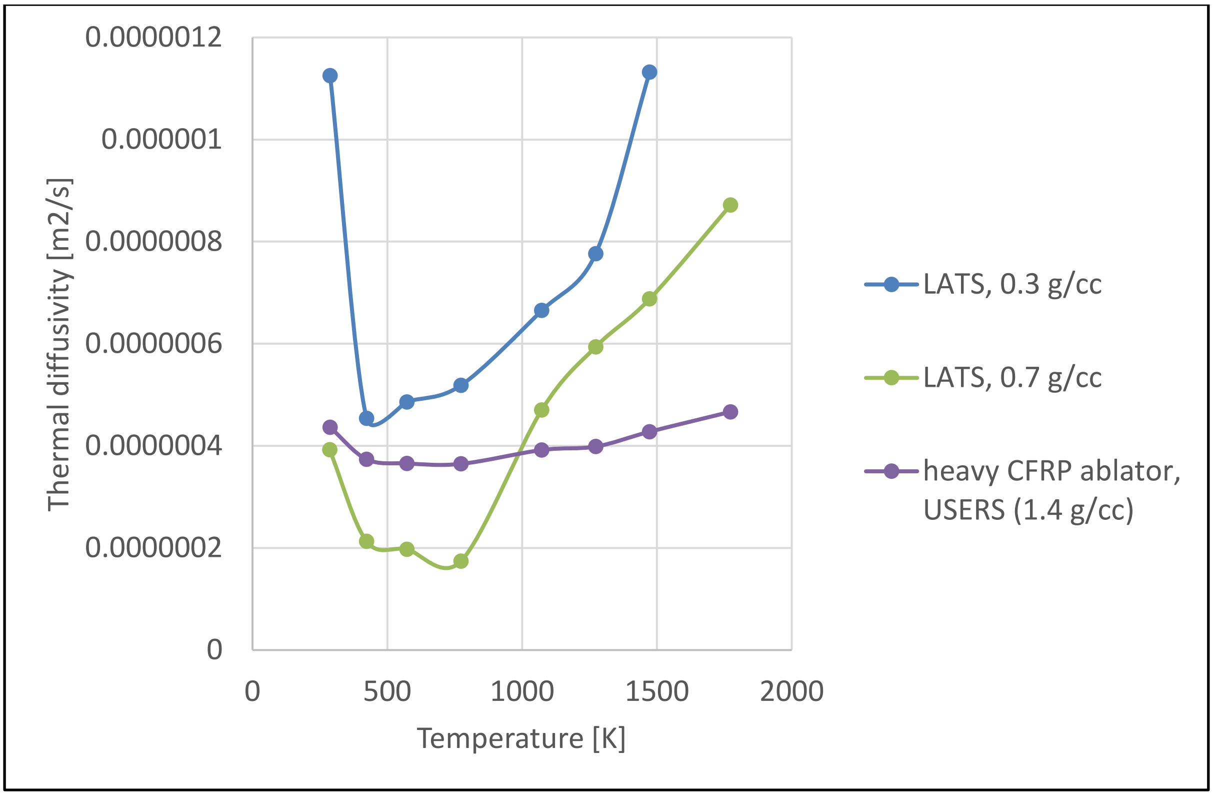

Fig.2-28 Thermal diffusivity for LATS and conventional ablators (USERS)

Regarding the surface recession rate, the dependency with the stagnation pressure in case of LATS, PICA and conventional CFRP ablator (USERS) can be seen in Fig.2-29.

Fig.2-30 shows the dependency of the mass recession rate with the surface temperature in case of LATS and USERS ablators. The values for USERS and PICA materials were taken from [2-21] and [2-22].

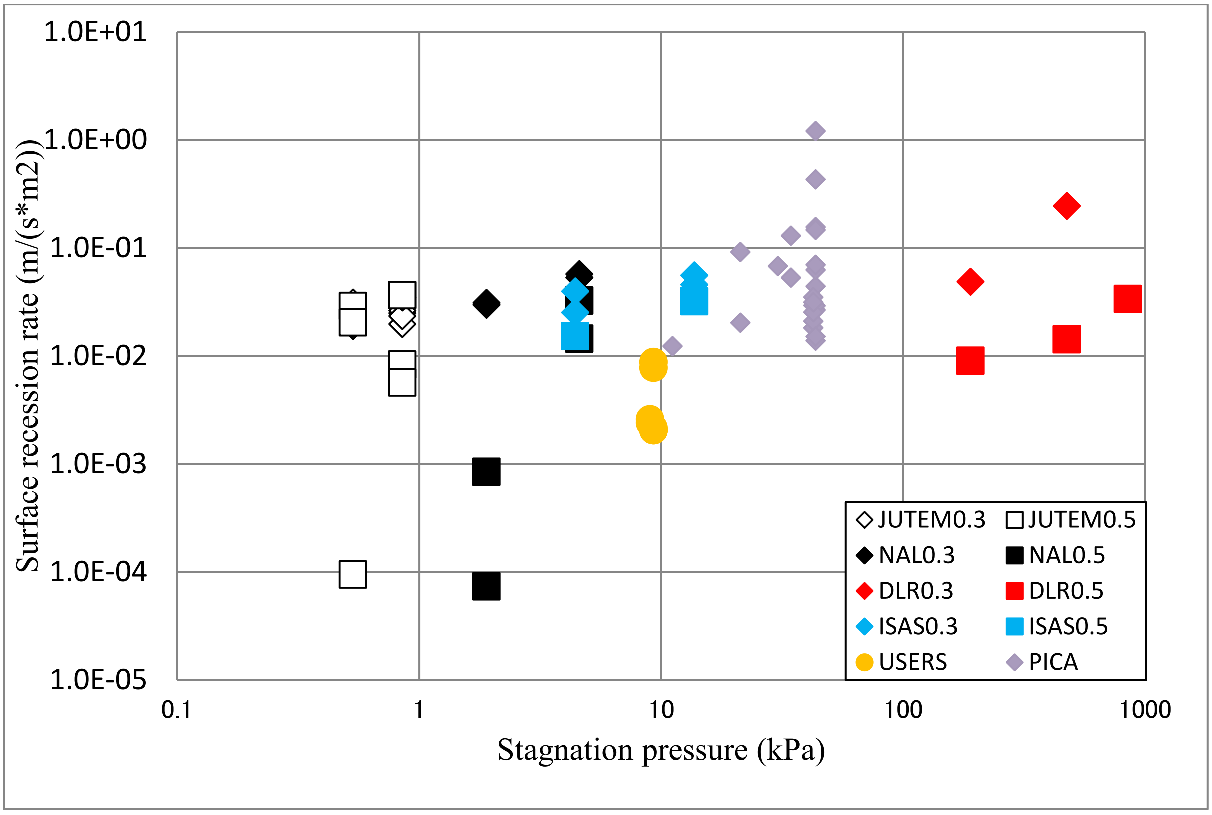

Fig.2-29 Dependency of surface recession rate with the stagnation pressure in case of LATS, PICA and conventional ablators (USERS)

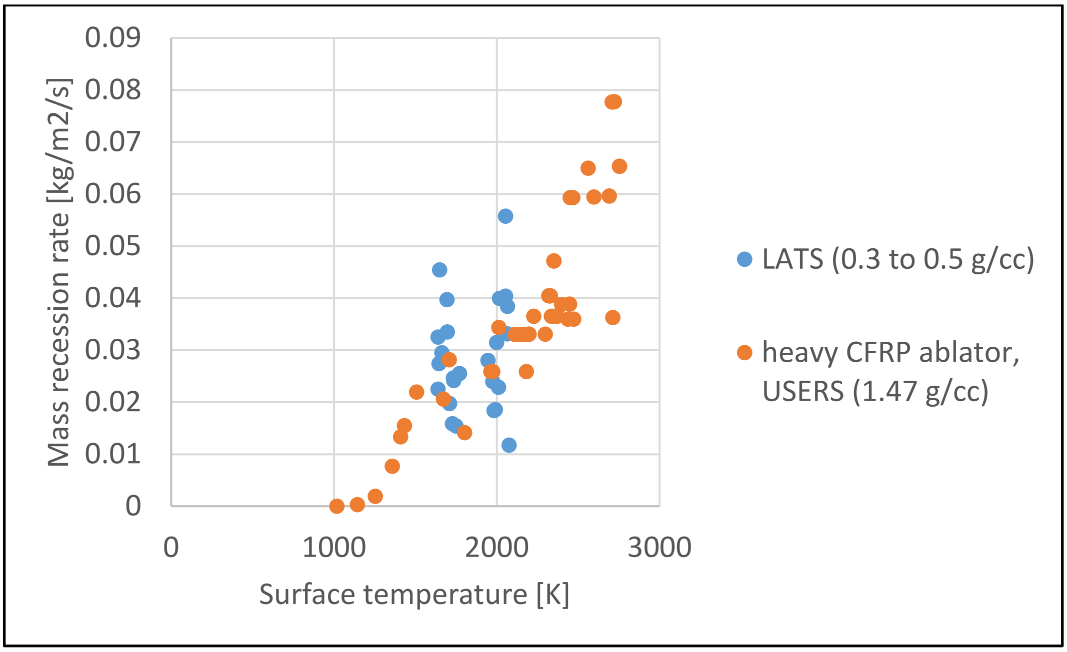

Fig.2-30 Dependency of the mass recession rate with the surface temperature in case of LATS and conventional ablators (USERS)

Even if the ablator is completely carbonized, the ablator thickness must have a value that can endure the aerodynamic load and the thermal load during re-entry. The mechanical properties, which affect the thermal stress generated between two components (like that between the two layers of two-layer type phenol CFRP), are the coefficient of thermal expansion, Young's modulus, and Poisson's ratio. Difference in the coefficient of thermal expansion, Young's modulus, and the temperature distribution determine the magnitude and the location of thermal stress [2-30].

According to [2-20], when the heat is applied to the ablator, the pyrolysis and the char layer are formed. The pyrolysis gas is generated in the pyrolysis layer and it is released towards the surface. The char layer suffers the effects of the pyrolysis gas pressure, the thermal stress, and the surface shear force by the high enthalpy flow. As a consequence, carbonaceous solid particles are released from the ablation surface into the flow (phenomenon called "Spallation"). Another phenomenon is the phenomenon of "coking" by which solid carbon is deposited when the pyrolysis gas passes through the porous char layer to the surface. Due to the coking phenomenon, increases the density of the char layer increases near the surface of the heated material [2-20].

The strength of this carbonized layer is generally low compared with virgin material. Therefore, one of the design techniques now in use is to leave a virgin material layer of high strength [2-30]. Although the heat shield system then becomes heavily, this technique can satisfy the strength requirement. However, if all the carbonized ablator is used as a structural member, the thickness of the heat shield system will decrease.

2.3.4 Previous empirical studies on lightweight ablators

Several studies were made in the past concerning the ablation phenomenon of charring ablators, including PICA or LATS materials. The concept of a thermal protection shield using a charring ablator is shown in Fig.2-31:

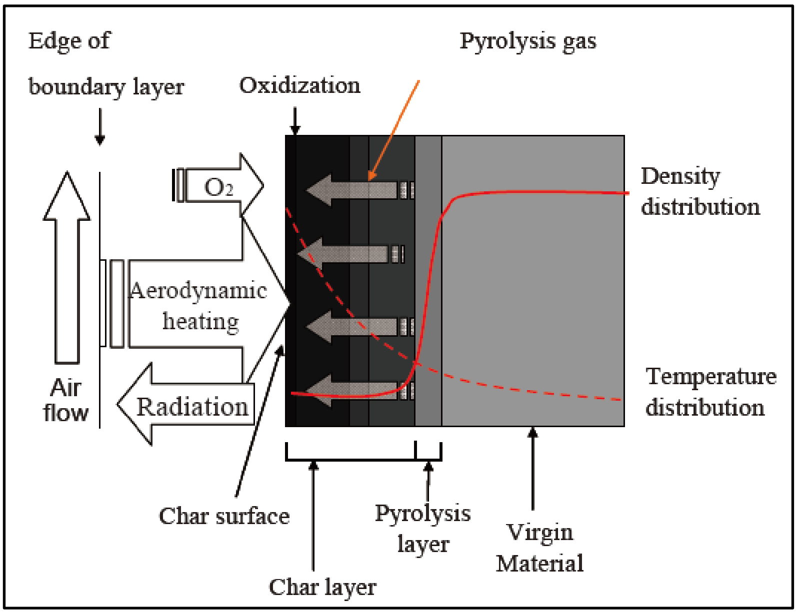

Fig.2-31 Concept of charring ablation [2-20]

The phenomena which occurs during ablation are summarized in [2-20] and are as follows:

- pyrolysis reaction in the resin of the ablator, after which the pyrolysis gas is generated and the resin is carbonized. As a result, the carbonized resin forms the porous char layer with neighboring refractory reinforcement fiber, and the pyrolysis gas are released out through the char surface;
- the loss in heat energy when the pyrolysis gas is released through the char layer; also, the heat which enters the ablator at the surface is blocked by the pyrolysis gas.
- The recession of the char layer recedes due to the process of thermochemistry (e.g., oxidation, sublimation, melting, evaporation) and a mechanical processes (e.g. spallation) and also the blocking of incoming heat by the formed gas
- The radiation energy emission at the char surface which has high temperature.

The Surface Energy Balance is given by the below Fig.2-32.

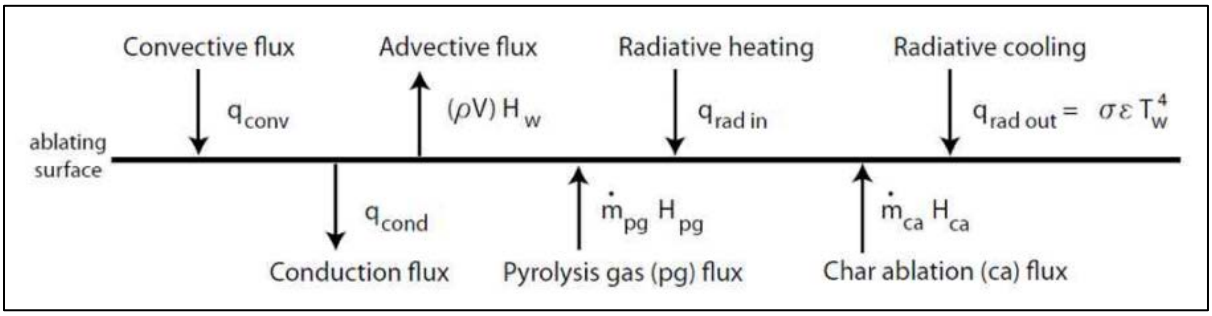

Fig.2-32 Surface Energy Balance [2-31]

One important observation to make is that phenolic-based ablators are porous materials and the recession may not recede uniformly due to the porosity. The materials may undergo volume ablation with two important consequences [2-32]:

- The material weakens in volume and is possibly subject to mechanical erosion (Spallation);
- The ablation enthalpy distributed in volume modifies the thermal response.

According to [2-30], in studying the performance of an ablator system, the recession characteristics play a crucial role. In this context, developing new methods to estimate recession rate would lead to a more efficient design of the future ablator systems for reentry spacecraft. The thermo-chemical ablation is the primary cause for recession, while the effect of mechanical erosion is secondary. Consequently, understanding the mechanism of thermo-chemical ablation is very important from the view point of structure design [2-33].

Surface recession rate was subject for previous empirical determination in the past, e.g. the study for Galileo spacecraft which entered the atmosphere of Jupiter, for which high-density ablator was used [2-34]. In those studies, the surface recession rate was assumed to be independent of density and a linear dependency with the heat flux was found [2-34].

For solving the chemical ablation problem for charring carbon based materials, several approaches were developed to calculate the temperature of body and the surface recession caused by chemical ablation. Most of the existing models are one-dimensional studies, in which the chemical reactions are seen as equilibrium processes [2-33].

For determining the mass recession rate, a multitude of factors have to be taken into consideration like the complex chemical ablation and particle erosion components, dependent upon near surface material density, surface temperature, altitude, velocity, environment [2-35].

There were several studies in the past for determining the mass recession rate. One of the scientists who made a significant contribution in the field was Metzger, who analyzed the mass loss characteristics of graphite in heated air. According to Metzger's study, there are three regions of temperature for considering the mass loss of graphite. As described also in [2-22], the first region is the rate-controlled oxidation region (below approximately 1,500 K), where the surface material mainly dissipates due to its oxidation by air. The second region is the diffusion-controlled oxidation region (between 1,500 K and 3,000 K). The third is the sublimation region for temperatures above 3,000 K, where the surface mass loss of graphite predominately occurs due to the sublimation of carbon: 3C(Solid)→C3(Gas). Regarding the first two regions, Park demonstrated that the surface mass loss of the graphite is give by the reaction C+O→CO [2-22].

For the first region, the following formula based on Arrhenius equation is widely used by scientists [2-36]:

$$\dot{m}_R = a_R \cdot \left(X_{O_2}P\right)^{0.5} \cdot exp[-E_R/(R \cdot T_W)] \tag{2-7}$$

where $a_R = 4.71 \times 10^5\ g/(cm^2 s)$, $X_{O_2} = 0.21$ – mole fraction (partial pressure) of oxygen in air, $E_R = 44 \times 10^3 cal/mole$, R is the universal gas constant, 1.987 *cal/mole/K*, P is the pressure and T_W is the wall temperature. [2-1]

There should be noted that (2-7) has a meaning only for the lowest ablating temperature range [2-34]. For the second region, above 1,500 K, (2-7) gives inaccurate results. [2-1]

According to [2-33], for the second region of diffusion-controlled oxidation, Metzger *et al.* deduced the total mass loss rate $\dot{m}_t$ in the diffusion-controlled oxidation region of the graphite:

$$\dot{m}_t = C_0\sqrt{P_{st}/R_B} \tag{2-8}$$

where C_0 is the diffusion-controlled mass-transfer constant, P_{st} is the stagnation pressure (Pa) and R_B is the curvature radius of the specimen. If the front surface of the ablator specimen is flat, R_B is 2.46 times the actual radius.

The equation of Metzger contains however flaws. As noted in [2-35], due to the fact that the graphite does not contain resin, the diffusion-controlled mass-transfer constant C_0 is constant. However, in case of LATS, which contains resin, its quantity depends on the density. The resin of a heated LATS decomposes; a part of the resin becomes gas and covers the surface of the material [2-35]. In conclusion, Metzger's theory cannot be applied to CFRP since CFRP contains a resin that undergoes thermal decomposition by heating [2-35].

For overcoming this difficulty in solving the mass recession rate for CFRP material, Okuyama *et al.* studied the mass recession of lightweight ablator system, made of CFRP, in a nitrogen gas atmosphere. The total mass recession rates $\dot{m}_t$ of the carbonized CFRP in a nitrogen atmosphere are given by the following equations, deduced by Okuyama *et al.*: $\dot{m}_t = 2.44 \times 10^{-5}(P_e/R_B)^{0.5}$, $1.72 \times 10^{-5}(P_e/R_B)^{0.5}$ and $0.713 \times 10^{-5}(P_e/R_B)^{0.5}$, respectively (different values for different test conditions). These results show that the total mass recession rate $\dot{m}_t$ becomes small as the amount of resin inside CFRP decreases [2-35]. Therefore, (2-8) is modified to (2-9).

$$\dot{m}_t = \theta\sqrt{P_{st}/R_B} \tag{2-9}$$

where θ is named as the diffusion-controlled mass-transfer modulus ($kg^{0.5}/m^2$), which can only be used in the diffusion-controlled regime and represents a new evaluation index of the heat shield performance of ablators [2-22].

In the present study, θ will be taken as being 2.44 ($kg^{0.5}/m^2$) since this value corresponds to a first series of tests for which no previous heating occurred. [2-1]

The measured and calculated results for mass loss rate, in case of LATS, PICA and high density CFRP ablators is given in the Fig.2-33.

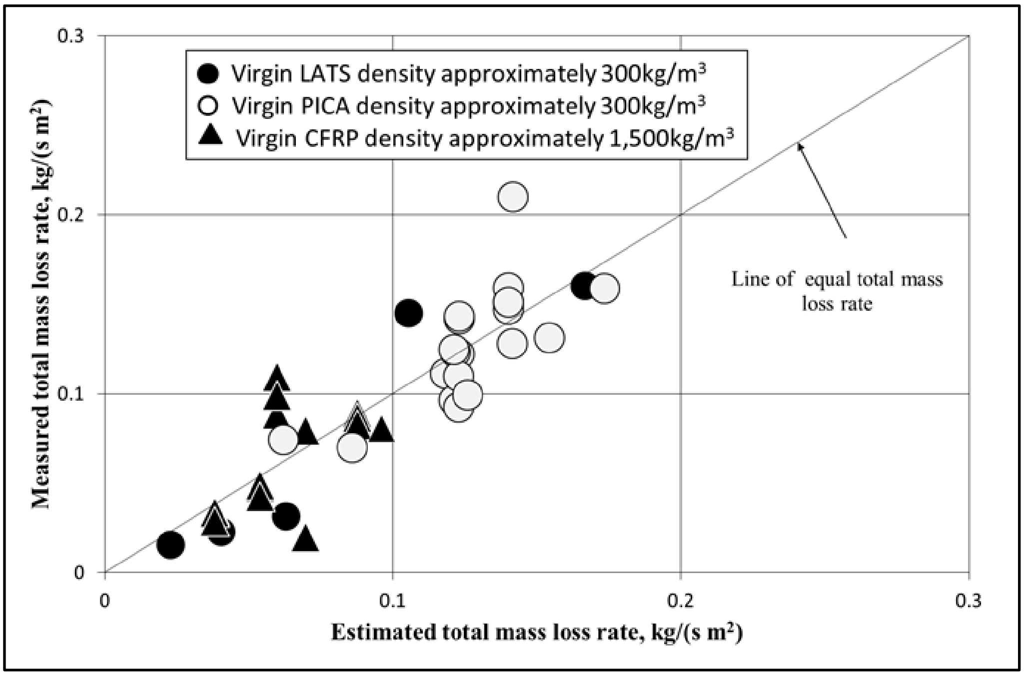

Fig.2-33 Relationship between measured and estimated total mass loss rate of charring CFRP [2-22]

According to [2-36], numerical prediction of ablation is ambitious and cpu-time demanding due to the complex multiphase physical and chemical processes that occur. Even in the present state-of-the-art numerical models, which couples a high-fidelity CFD flow solver with a material thermal response code [2-36], some major restrictions are still present [2-2]:

- Surface chemical equilibrium assumption;

- Non-ablating flow field prediction;
- Simplified diffusion modeling based on transfer coefficient.

The ablation recession rate is generally computed by the material response code using thermochemical tables and extremely simplified diffusion models based on transfer coefficients and semi-empirical relations relating mass and energy transfer [2-36].

For designing the thermal protection system, the thermal behaviour of the ablator when it is facing severe aerodynamic heating environments during the atmospheric re-entry should be predicted [2-20].

References

[2-1] Bianca Szasz, Keiichi Okuyama, *A New Method for Estimating the Mass Recession Rate for Ablator Systems*, International Science Index, Vol.8, No.:11, 2014, London, UK.

[2-2] Bianca Szasz, Kei-ichi Okuyama, Sumio Kato, Takayuki Shimoda, *Empirical Study of the Lightweight Ablator Series for Transfer Vehicle Systems (LATS)*, Transaction of JSASS, Aerospace Technology Japan, scheduled for publication;

[2-3] Garzon, M., *Development and Analysis of the Thermal Design for the Osiris 3U Cubesat*. Pennsylvania: The Pennsylvania State University, 2012.

[2-4] Lee-Her, H., Ming-Shong, C., & Jih-Run, T., *Thermal Control Design and Analysis for Picosatellite Yamsat*, Transaction of the Aeronautical and Astronautical Society of the Republic of China, Vol 35, 227-233, 2003.

[2-5] Karam, R., *Satellite thermal Control for Systems Engineers*. Virginia, American Institute of Aeronautics, 1998.

[2-6] David G. Gilmore, *Satellite Thermal Control Handbook*, The Aerospace Corporation Press, California, U.S.A, 1994.

[2-7] The Japan Carbon Fiber Manufacturers Association website, *Carbon Fiber*, URL: http://www.carbonfiber.gr.jp/english/index.html , 2016.

[2-8] Central Carbon Fiber website, *CFRTS & CFRTP*, URL: http://www.centralcarbonfiber.com/cfrts_cfrtp/index.html (July 2016).

[2-9] Taro Nakamura, Yi Wan, Haowen Wei, Isamu Ohsawa, Jun Takahashi, *"Investigation of sandwich panel made by CFRTS and CFRTP*," 13th Japan International Sampe Symposium and Exhibition, December 2015.

[2-10] Kazuto Tanaka, Ryuma Sukena, Syota Mizuno and Tsutao Katayama, "*Roll forming of CFRTP Prepreg and Evolution of its Mechanical Property"*, The Science and Engineering Review of Doshisha University, Vol.55, No.3, October 2014.

[2-11] S. Pimenta, S.T. Pinho, *"Recycling carbon fiber reinforced polymers for structural applications: Technology review and market outlook,"* Waste Management, vol.31, pp.378-392, 2011.

[2-12] S. Pimenta, S.T. Pinho, "*The effect of recycling on the mechanical response of carbon fibers and their composites,*" Composite Structures, vol.94, pp.3669-3684, 2012.

[2-13] Hiroaki Takei, Michelle Salvia, Alain Vautrin, Akira Tonegawa and Yoshitake Nishi, *"Effects of Electron Beam Irradiation on Elasticity of CFRTP (CF/PEEK),"* Materials Transactions, Vol.52, No.4 (2011), pp.734 to 739.

[2-14] Jun Takahashi and Takashi Ishikawa, *"Current Japanese Activity in CFRTP for Industrial Application*", Leuven and TexComp -11 Conference, 16-20 September 2013, Leuven.

[2-15] Jun Takahashi, Kiyoshi Uzawa and Tsuyoshi Matsuo, "*Development of CFRTP for Mass Produced Automobile,*" The University of Tokyo, CDW-15, Kanazawa, Japan, October 18-19, 2010.

[2-16] M. Makihara: *Plastics 53 (2002)* 119-122.

[2-17] M. Kuehnel, A. Schuster, A. Buchheim, T. Gergross and M. Kupke, *"Automated Near-Net-Shape Preforming of Carbon Fiber Reinforced Thermoplastics (CFRTP)",* ICS of the JEC Europe 2014, Paris, March 11-13.

[2-18] Daniele Bianchi, *Modeling of ablation phenomena in space applications*, Ph.D. Thesis, Universita degli Studi di Roma "La Sapienza", 2007.

[2-19] Okuyama, K., Kato., S., Kanno, Y., Uto, M., Sakata, R., Hama, K., *A Lightweight Heat Shield System using a Phenol CFRP Material*, Journal of Hot Structures and Thermal Protection Systems for Space Vehicles, Proceedings of the 4th European Workshop held 26-29 November, 2002, Italy, edited by A. Wilson, ESA SP-521, 2003, p.303.

[2-20] Sumio Kato, Kei-ichi Okuyama, Kenta Gibo, Takuma Miyagi, Toshiyuki Suzuki, Kazuhisa Fujita, Takeharu Sakai, Seiji Nishio, and Akihiro Watanabe, *Thermal Response Simulation of Ultra Light Weight Phenolic Carbon Ablator by the Use of the Ablation Analysis Code*, Transactions of the Japan Society for Aeronautical and Space Sciences, Japan, 2012.

[2-21] Tran, H.K., Johnson, C.E., Rasky, D.J., Hui, F.C.L., Hsu, M., Chen, T., Chen, Y.K., Paragas, D. and Kobayashi, L.: *Phenolic Impregnated Carbon Ablators (PICA) for Discovery Missions*, NASA Technical Memorandum 110440, 1997, pp. 1-69.

[2-22] Keiichi Okuyama, Sumio Kato and Hiroaki Ohya: *Thermochemical Performance of a Lightweight Charring Carbon Fiber Reinforced Plastic*, Trans. Japan Soc. Aero. Space Sci., Vol.56, No.3, pp. 159-169, 2013.

[2-23] Yoseph Bar-Cohen, *High Temperature Materials and Mechanisms*, CRC Press, Taylor & Francis Group, LLC, 2014, International Standard Book Number-13:978-1-4665-6645-3.

[2-24] M. Stackpoole *et al.*, *Post-Flight Evaluation of Stardust Sample Return Capsule Forebody Heatshield Material*, AIAA 2008-1202.

[2-25] Huy K. Tran, Christine E. Johnson, Daniel J. Rasky, Frank C.L. Hui, Ming-Ta Hsu, Timothy Chen, Y.K. Chen, Daniel Paragas, and Loreen Kobayashi, *Phenolic Impregnated Carbon Ablators (PICA) as Thermal Protection Systems for Discovery Missions*, NASA Technical Memorandum 110440, 1997.

[2-26] DSC Beginners Guide, URL: https://www.perkinelmer.com/CMSResources/Images/44-74542GDE_DSCBeginnersGuide.pdf.

[2-27] TA-DSC, URL: http://www.hic.ch.ntu.edu.tw/TA/TA-DSC-TR-PRIN.pdf

[2-28] Ethiraj Venkatapathy and James Reuther, NASA Crew Exploration Vehicle, *Thermal Protection System, Lessons Learned*, 6th International Planetary Probe Workshop, June 26th, 2008.

[2-29] William M. Congdon, *Development of Design and Production Processes for Block-Ablator Heatshields with Preliminary Test Results*, ARA Ablatives Laboratory, URL: https://solarsystem.nasa.gov/docs/p477.pdf (July 2016).

[2-30] Keiichi Okuyama, Sumio Kato and Tetsuya Yamada: *Thermo-chemical recession characteristics of CFRP in an earth atmospheric reentry environment*, TANSO, 2005, No.219, pp. 232-237.

[2-31] J. Lachaud, T.E. Magin, I. Cozmuta, and N.N. Mansour, *A Short Review of Ablative-Material Response Models and Simulation Tools*, NASA Archive, URL: http://ntrs.nasa.gov/archive/nasa/casi.ntrs.nasa.gov/20110014340.pdf .

[2-32] Jean Lachaud, Ioana Cozmuta, and Nagi N. Mansour, *Ablation of PICA-like Materials. Surface or Volume Phenomenon?*, Proceedings of the 6th International Planetary Probe Workshop, Atlanta, June 2008.

[2-33] Tiantian Yin, Zhongwei Zhang, Xiaofeng Li, Xiang Feng, Zhihai Feng, Yu Wang, Linghui He, Xinglong Gong, *Modelling ablative behaviour and thermal response of carbon/carbon composites*, Journal of Computational Materials Science 95 (2014) 35-40, Elsevier, 2014.

[2-34] Jesse W. Metzger, *Response of Galileo Aft Cover Components to Laser Radiation*, Paper No. 82-0853, 3rd AIAA/ASME Joint Thermophysics, Fluids, Plasma & Heat Transfer Conference, 1982.

[2-35] Robert L. Potts, *Analysis of an Integral Method for Computing Reentry Vehicle Heat Conduction in Systems Level Computer Codes*, Science Applications, Inc., El Segundo, California.

[2-36] Daniele Bianchi, Alessandro Turchi, F. Nasuti, M. Onofri, *CFD Ablation Predictions with Coupled GSI Modeling for Charring and non-Charring Materials*, 5th Ablation Workshop, Lexington, Kentucky, U.S.A., February 28 – March 1, 2012, available at http://uknowledge.uky.edu/ablation/2012/Coupling/3/ .

III. Ultra-light thermal control method for Shinen2 deep space probe

3.1 Outline of Shinen2 deep space mission

Shinen2 was developed by Kyushu Institute of Technology in collaboration with Kagoshima University (Japan) and Prairie View A&M University (U.S.A.). Shinen2 was launched from Tanegashima Space Center, on December 3rd, 2014, together with the asteroid probe "Hayabusa2", Procyon and Despatch [3-1].

The mission success of Shinen2 can be defined on different levels [3-1]:

1) Minimum Success

- Establishing a communication technology near Moon orbit;
- Demonstration in deep space of a structure made of CFRTP (Carbon Fiber Reinforced Thermo Plastics) composite materials;
- Measurement of the spatial distribution of cosmic radiation through the Van Allen belts.

2) Full Success

- Establishing a communication technology above 1 million km distance from Earth;
- Measurement of the spatial distribution of the cosmic radiation above 1 million km distance from Earth.

3) Extra Success

- Establishing a communication technology above 3 million km distance from Earth;
- Measurement of the spatial distribution of the cosmic radiation above 3 million km distance from Earth.

Regarding the communication via ham radio in deep space, the long-distance communication between Shinen2 and the ground stations was achieved by WSJT (Weak Signal Communication, K1JT). The International Telecommunications Union defines "deep space" to start at a distance of 2 million *km* from the Earth's surface [3-4] and Shinen2 could achieved a communication distance of 2,250,000 *km*. [3-1]

Shinen2 (Fig.3-1) was launched together with Hayabusa2 (Fig.3-2), Despatch and Procyon deep space probes. Hayabusa2 mission aims at a round trip mission to the asteroid 1993JU3 which is a C-type asteroid, which might contain organic matters and hydrated minerals. After a successful sample collection, the scientists will be able to gather more knowledge about the origin and evolution of the planets, especially in the matters like the origin of water and organic matters [3-5].

Fig.3-1 Shinen2, Flight Model

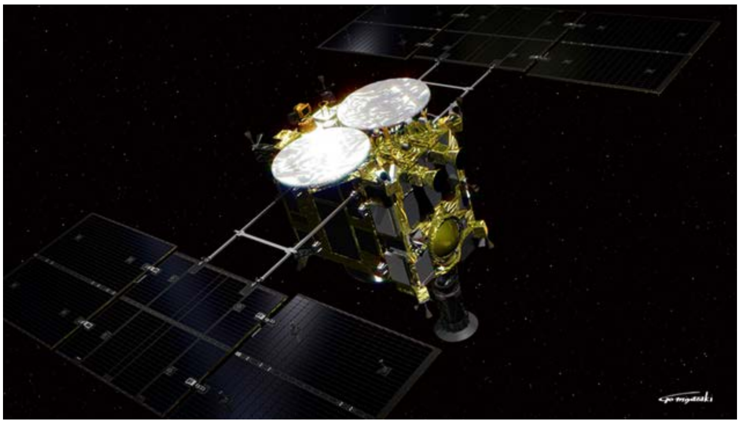

Fig.3-2 Asteroid probe Hayabusa 2 [3-5]

For achieving the main mission objectives for Shinen2, thermal design plays a very important role due to the fact that it must assure the survival of electric components including the communication system through which the ground stations will be kept in contact with the space probe. For thermal analysis of Shinen2 in deep space for the hot and cold worst conditions, SINDA equations-solver has been used. According to [3-2], to verify the validity of the thermal analysis, the results are compared with the results from the thermal balance tests, in this way a thermal design method for ultra-small spacecraft which flies in deep space being realized.

3.2 Passive thermal control using CFRP materials

For obtaining an optimum performance and assuring the success of the mission, the thermal control plays a very important role. If the temperature of a component is too low or too high, the respective component can be damaged or its performance can be severely affected.

When a passive thermal system is used, the complexity of a satellite is reduced, and there are more resources available on small satellites to be used for payload function [3-3]. According to [3-6], the most applied means for realization of passive thermal control satellite design are the multilayer insulation, painted surfaces, optical coatings, heat conductive elements, heat insulation supports and thermal conductive gaskets.

In case of Shinen2, the passive thermal control system will consist of painted surfaces, in this way, the simplicity of thermal system being assured and the costs being kept at minimum. The passive thermal control system of Shinen2 consists mainly in using a combination of white and black paint. To assure more storage of heat inside, the inside components are painted black. For the outer surfaces, the white paint is used in order to prevent too much heat from the Sun to enter inside the space probe. [3-2]

The heat transfer inside is accomplished by conduction and radiation. To allow more heat transfer between internal components and outer panels, the structure of the main frame was changed after STM model. Instead of having a big case for main frame, for EM and FM models there are four strong pillars which host inside the two batteries and Radiation Detector Sensor (Fig.3-3). Before this change, there was a big difference in temperatures between 0.9 and 1.1 AU (of around 40 degrees Celsius), but for the EM and FM models, the difference are of only 20 degrees Celsius between the worst hot case and worst cold case scenarios. [3-1]

In case of Shinen2, the most delicate devices are batteries and the payload (Radiation sensor), which can be seen in Fig.3-4. Average heat generation inside Shinen2 is between 10 and 15 *W*. [3-3]

Also, another important aspect is that the solar cells are body-mounted, they are placed on CFRTP panels, being attached on all lateral sides of the satellite and on the top panel. [3-3]

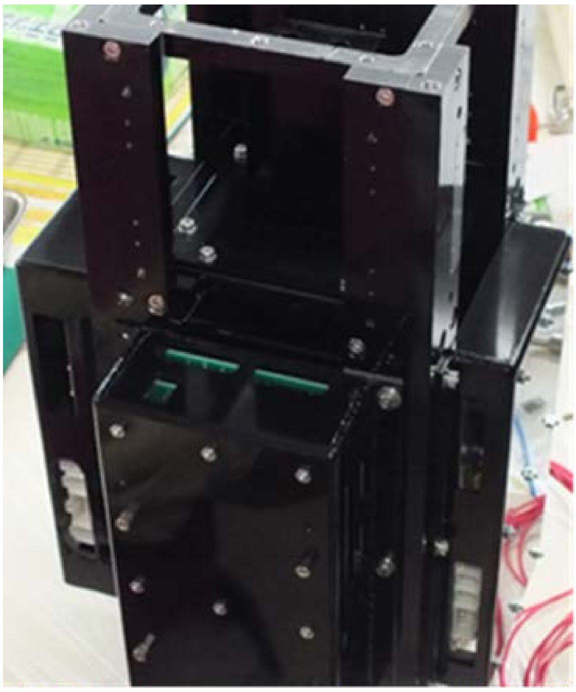

Fig.3-3 The internal structure of Shinen2 (EM Model) [3-3]

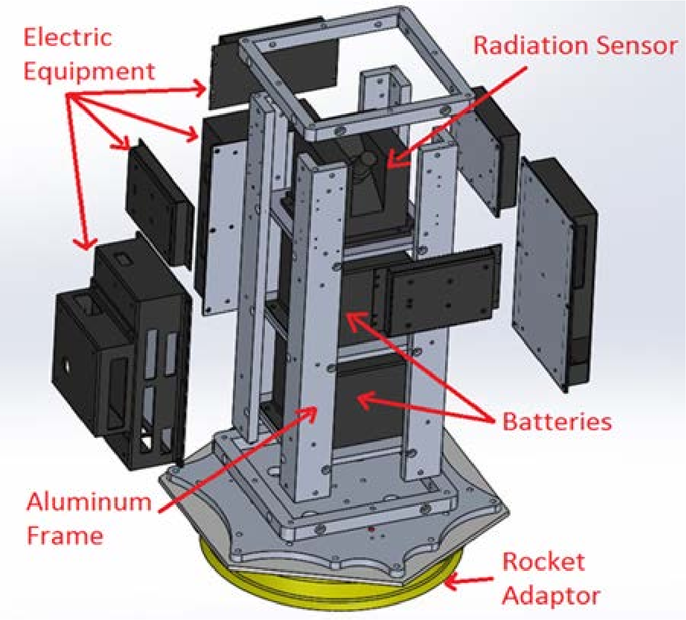

Fig.3-4 Overview of the internal structure of Shinen2 [3-3]

3.3 Thermal environment in space. Orbit analysis

Right after the separation and after escaping from the Earth's sphere of influence, Shinen2 followed an elliptical orbit around the Sun [3-2]. The distance between Shinen2 and the Sun varies, the perihelion being at 0.9 AU and the aphelion at 1.1 AU, the trajectory being calculated considering two stages: hyperbolic escape trajectory and the elliptical orbit around the Sun. The thermal environments for 0.9 AU and 1.1 AU are quite different, the Solar Constant being 1699 W/m^2, respectively 1137 W/m^2. Because Shinen2 has an elliptical orbit around the Sun, the most important environmental factor is the Sun's influence [3-3].

Shinen2 doesn't possess a propulsion system, its trajectory is determined solely by the impulse given by the rocket at the separation phase. To calculate its exact orbit in space is crucially important since the thermal design and communication mission depends on it. Since Shinen2 mission is designed in the academia environment, it is important to maintain the involved resources at minimum and, therefore, developing easy methods to calculate the trajectory of the space probe is desirable. For this purpose, a simple orbit calculation method has been developed and its results were compared with the results given by an open source software, GMAT (General Mission Analysis Tool), of NASA (National Aeronautics and Space Administration, U.S.A.). The compatibility between the results of orbit calculation proves that the simple orbit calculation method can be used for the deep space missions, led by universities, where the cost of the resources must be kept at minimum. [3-1]

Trajectory design is a crucial process in the early mission design. The trajectory is composed by 2 important stages: the hyperbolic escape trajectory around the Earth (until 925 000 km from the center of Earth, this location corresponding to the edge of Earth's sphere of influence) and the elliptical orbit around the Sun. For computing the trajectory for these 2 stages, the two-body problem assumption is used, where all the perturbations like the third-body attractions, the non spherical Earth shape, the solar-radiation pressure are ignored. To confirm the preciseness of this simple method, a comparison with the results given by the open source GMAT software (General Mission Analysis Tool) is made. [3-1]

Based on the analysis data, Shinen2 was expected to come back near Earth one year after the launch and the closest distance to be about 5.7 million km, at 4th December 2015 when a communication attempt with the space probe was made by Green Bank Telescope (U.S.A.) [3-1].

For establishing the communication in deep space based on ham radio, it is crucially important to know the exact position of Shinen2 at any given time. To describe the motion of Shinen2 in space, the trajectory must be defined in an inertial coordinate system, having the Earth at the origin of coordinates, for the first part of the trajectory, then the Sun, for the second part. In the trajectory analysis, the Geocentric Equatorial Inertial and Heliocentric Aries Ecliptic coordinate systems were used [3-1].

In the calculations, the J2000 standard equinox and epoch system is used (January 1, 2000 at 12:00 UT). The prefix "J" indicates that it is a Julian epoch. The equinox addresses changes in the coordinate system (due to the change in the position of the Earth's axis relative to the ecliptic, change caused by forces exerted by the Sun, Moon and planets), while the epoch addresses changes in the position of the celestial body itself [3-7].

The input data for Shinen2's orbit calculation were given by JAXA, prior to launch day. The input data are described in Table 3-1. [3-1]

Table 3-1 Input parameters for orbit calculation of Shinen2 [3-1]

Time of separation (after launch)	6835	*seconds*
Distance from the center of Earth	9244.915	*km*
Latitude	0.034	*degrees North*
Longitude	189.94	*degrees East*
Inertial Velocity	10357.221	*m/s*
Inertial velocity Elevation angle	34.644	*degrees*
Inertial velocity Azimuth angle	119.877	*degrees*
Japan time of launching	13:22:48	3-Dec-14

Based on these parameters, the trajectory of Shinen2 in the Solar System was deduced. The trajectory consists of 2 phases: the escape hyperbola around the Earth (inside the Earth's sphere of influence) and the elliptical orbit around the Sun (beyond the Earth's sphere of influence) [3-1].

The origin of the latitude-longitude coordinate system is the geocenter. The fundamental plane is the equator, and the principal axis in the fundamental plane points towards the Greenwhich meridian. The geocentric latitude is the acute angle measured perpendicular to the equatorial plane between the equator and a ray connecting the geocenter with a point on the Earth's surface; $-90\ deg \leq \phi \leq 90\ deg$. The east longitude is the angle measured eastward from the prime meridian in the equatorial plane to the meridian containing the surface point; $0\ deg \leq \lambda_E \leq 360\ deg$ [3-8].

Since the distance from Earth, the latitude and longitude angles, the inertial velocity and its angles are known, the position and velocity in the Geographic Coordinate System can be deduced. The X-axis of the Geographic Coordinate System is given by the intersection of Greenwich meridian and geographic equator and the Z-axis is towards the Geographic North Pole. The Y-axis completes a right-handed Cartesian triad [3-1].

The formula for calculating the position in the GEO system are given below [3-9]:

$$x_{GEO} = R * cos\phi * cos\lambda$$

$$y_{GEO} = R * cos\phi * sin\lambda$$

$$z_{GEO} = R * sin\phi \tag{3-1}$$

where R is the radial distance from the center of Earth, ϕ is the latitude angle and λ is the longitude angle. For velocity, similar formula are applied:

$$Vx_{GEO} = V * \cos(Ve) * \cos(Va)$$

$$Vy_{GEO} = V * \cos(Ve) * \sin(Va)$$

$$Vz_{GEO} = V * \sin(Ve) \tag{3-2}$$

where V is the inertial velocity, Ve is the inertial velocity elevation angle and Va is the inertial velocity azimuth angle.

Several coordinate systems are used in the study of the motions of the Earth and other celestial bodies. Since it is desirable to calculate the trajectory of Shinen2 independently of Earth's rotation around its own axis, a transformation from the Geographic Reference System (GEO) to the Geocentric Equatorial Inertial System (GEI) is required. GEI System has the X-axis pointing towards the First Point of Aries and the Z-axis towards the Geographic North Pole. The GEI coordinate system is not fixed to the Earth and turning with it; rather, the geocentric-equatorial frame is nonrotating with respect to the stars (except for precession of the equinoxes), and the Earth turns relative to it [3-8].

For performing the transformation mentioned above, the time in Julian centuries, corresponding to the separation time, must be calculated first. The rotational orientation of the Earth is conventionally determined by specification of the Greenwhich hour angle of the vernal equinox, which is measured positively westward along the celestial equator from the Greenwhich meridian to the vernal equinox. Greenwhich hour angle is measured either in degrees or in hours, the conversion factor being exactly 15 *deg/h* [3-8]. The Julian day number is a uniform time scale often used in astronomy and related applications. It is defined to be the total number of days elapsed since 12 *h* UT (universal time) on Monday, January 1, 4713 B.C.

(on the Old Style, or Julian, calendar). The Julian Day Number for the 3rd December 2014, the day of launch, is 2456994.5, for 0h UT [3-10]. The separation time was at 15h15’, Japan time, which means 6h15’ UT. The Julian Day number, for that time, will be: 2456994.5+6.25/24=2456994.76.

The Greenwich Mean Sidereal time can be calculated as follows [3-1]:

$$GMST = 367 * year - INT(7 * (year + INT((month + 9)/12))/4) + INT(275 * month/9) + day - 730531.5 + (h + min/60 + sec/3600)/24 \tag{3-3}$$

Knowing the GMST, the position and the velocity of Shinen2 in GEI coordinate system can be found out [3-9]:

$$x_{GEI} = x_{GEO} * \cos(GMST) - y_{GEO} * \sin(GMST)$$

$$y_{GEI} = x_{GEO} * \sin(GMST) + y_{GEO} * \cos(GMST)$$

$$z_{GEI} = z_{GEO} \tag{3-4}$$

$$vx_{GEI} = vx_{GEO} * \cos(GMST) - vy_{GEO} * \sin(GMST)$$

$$vy_{GEI} = vx_{GEO} * \sin(GMST) + vy_{GEO} * \cos(GMST)$$

$$vz_{GEI} = vz_{GEO} \tag{3-5}$$

The equations of motion for a satellite moving under the attraction of a point mass planet without any other perturbations can be given in the planet-centered coordinates as [3-8]:

$$d^2\vec{r}/dt^2 = -\mu\vec{r}/r^3 \tag{3-6}$$

where:

$\vec{r}$ – position vector of the satellite;

μ – gravitational constant;

t – time.

Equation (3-6) is a set of three simultaneous second-order nonlinear differential equations. There are six constants of integration. The solution of Eq. (3-6) can be either in terms of initial position and velocity: $x_0, y_0, z_0, \dot{x}_0, \dot{y}_0, \dot{z}_0$; or in terms of the six orbit elements: *a*, *e*, *i*, *Ω*, *ω*, *M* [3-8].

The motion of a body around an attractor body can be described by a three-scalar second-order differential equation. The integration of these equations of motion gives the six constants of integration which are called the orbital elements [3-8].

The closed-form conic solutions of the two-body equations of motion may be expressed in a general functional form as [3-8]:

$$\vec{r}(t) = \vec{r}(x_0, y_0, z_0, \dot{x}_0, \dot{y}_0, \dot{z}_0, t) \tag{3-7a}$$

Or

$$\vec{r}(t) = \vec{r}(a, e, i, \Omega, \omega, M) \tag{3-7b}$$

Five of the six orbit elements ($a - \omega$) in the preceding expression are constants, and M is the mean anomaly defined by [3-8]:

$$M = M_0 + n(t - t_0) \tag{3-8}$$

where

$M_0 =$ mean anomaly at epoch, t_0

$n =$ mean angular motion $= \sqrt{\mu/a^3}$

The orbital elements are: the semimajor axis (the size of the orbit), eccentricity (the shape of the orbit), time or perigee passage (often replaces by the mean anomaly at some arbitrary time), inclination of the orbit plane with respect to the reference plane), right ascension of the ascending node (measured counterclockwise in the equator plane, from the direction of the vernal equinox to the point at which the satellite makes its south-to-north crossing of the equator), argument of perigee (measured in the orbit plane in the direction of motion, from the ascending node to perigee). The orbital elements are summarized in Table 3-2. Another way to represent an orbit is by using Cartesian orbital elements which are also referred to as orthogonal orbital elements. [3-1]

Table 3-2 Display of Kepler orbital elements [3-1]

Orbital element	**Symbol [Units]**
Major semi-axis	a [*km* or *AU*]
Eccentricity	e [dimensionless]
Angle of inclination	i [*degree* or *rad*]
Right ascension of ascending node	Ω [*degree* or *rad*]
Argument of perigee	ω [*degree* or *rad*]
Mean anomaly	M [*degree* or *rad*]

After the separation, Shinen2 went into an escape hyperbolic orbit around the Earth, until it reached the edge of the Earth's sphere of influence, located at about 925,000 km. For the hyperbolic orbit, the influence of Sun's gravitational force is neglected and only Earth is considered as the attracting body.

For the calculations of the hyperbolic orbit, the following constants are considered (Table 3-3):

Table 3-3 Physical constants used for the calculation of the hyperbolic orbit [3-1]

Parameter	**Notation and measurement unit**	**Value**
Earth's gravitational parameter	µ $[km^3/s^2]$	398600.4418
Radius of the Earth's sphere of influence	R-for v∞ $[km]$	925000
Earth - planetary speed	Vp [*km/s*]	29.8

The formula that have been used for the calculation of orbital parameters are described in [3-8].

Angular momentum is given by:

$$\begin{aligned} hx &= y_{GEI} * vz_{GEI} - z_{GEI} * vy_{GEI} \\ hy &= z_{GEI} * vx_{GEI} - x_{GEI} * vz_{GEI} \\ hz &= x_{GEI} * vy_{GEI} - y_{GEI} * vx_{GEI} \end{aligned} \tag{3-9}$$

$$h = \sqrt{(hx^2 + hy^2 + hz^2)} \tag{3-10}$$

Inner product of the position vector and the velocity vector are given by:

$$\vec{r} \cdot \vec{v} = x_{GEI} * vx_{GEI} + y_{GEI} * vy_{GEI} + z_{GEI} * vz_{GEI} \tag{3-11}$$

Vector pointing towards ascending node:

$$\begin{aligned} nx &= -hy \\ ny &= hx \\ nz &= 0 \end{aligned} \tag{3-12}$$

$$n = \sqrt{(nx^2 + ny^2 + nz^2)} \tag{3-13}$$

Eccentricity:

$$ex = (x_{GEI} * (V^2 - \mu/R) - (\vec{r} \cdot \vec{v}) * vx_{GEI})/\mu$$

$$ey = (y_{GEI} * (V^2 - \mu/R) - (\vec{r} \cdot \vec{v}) * vy_{GEI})/\mu$$

$$ez = (z_{GEI} * (V^2 - \mu/R) - (\vec{r} \cdot \vec{v}) * vz_{GEI})/\mu \tag{3-14}$$

$$e = \sqrt{(ex^2 + ey^2 + ez^2)} \tag{3-15}$$

The scalar product of the vector pointing towards the ascending node and eccentricity vector is defined as:

$$\vec{n} \cdot \vec{e} = nx * ex + ny * ey + nz * ez \tag{3-16}$$

The semi-major axis:

$$a = (\mu * R)/(2 * \mu - R * V^2) \tag{3-17}$$

The semi-latus rectum:

$$p = a * (1 - e^2) \tag{3-18}$$

Orbital inclination:

$$i = \mathrm{acos}(hz/h) \tag{3-19}$$

Argument of perigee:

$$\omega = \mathrm{acos}(((n^{\rightarrow} \cdot e^{\rightarrow}))/(n * e)); \text{ if ez<0, then } \omega = 360 - \mathrm{acos}(((n^{\rightarrow} \cdot e^{\rightarrow}))/(n * e)) \tag{3-20}$$

Right ascension of ascending node:

$$\Omega = \mathrm{acos}(\mathrm{nx}/\mathrm{n}); \text{ if ny<0, then } \Omega = 360 - \mathrm{acos}(\mathrm{nx}/\mathrm{n}) \tag{3-21}$$

True anomaly:

$$\theta 1 = \mathrm{acos}((p - r)/(r * e)) \tag{3-22}$$

$$\text{if } r \cdot v < 0, \text{ then } \theta 1 = 360 - \mathrm{acos}((p - r)/(r * e)) \tag{3-23}$$

For the position of Shinen2 at a distance of 925000 *km*, the true anomaly can be calculated with the following formula:

$$\text{if } r \cdot v < 0, \text{ then } \theta 1 = 360 - \operatorname{acos}((p - r)/(r * e)) \tag{3-24a}$$

$$\text{Otherwise: } \theta 1 = \operatorname{acos}((p - r)/(r * e)) \tag{3-24b}$$

Knowing the orbital parameters and true anomaly for the location at 925000 *km* away from Earth, the position and the velocity at that location (represented by the index 1) can be calculated [3-11]:

$$x1 = R_{925000} * (\cos(\Omega) * \cos(\omega + \theta 1) - \sin(\Omega) * \sin(\omega + \theta 1) * \cos(i))$$

$$y1 = R_{925000} * (\sin(\Omega) * \cos(\omega + \theta 1) + \cos(\Omega) * \sin(\omega + \theta 1) * \cos(i))$$

$$z1 = R_{925000} * \sin(i) * \sin(\omega + \theta 1) \tag{3-25}$$

$$vx1 = (\mu/h) * e * \sin(\theta 1) * (\cos(\Omega) * \cos(\omega + \theta 1) - \sin(\Omega) * \sin(\omega + \theta 1) * \cos(i)) + \left(\frac{\mu}{h}\right) * (1 + e * \cos(\theta 1)) * (-\cos(\Omega) * \sin(\omega + \theta 1) - \sin(\Omega) * \cos(\omega + \theta 1) * \cos(i))$$

$$vy1 = (\mu/h) * e * \sin(\theta 1) * (\sin(\Omega) * \cos(\omega + \theta 1) + \cos(\Omega) * \sin(\omega + \theta 1) * \cos(i)) + \left(\frac{\mu}{h}\right) * (1 + e * \cos(\theta 1)) * (-\sin(\Omega) * \cos(\omega + \theta 1) + \cos(\Omega) * \cos(\omega + \theta 1) * \cos(i))$$

$$vz1 = (\mu/h) * e * \sin(\theta 1) * (\sin(\omega + \theta 1) * \sin(i)) + \left(\frac{\mu}{h}\right) * (1 + e * \cos(\theta 1)) * (\cos(\omega + \theta 1) * \sin(i)) \tag{3-26}$$

Knowing the position and velocity at the boundary of the Earth's sphere of influence, the elliptical orbit around the Sun can be deduced. First, a transformation between GEI (Geocentric equatorial inertial) reference system to GSE (Geocentric solar ecliptic) reference system is required [3-1].

The time of reaching 925,000 km from Earth is December 5, 10:27:36 UTC. From this information, the time in Julian centuries can be deduced. The Julian Day Number for the 5th December 2014 is 2456996.5, for 0 h UTC [3-11]. The Julian Day (JD) for the time of reaching 925000 km, will be JD=2456996.5+10/24+27/1440+36/86400=2456996.936.

MJD, which stands for "Modified Julian Date", is introduced to reduce the number of significant digits that must be carried in the computation without loss of precision or the need to invoke double precision operations. MJD is related to Julian date (JD) by the following [3-9]:

$$MJD = JD - 2400000.5 \tag{3-27}$$

A Julian day is reckoned from noon to noon of the following day. A modified Julian day is from midnight to midnight of the following day [3-9]. Then, the Julian centuries to J2000.0 can be calculated [3-9]:

$$t = (MJD - 51544.5)/36525 \tag{3-28}$$

To make a coordinate transformation between the Geocentric Equatorial Inertial reference system to the Geocentric Solar Ecliptic (a reference system having X-axis being the Earth-Sun line and Z-axis towards Ecliptic North Pole), two rotations are needed [3-9]:

1) rotation from the equator of Earth to the plane of the ecliptic;

2) rotation from the First Point of Aries to the Earth-Sun direction (in the ecliptic plane).

The transformation matrix is defined as following:

$$T_2 =< \lambda_{O,}Z >*< \varepsilon, X > \tag{3-29}$$

where ε, the obliquity of the ecliptic, and λ_O, the Sun's ecliptic longitude, are deduced based on the following equations [3-9]:

$$\varepsilon = 23.439 - 0.013 * t \tag{3-30}$$

$$M = 357.528 + 35999.05 * t + 0.04107 * UT \tag{3-31}$$

$$\Lambda = 280.46 + 36000.772 * t + 0.04107 * UT \tag{3-32}$$

$$\lambda_O = \Lambda + (1.915 - 0.0048 * t) * \sin(M) + 0.02 * \sin(2 * M) \tag{3-33}$$

Using these values, the position and velocity values in the GSE reference system are determined using the following equations [3-1]:

$$x_{GSE} = x_{GEI} * \cos(\lambda_o) + y_{GEI} * \sin(\lambda_o) * \cos(\varepsilon) + z_{GEI} * \sin(\lambda_o) * \sin(\varepsilon)$$
$$y_{GSE} = -x_{GEI} * \sin(\lambda_o) + y_{GEI} * \cos(\lambda_o) * \cos(\varepsilon) + z_{GEI} * \cos(\lambda_o) * \sin(\varepsilon)$$
$$z_{GSE} = -y_{GEI} * \sin(\varepsilon) + z_{GEI} * \cos(\varepsilon) \quad (3\text{-}34)$$

$$vx_{GSE} = vx_{GEI} * \cos(\lambda_o) + vy_{GEI} * \sin(\lambda_o) * \cos(\varepsilon) + vz_{GEI} * \sin(\lambda_o) * \sin(\varepsilon)$$
$$vy_{GSE} = -vx_{GEI} * \sin(\lambda_o) + vy_{GEI} * \cos(\lambda_o) * \cos(\varepsilon) + vz_{GEI} * \cos(\lambda_o) * \sin(\varepsilon)$$
$$vz_{GSE} = -vy_{GEI} * \sin(\varepsilon) + vz_{GEI} * \cos(\varepsilon) \quad (3\text{-}35)$$

Knowing the location of Shinen2 in the Geocentric Solar Ecliptic (GSE), a transformation to a heliocentric reference system (HEE - Heliocentric Earth Ecliptic), having the Sun in the center in the origin, is possible [3-1].

Firstly, the exact value of the distance between Earth and Sun, at a specific point in time, must be known [3-9]:

$$\rho = 149598500\ km - mean\ distance\ Earth - Sun$$

$$e = 0.016709 - 0.0000418 * t \quad (3\text{-}36)$$

$$\omega = 282.94 + 1.72 * t \quad (3\text{-}37)$$

$$v = (\lambda_o - \omega) \quad (3\text{-}38)$$

$$R_O = \frac{\rho * (1 - e^2)}{1 + e * \cos(v)} \quad (3\text{-}39)$$

where e is the eccentricity of the Sun's apparent orbit around the Earth, ω is the longitude of perigee of that orbit and v is the true anomaly. In addition, revolution speed of Earth around the Sun (V_p) is calculated by the following equation by using the semi-major axis (*am*) of Earth's orbit:

$$\text{am} = \left(\frac{\mu s(365.25 * 24 * 60 * 60)}{2\pi}\right)^{\frac{2}{3}} \quad (3\text{-}40)$$

$$\text{V}_p = \sqrt{\mu s\left(\frac{2}{R_O} - \frac{1}{am}\right)} \quad (3\text{-}41)$$

Using the parameters above, a coordinate transformation between GSE to HEE (Heliocentric Aries ecliptic) system, is possible. The HEE system has the X-axis pointing to Earth from Sun and the Z-axis oriented towards the Ecliptic North Pole. Y-axis completes a right-handed Cartesian triad. The transformation between the two coordinate system is given in the following equation:

$$Q_{HEE} = R + < 180°, Z > * \; Q_{GSE} \tag{3-42}$$

Based on (3-42), the position components in GSE reference system can be determined:

$$\begin{gathered} x_{HEE} = R - x_{GSE} \\ y_{HEE} = -y_{GSE} \\ z_{HEE} = z_{GSE} \end{gathered} \tag{3-43}$$

For deducing the velocity components, the *R* matrix is ignored in (3-42).

$$\begin{gathered} vx_{HEE} = -vx_{GSE} \\ vy_{HEE} = -vy_{GSE} + Vp \\ vz_{HEE} = vz_{GSE} \end{gathered} \tag{3-44}$$

Knowing the position and velocity in HEE reference system, the position and velocity in HAE (Heliocentric Aries ecliptic) reference system can be found out [3-9]. HAE reference system has X-axis pointing towards the First Point of Aries and Z-axis towards the Ecliptic North Pole and Y-axis completes the right-handed Cartesian triad [3-1].

The transformation between HEE and HAE reference system is given by [3-9]:

$$Q_{HEE} = < \lambda_O + 180°, Z > * \; Q_{HAE} \tag{3-45}$$

Based on Eq. (3-45), the position and velocity components in HAE can be calculated as follows:

$$\begin{gathered} x_{HAE} = x_{HEE} * \cos(\lambda_o + 180°) - y_{HEE} * \sin(\lambda_o + 180°) \\ y_{HAE} = x_{HEE} * \sin(\lambda_o + 180°) + y_{HEE} * \cos(\lambda_o + 180°) \\ z_{HAE} = z_{HEE} \end{gathered} \tag{3-46}$$

$$\begin{gathered} vx_{HAE} = vx_{HEE} * \cos(\lambda_o + 180°) - vy_{HEE} * \sin(\lambda_o + 180°) \\ vy_{HAE} = vx_{HEE} * \sin(\lambda_o + 180°) + vy_{HEE} * \cos(\lambda_o + 180°) \\ vz_{HAE} = vz_{HEE} \end{gathered} \tag{3-47}$$

Knowing the position and velocity in HAE reference system, the orbital elements can be calculated:

Angular momentum:

$$hx = y_{HAE} * vz_{HAE} - z_{HAE} * vy_{HAE}$$
$$hy = z_{HAE} * vx_{HAE} - x_{HAE} * vz_{HAE}$$
$$hz = x_{HAE} * vy_{HAE} - y_{HAE} * vx_{HAE} \tag{3-48}$$

$$h = \sqrt{(hx^2 + hy^2 + hz^2)} \tag{3-49}$$

Scalar product of position and velocity vectors:

$$\vec{r} \cdot \vec{v} = x_{HAE} * vx_{HAE} + y_{HAE} * vy_{HAE} + z_{HAE} * vz_{HAE} \tag{3-50}$$

Vector pointing towards the ascending node:

$$nx = -hy$$
$$ny = hx$$
$$nz = 0 \tag{3-51}$$

$$n = \sqrt{(nx^2 + ny^2 + nz^2)} \tag{3-52}$$

Eccentricity:

$$ex = (x_{HAE} * (V^2 - \mu/R) - (\vec{r} \cdot \vec{v}) * vx_{HAE})/\mu$$
$$ey = (y_{HAE} * (V^2 - \mu/R) - (\vec{r} \cdot \vec{v}) * vy_{HAE})/\mu$$
$$ez = (z_{HAE} * (V^2 - \mu/R) - (\vec{r} \cdot \vec{v}) * vz_{HAE})/\mu \tag{3-53}$$

$$e = \sqrt{(ex^2 + ey^2 + ez^2)} \tag{3-54}$$

Scalar product between the vector pointing towards the ascending node and eccentricity vector:

$$\vec{n} \cdot \vec{e} = nx * ex + ny * ey + nz * ez \tag{3-55}$$

Semi-latus rectum:

$$p = h^2/\mu \tag{3-56}$$

Orbital inclination:

$$i = \mathrm{acos}(\frac{hz}{h}) \tag{3-57}$$

Argument of perigee:

$$\omega = \mathrm{acos}\left(\frac{(\vec{n} \cdot \vec{e})}{n * e}\right); \text{ if ez<0, then } \omega = 360 - \mathrm{acos}\left(\frac{(\vec{n} \cdot \vec{e})}{n * e}\right) \tag{3-58}$$

Longitude of Ascending Node:

$$\Omega = \mathrm{acos}(\frac{\mathrm{nx}}{\mathrm{n}}); \text{ if ny<0, then } \Omega = 360 - \mathrm{acos}(\frac{\mathrm{nx}}{\mathrm{n}}) \tag{3-59}$$

Major semiaxis:

$$a = \frac{p}{1-e^2} \tag{3-60}$$

True anomaly:

$$\theta 1 = \mathrm{acos}((a * (1 - e^2) - r)/(r * e)) \tag{3-61}$$

Periapsis and apoapsis can be calculated with the following formula:

$$rp = a * (1 - e) \tag{3-62}$$

$$ra = a * (1 + e) \tag{3-63}$$

For knowing the position of Shinen2 at any time, a reverse calculation is performed. The eccentric and mean anomaly will be computed first, based on knowing the true anomaly at the edge of the Earth's sphere of influence. Their formula are given below:

$$E_O = \mathrm{acos}((e + \cos(\theta 1))/(1 + e * \cos(\theta 1)\ )) \tag{3-64}$$

$$M_O = E - e * \sin(E) \tag{3-65}$$

$$n = \sqrt{\mu/a^3} \tag{3-66}$$

Deciding a certain time step, *Δt*, the true anomaly can be deduced for any time, based on mean and eccentricity anomaly, calculated with Kepler's equation for elliptical motion, described below [3-1]:

$$M = n * \Delta t + M_O \tag{3-67}$$

$$E_1 = M \tag{3-68}$$

$$E_2 = M + e * \sin(E_1) \tag{3-69}$$

$$E_3 = M + e * \sin(E_2) \tag{3-70}$$

$$E_4 = M + e * \sin(E_3) \tag{3-71}$$

$$E_5 = M + e * \sin(E_4) \tag{3-72}$$

$$\theta = 2 * \mathrm{atan}(\surd(((1 + e)/(1 - e)) * \tan(E_5/2))\ ) \tag{3-73}$$

Knowing the true anomaly, the distance between Shinen2 and Sun can be calculated:

$$R = p/(1 + e * \cos(\theta)) \tag{3-74}$$

Based on the R value, the position and velocity components can be computed at any given time:

$$X_{HAE} = Rs * (\cos(\Omega) * \cos(\omega + \theta) - \sin(\Omega) * \sin(\omega + \theta) * \cos(i))$$

$$Y_{HAE} = Rs * (\sin(\Omega) * \cos(\omega + \theta) + \cos(\Omega) * \sin(\omega + \theta) * \cos(i))$$
$$Z_{HAE} = Rs * \sin(i) * \sin(\omega + \theta) \tag{3-75}$$

$$\begin{aligned} Vx_{HAE} = \left(\frac{\mu s}{h}\right) * e * \sin(\theta) \\ &* (\cos(\Omega) * \cos(\omega + \theta) - \sin(\Omega) * \sin(\omega + \theta) * \cos(i)) + \left(\frac{\mu s}{h}\right) \\ &* (1 + e * \cos(\theta)) \\ &* (-\cos(\Omega) * \sin(\omega + \theta) - \sin(\Omega) * \cos(\omega + \theta) * \cos(i)) \end{aligned}$$

$$\begin{aligned} Vy_{HAE} = \left(\frac{\mu s}{h}\right) * e * \sin(\theta) \\ &* (\sin(\Omega) * \cos(\omega + \theta) + \cos(\Omega) * \sin(\omega + \theta) * \cos(i)) + \left(\frac{\mu s}{h}\right) \\ &* (1 + e * \cos(\theta)) \\ &* (-\sin(\Omega) * \cos(\omega + \theta) + \cos(\Omega) * \cos(\omega + \theta) * \cos(i)) \end{aligned}$$

$$\begin{aligned} Vz_{HAE} = \left(\frac{\mu s}{h}\right) * e * \sin(\theta) * (\sin(\omega + \theta) * \sin(i)) + \left(\frac{\mu s}{h}\right) * (1 + e * \cos(\theta)) \\ * (\cos(\omega + \theta) * \sin(i)) \end{aligned} \tag{3-76}$$

For the communication mission, it is crucial to know the position of Shinen2 on the sky, at any given time. For this purpose, the position of Earth in the heliocentric coordinates must be determined. The following equations are used [3-1]:

$$\theta_E = 360 + (\lambda_0 - \omega_E) \tag{3-77}$$

where λ_o and ω_E are calculated in the same way as in Eq. (3-33) and (3-37).
The distance between Earth and Sun, at any given time, is deduced by the following equation:

$$R_E = ((R_O * (1 - e^2))/(1 + e * \cos(\theta_E)) \tag{3-78}$$

The magnitude of Earth's speed can be calculated as follows:

$$V_E = \sqrt{}(\mu * (2/R_E - 1/a_E)) \tag{3-79}$$

Knowing the magnitude of position and velocity, their values can be expressed in HEE coordinate system as the x-coordinate for position and y-coordinate for velocity [3-1]:

$$XE_{HEE} = R_E$$

$$YE_{HEE} = 0$$

$$ZE_{HEE} = 0 \tag{3-80}$$

$$VX\_E_{HEE} = 0$$

$$VY\_E_{HEE} = V_E$$

$$VZ\_E_{HEE} = 0 \tag{3-81}$$

The transformation between HEE and HAE can be then made, using a coordinate transformation as in Eq. (3-45), following the indications given in [3-9]. Then, knowing the position of Earth and Shinen2 in HAE reference system (relative to the Sun), the distance between Earth and Shinen2 can be calculated as follows [3-1]:

$$\Delta d = \sqrt{(X_{HAE} - XE_{HAE})^2 + (Y_{HAE} - YE_{HAE})^2 + (Z_{HAE} - ZE_{HAE})^2} \tag{3-82}$$

In Fig.3-5 and Fig.3-6, a 3-dimensional view, respectively a 2-dimensional view of the Shinen2 and Earth's orbit around the Sun can be seen. [3-1]

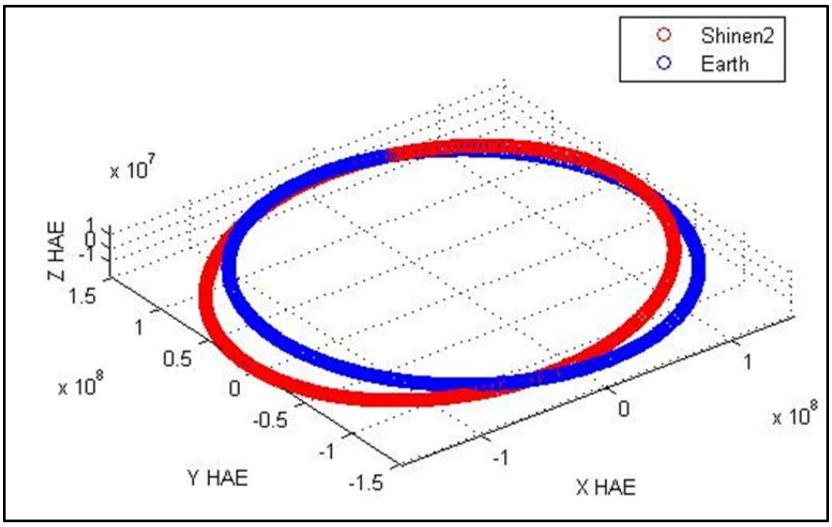

Fig.3-5 3-dimensional view of Shinen2 and Earth's orbit around the Sun [3-1]

To know the distance between Shinen2 and Earth at any given time is very important for the communication mission. In Fig.3-7, the distance is represented as a function of time.

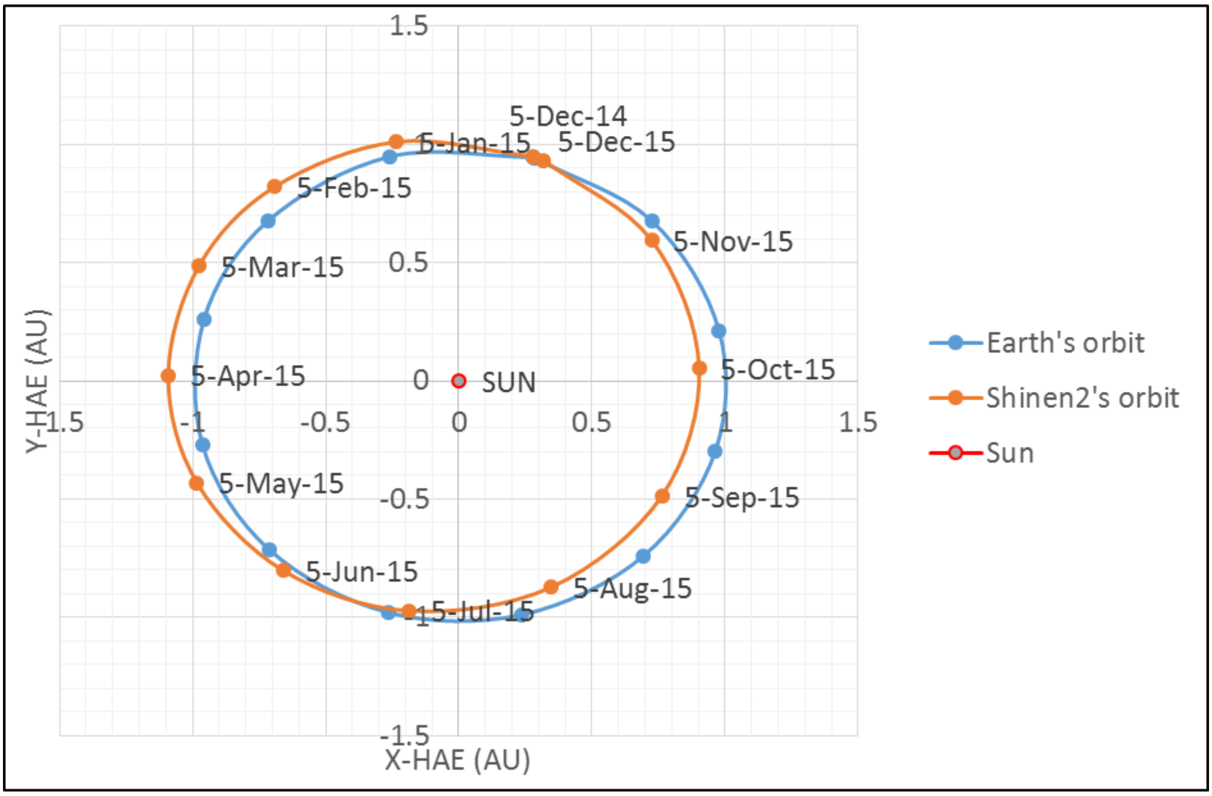

Fig.3-6 2-dimensional view of Shinen2 and Earth's orbit around the Sun

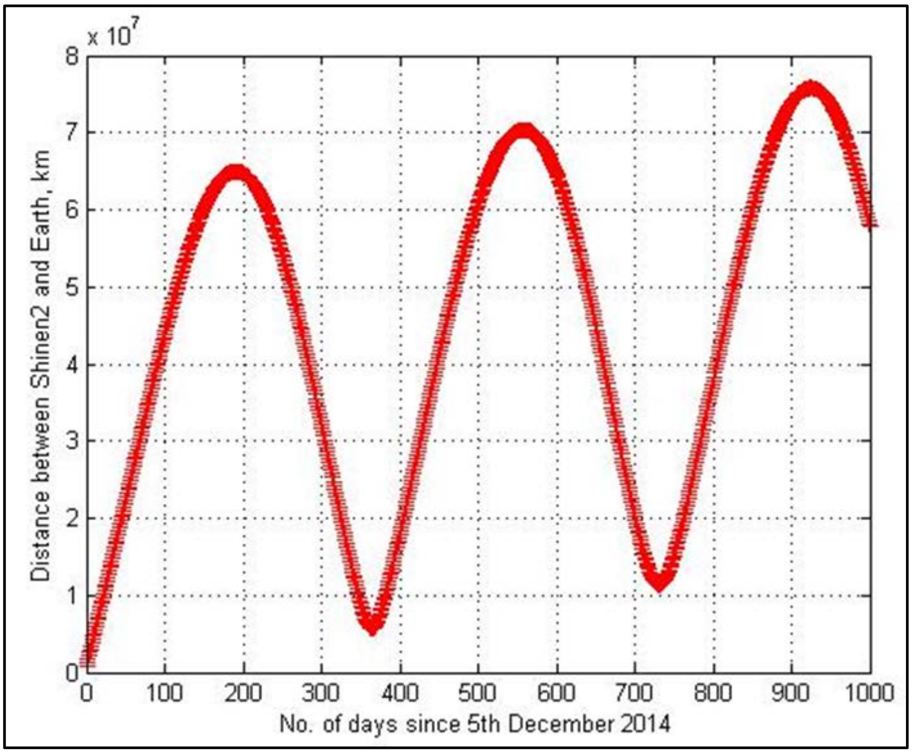

Fig.3-7 Distance between Shinen2 and Earth, for a period of 1000 days since 5th December 2014 [3-1]

From the position values in HAE, a series of coordinate transformation can be made to find the coordinate of Shinen2 in GEI reference system, by applying a reverse calculation at each time.

Details about the coordinate transformations can be found in [3-9]. Knowing the coordinates in GEI reference system, Declination and Right Ascension can be calculated [3-1]:

$$\delta = \mathrm{asin}(\frac{Z_{GEI}}{R_{GEI}}) \tag{3-83}$$

$$RA = \mathrm{acos}(\frac{X_{GEI}}{R_{GEI} * \cos(\delta)}) \tag{3-84}$$

Having the geographical latitude and longitude of a ground station and the Declination and Right Ascension of Shinen2, the precise location of Shinen2 on the sky, for a certain position on Earth of the ground station, can be calculated in terms of Elevation and Azimuth [3-1].

To validate the accuracy of orbit analysis, the results were compared with the ones given by the General Mission Analysis Tool (GMAT). According to [3-12], the General Mission Analysis Tool (GMAT) is an open source software system for space mission design, optimization, and navigation. The software simulate missions ranging from low Earth orbit deep space missions. General Mission Analysis Tool is developed by a team of NASA, private industry, private and public contributors and is widely used for real-world mission support, engineering studies, as a tool for education, and public engagement [3-13].

Most orbit modeling methods are solving the two-body problem and adding several perturbing forces (gravitational attraction from other bodies besides the primary, solar wind, drag, magnetic fields, and propulsive forces [3-14]). For an accurate orbit simulation, these perturbation forces should be included.

There are analytical solutions for simple two-body and three-body problems, but none have been found for the n-body problem (except for certain special cases). Another challenge is that even the two-body problem becomes invalid if one of the bodies is irregular in shape (Earth is not a perfect sphere and also its mass is not evenly distributed). According to [3-12], due to these issues, the two-body problem becomes inaccurate for orbits around the Earth, especially for Low Earth orbits.

Solar radiation pressure causes perturbations to orbits. For satellites orbiting around Earth, solar radiation pressure is stronger than the drag force above 800 km altitude. The value is proportional with the cross-sectional area and inverse proportional with the mass of the spacecraft [3-12].

For orbit simulation, in GMAT software, a complex modelling of perturbing accelerations is performed. Two-body solutions can give approximations for the orbit ephemeris, but, for a precise solution, the effects of perturbing accelerations must be taken into consideration especially in certain situations [3-1].

The equations of motion for the case where perturbations are modeled, can be written in a general form as [3-8]:

$$d^2\vec{r}/dt^2 = -\mu\,(\vec{r}/r^3) + \vec{a}_P \tag{3-85}$$

where $\vec{a}_P$ is the resultant vector of all the perturbing accelerations. $\vec{a}_P$ may consist of the types of perturbing accelerations presented in Table 3-4 [3-1].

Table 3-4 Examples of perturbing accelerations [3-8]

Gravitational	Third-body (sun/moon) attractions
	The nonspherical Earth
Nongravitational	Atmospheric drag
	Solar-radiation pressure
	Outgassing (fuel tank leaks on the spacecraft)
	Tidal friction effect

According to [3-8], in the presence of perturbations, such as drag, third-body attraction, and Earth gravity harmonics, the Keplerian orbit elements are no longer constant. The orbit elements vary in such a way that, at any instant, the coordinates and velocity components can be computed from a unique set of two-body elements as if there were no perturbations. The equations of the variations can be derived from the concept of perturbed variations. There are two basic approaches to obtain the variational equations in celestial mechanics: the force components approach (Gaussian method) and the perturbing function approach (Lagrangian method) [3-1].

In GMAT the inertial system which is used for orbit simulation is called the FK5 system or F_{J2K}. According to [3-12], the F_{J2K} system is referenced to the Earth's equator and the Earth's orbit about the sun. Due to the fact that these two planes are fixed in space, an epoch and inertial system based on the geometry at that epoch must be selected. The epoch is chosen to be J2000 epoch. The transformation from F_{J2K} to the Earth Fixed system is called FK5 reduction [3-12].

The nominal z-axis of F_{J2K} is normal to the Earth's equatorial plane and the nominal x-axis points along the intersection line between the Earth's equatorial plane and the ecliptic plane, in the direction of Aries. The nominal y-axis completes the right-handed system. According to [3-12], due to the fact that the dynamic orientation of the Earth is complicated to be precisely modeled, FK5 reduction is a combination of dynamics models and empirical observations that are updated daily.

In case of Earth's orientation, three types of motion are considered: the first type, including precession and nutation (the Earth's principal moment of inertia changes with respect to inertial space), second type called sidereal time and the third one, of the Earth's instantaneous spin axis with respect to the Earth's surface (the Earth's spin axis is not constant with respect to the Earth's crust and its motion is called Polar Motion). Among all, nutation is considered to be the most complex motion in FK5 reduction and it is described as "the short period motion of the Earth's rotation axis with respect to a space-fixed coordinate system" by Seidelmann [3-12].

Using GMAT software with its advanced modelling techniques, the trajectory of Shinen2 was simulated and the results were compared with the ones given by using the simple orbit prediction presented in Chapter 3. Two stages of the orbit were considered also: first stage in the Earth's sphere of influence (where Runge-Kutta algorithm is used) and the second stage, beyond the Earth's sphere of influence, in deep space (where Dormand-Prince algorithm integration is used).

The differences between the two methods are described in Fig.3-8 and Fig.3-9. [3-1]

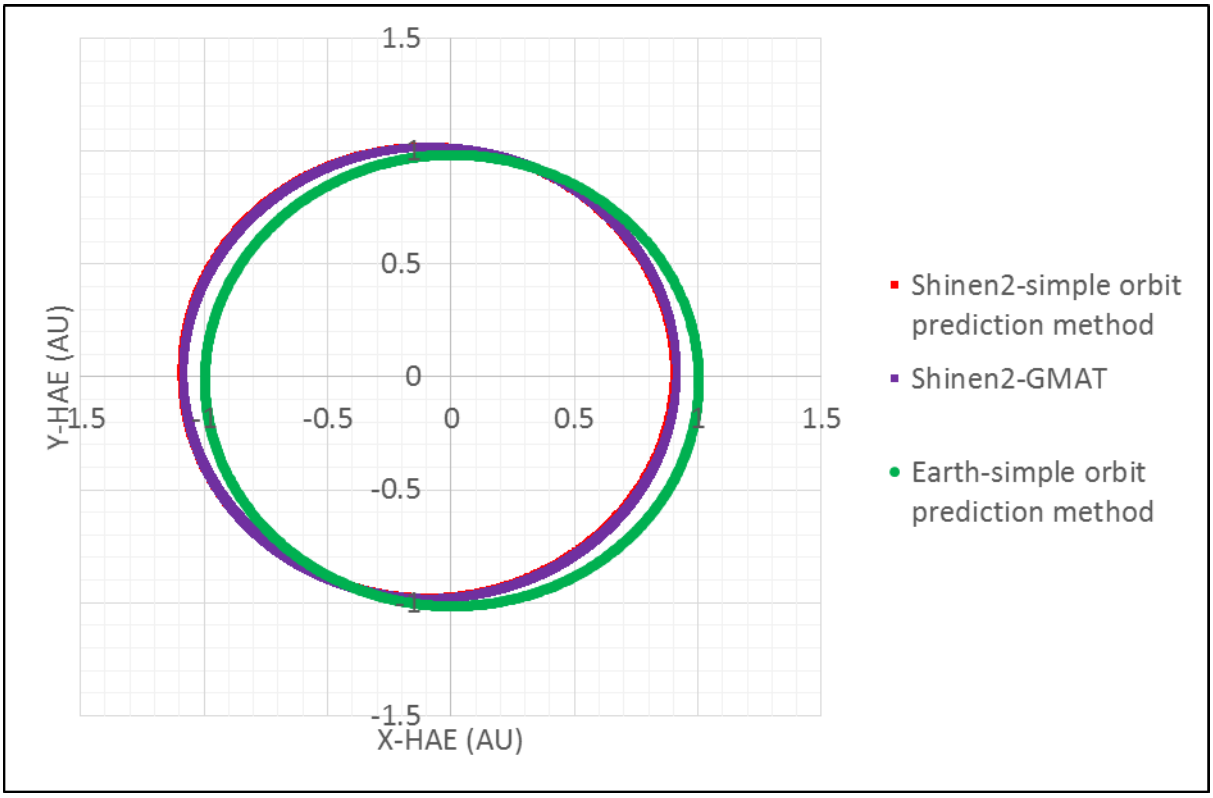

Fig.3-8 2d orbit representation of Shinen2 and Earth using simple method prediction and GMAT software [3-1]

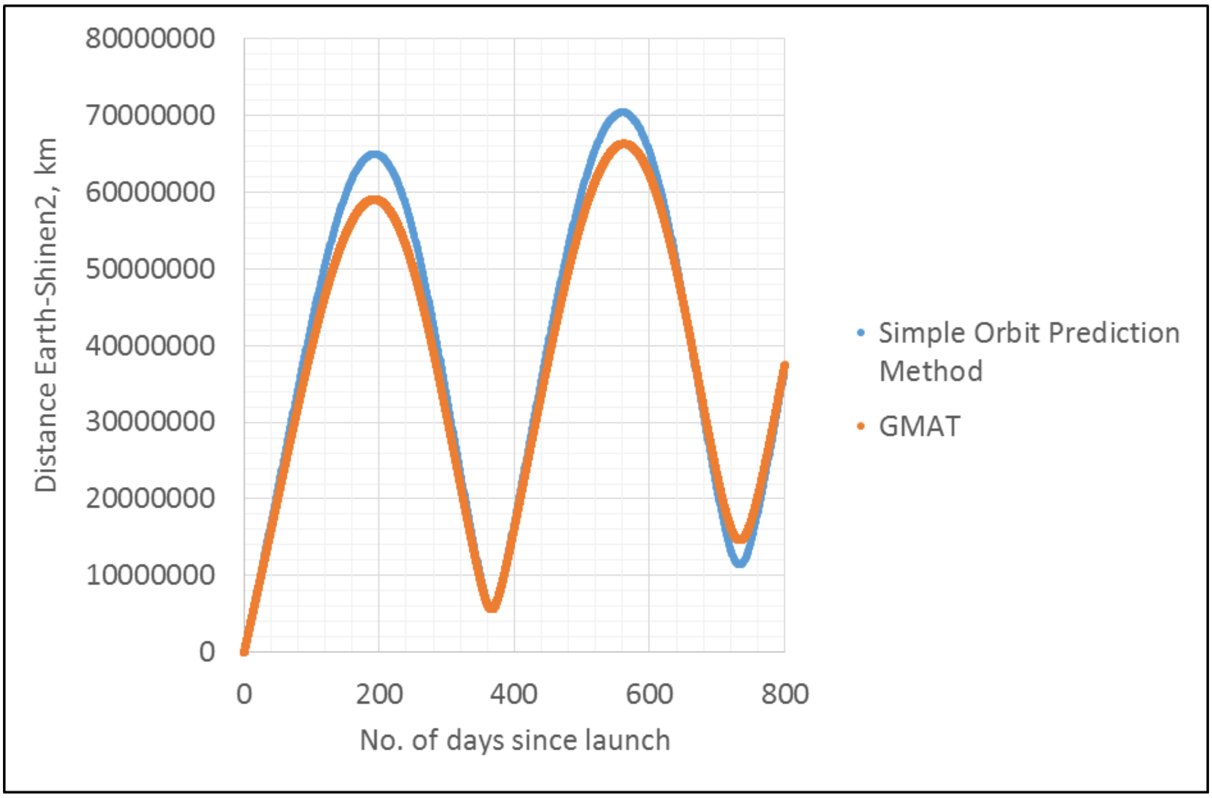

Fig.3-9 Distance between Shinen2 and Earth in time (using simple orbit method prediction and GMAT software) [3-1]

In case of GMAT solution, the perihelion was found to be 0.92 AU and the aphelion 1.09 AU. In comparison, when using the Simple Prediction Method, the perihelion was found to be 0.91 AU and the aphelion 1.1 AU. The Earth's gravitational influence may play a role in explaining the differences between the two orbit analysis methods.

One interesting observation to make is that the orbital period is almost the same, but the eccentricity is different. According to [3-13], the most important orbital elements which affect the orbit of a satellite are inclination and eccentricity. The mathematical models demonstrated that the value of the semi major axis is not influenced by third-body perturbations, except for short periodic oscillations with small amplitudes. Also, the argument of periapsis and the right ascension of the ascending node do not affect very much the orbit of a satellite, as they do not change the regions of the celestial body that is covered by the satellite.

In Fig. 3-10, there can be seen that the maximum difference between the two methods is at about 200 days after launch. On 4th December 2015, a communication attempt with Shinen2 was made. For that date, the coordinates values of Shinen2, in the Geocentric Equatorial Inertial (GEI), and the distance to Earth, calculated by using the two methods, can be seen in Table 3-5 [3-1].

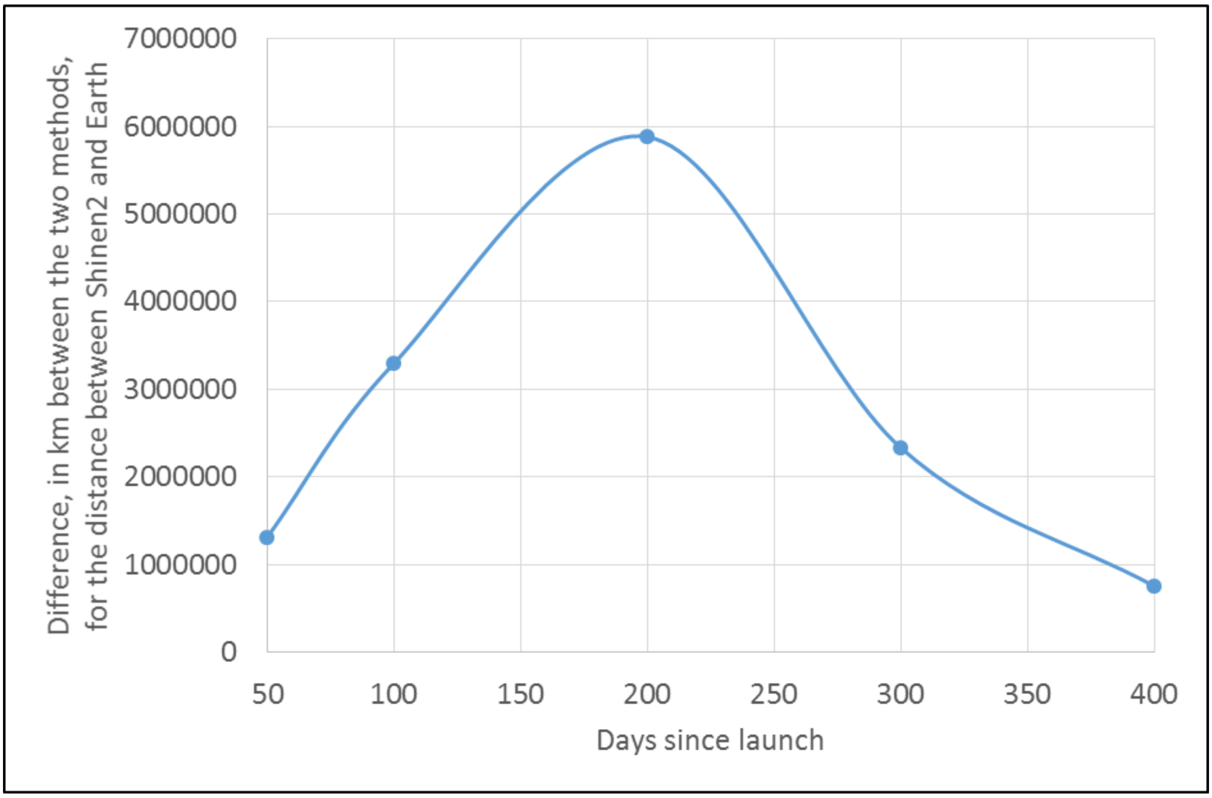

Fig.3-10 Difference in kilometers between the two methods (GMAT and simple orbit prediction), for the distance between Shinen2 and Earth [3-1]

Table 3-5 Differences between the values of coordinates in GEI and of the distance Shinen2-Earth, obtained with the two methods [3-1]

Parameter	GMAT	Simple Orbit Prediction Method	Difference between the two methods
x-GEI	5255735.108 *km*	5574686.775 *km*	318951.667 *km*
y-GEI	-2038297.269 *km*	-1219682.838 *km*	818614.431 *km*
z-GEI	-490316.3766 *km*	-819995.0001 *km*	329678.6235 *km*
Δd	5658428.884 *km*	5765475.704 *km*	107046.82 *km*

The difference in coordinates are of the order of 10E+5 *km* which can be significant when trying to locate precisely the spacecraft on the sky. The difference might be negligible if the orbit analysis is performed solely to estimate the variation of the solar radiation along the orbit (which is an important issue for thermal design), but to locate precisely the spacecraft on the sky, for the purpose of communication, a more complex software as is GMAT software with its advanced orbit modelling techniques is preferable.

The new orbit analysis method can represent a first step in building a computer program which can be implemented in a micro-computer, installed in an ultra-small space probe, and it can serve for the autonomous control of the space probe. In case of an attitude control failure, the new program can recalculate the orbit so that the new thermal conditions can be found out and the value of the generated heat power can be adjusted according to the new thermal environment.

3.4 Thermal analysis model

Orbit prediction helps the engineers to predict the thermal environment through which the space probe passes. Knowing the thermal environment, a thermal analysis model can be built.

As outlined by [3-14], performing thermal analysis is the primary means by which can be verified if a thermal control subsystem meets the design requirements. In case of Shinen2, a SINDA model was developed to help predict the temperatures of the components [3-2]. The most delicate devices are batteries and the payload (NASA sensor). Average heat generation inside Shinen2 is between 10 and 15 W. Also, another important aspect is that the solar cells are placed on CFRP panels and attached on all lateral sides of the satellite and on the top panel [3-2].

For thermal analysis, a SINDA model of 47 nodes was built. For thermal analysis of Shinen2 in deep space, SINDA equations-solver has been used. SINDA is a thermal analyzer which uses a conductor-capacitor network representation, providing a powerful thermal programming language [3-15].

For estimating the optical properties of the outer surfaces, the presence of solar cells was carefully considered. The values for the Solar Constant are presented in Table 3-6.

Table 3-6 Variation of Solar Constant for Shinen2 mission

	Near Earth ($1\ AU$)	**Worst hot case ($0.9\ AU$)**	**Worst cold case ($1.1\ AU$)**
Solar Constant (W/m^2)	**1376**	**1699**	**1137**

In the thermal design of spacecraft, several parameters, like absorptivities and emissivities of the outer structures, emissivities of the inner components and structure, the thermal conductances, the heater powers generated inside, need to be determined so that the components will stay in their design temperature ranges. For estimating the optical properties of the outer surfaces, the presence of solar cells was carefully considered and the averaged optical properties are described in the Table 3-7. [3-2]

Table 3-7 Averaged values of Optical Properties of outer panels [3-3]

	Average absorptance (α)	**Average emissivity (ε)**
White Paint	0.39	0.75
Black Paint	0.69	0.75

Two cases were considered previously: one with the outer panels painted in white and one with the outer panels painted in black. After performing thermal analysis, it was found out that, for the white model, the internal temperatures for the electric components, payload and batteries are in the operating range, while for the black model, the internal temperatures are exceeding the operating range (Table 3-8). In Table 3-8, TX means transmitters, RX means receivers, SCU is Shinen2 Control Unit, PCU is Power Control Unit and CCU is Communication Control Unit. Both worst cold case and hot case were performed assuming that the interior components are painted in black and assuming also the internal heat generation inside Shinen2 (Table 3-9) [3-3]. The two kinds of range, the survival range and operational range, are frequently defined in case of thermal design. Operational limits are the limits within which the components must remain while operating and survival limits are the limits in which the components must remain at all times, even when not powered.

It was decided to use white paint for outer surfaces and black paint for the internal equipment. The optical properties of the materials used for Shinen2 can be seen in Table 3-10 [3-3].

Table 3-8 Survival and Operation Range of Temperatures [3-3]

Component	**Survival Range (Power off), (°C)**	**Operational Range, (°C)**
Radiation detector sensor	-30→60	-20→50
Batteries	-10→50	0→40
TX & RX	-30→60	-20→50
SCU, PCU, CCU	-40→80	-30→70

Regarding the materials, CRRP and CFRTP were used for the outer panels and Aluminum for the internal equipment. The properties of the materials are described in Table 3-11. Also, the PCB plates on which solar cells are mounted, were carefully taken into consideration in thermal analysis. [3-3]

To assure the survival of electric components and batteries, the SINDA program was run for the two cases: the worst hot case (0.9 *AU*) and the worst cold case (1.1 *AU*) [3-3].

Table 3-9 The internal heat generation [3-3]

Component	Heat Power [W]
Radiation Detector Sensor	1.25/0.1
Top Battery	0.5
Bottom Battery	0.5
TX top, -z (1)	0.1
TX top, -z (2)	0.1
A_CCU_PCU	0.2
TX, +z	5.0
B_PCU_CCU, +z	0.1
A_PCU_IF, -y	0.2
TX, +y	5.0

Table 3-10 The optical properties [3-3]

Material	Absorptivity (α)	Emissivity (ε)	α/ε
Aluminum	0.13	0.30	0.43
PCB	0.25	0.88	0.28
CFRTP	0.94	0.91	1.03
CFRP	0.85	0.85	1.00
White Paint	0.25	0.88	0.28
Black Paint	0.90	0.80	1.13

Table 3-11 The properties of the materials [3-3]

Material	Density (kg/m^3)	Thermal conductivity ($W/m/K$)	Specific Heat ($J/kg/K$)
Aluminum	2700	167	896
PCB	1300	0.274	1421
CFRTP	1520	0.766	913
CFRP	1600	0.766	1000

3.5 Validation of thermal analysis model by thermal vacuum tests

The SINDA model was validated by the thermal vacuum tests performed. In thermal vacuum tests, 50 thermocouples were used (Fig.3-11), positioned almost in the same location as the nodes in the SINDA model. A heaters cage was used to provide power (Fig.3-12). During the tests, the heaters were turned on and they have been kept working until the temperatures inside Shinen2 reached more than 35 degrees Celsius. Afterwards, the heaters were turned off, the temperatures dropped to the room temperature and afterwards the cooling system was activated. The temperatures of batteries were kept at 5 degrees Celsius 21 hours (time of reaching the Moon orbit) [3-2].

In SINDA, there were implemented the same conditions as for thermal vacuum tests and the differences are maximum 3 degrees Celsius (Table 3-12). The small differences (the average difference between the measured and calculated data being 1.45 degrees Celsius) show that the SINDA model represents accurately the real model so that it can be used to estimate thermal environment in deep space [3-2].

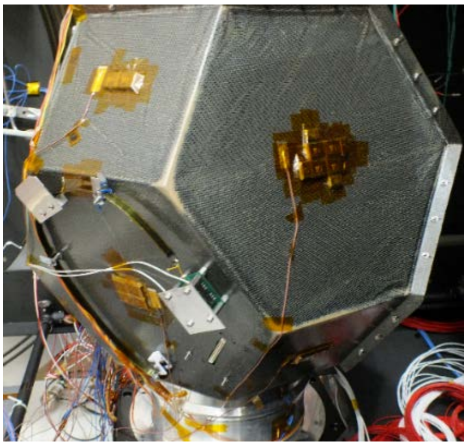

Fig.3-11 Preparations of EM model (with thermocouples attached in 50 locations) for thermal vacuum tests [3-2]

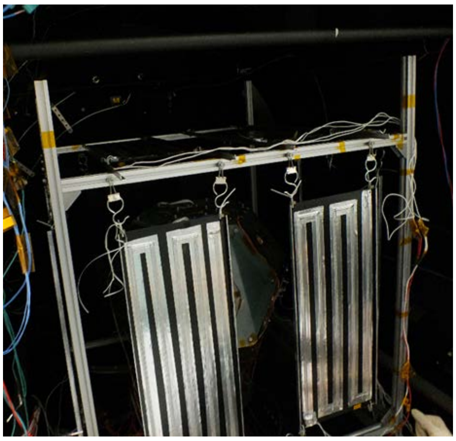

Fig.3-12 Heaters cage for thermal balance tests [3-2]

Table 3-12 Validation of Thermal Analysis Model [3-3]

Component	**Thermal tests results Temp. (℃)**	**Sinda results Temp. (℃)**	**Difference in Temp. (℃)**
Top Battery, top	36.0	34.3	1.70
Top Battery, bottom	35.8	34.3	1.50
Top Battery, lateral side	34.8	34.3	0.50
Top Battery, inside	36.0	34.3	1.70
Bottom Battery, top	35.5	34.1	1.40
Bottom Battery, bottom	35.7	34.1	1.60
Bottom Battery, lateral side	35.7	34.1	1.60
Bottom battery, inside	36.9	34.1	2.80
Radiation sensor, top	36.3	32.5	3.80
Radiation sensor, bottom	35.9	32.5	3.40
Top panel	32.8	31.4	1.40
SUBPCU	34.8	35.1	0.30
Bottom plate, CFRTP	31.3	33.5	2.20
CCU	34.9	34.6	0.30
SCU	35.9	36.6	0.70
TPD TX	34.3	34.9	0.60
TPR PCU -z	35.4	35.9	0.50
Main Transmitter	33.4	34.4	1.00
Access panel	29.4	28.7	0.70
Main Frame	34.4	33.7	0.70
Bottom Aluminium plate	35.0	33.8	1.20
Morse Transmitter	40.2	42.6	2.40

3.6 Thermal analysis results for space environment

To simulate the extreme thermal environment in space, the SINDA program was run for the two cases: the worst hot case (0.9 *AU*) and the worst cold case (1.1 *AU*). The results consist of temperatures between 25 and 50 °C for 0.9 *AU* and between 10 and 37 °C for 1.1 *AU* and these results are in the allowable and working temperature range [3-2].

As mentioned in [3-2], because the results of thermal analysis are in the allowable and working temperature range for electric components and batteries, the solution with white paint outside and black paint inside is considered a good solution for thermal control system of Shinen2.

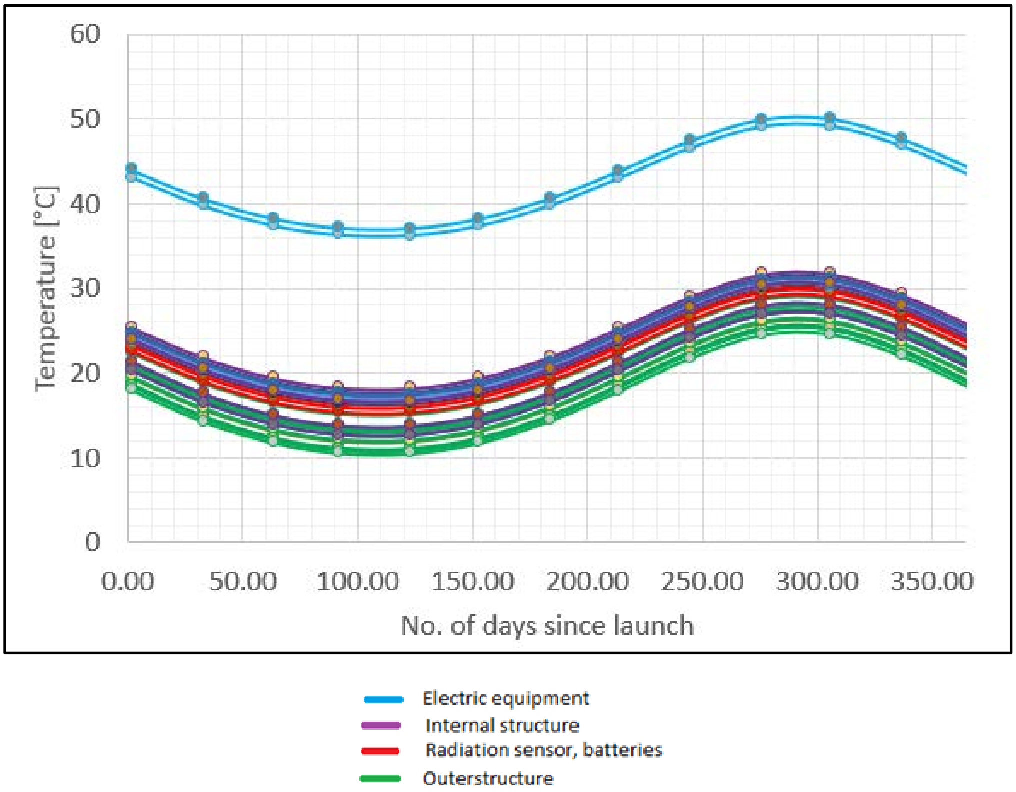

Fig.3-13 The analysis results in temperatures for one year period of time [3-3]

In Fig.3-14, the temperatures of Radiation Detector Sensor and of batteries are represented for one year (the orbit period of Shinen2) and, in Table 3-13, the exact values for NASA sensor and batteries are described in case of the worst hot and cold cases. [3-3]

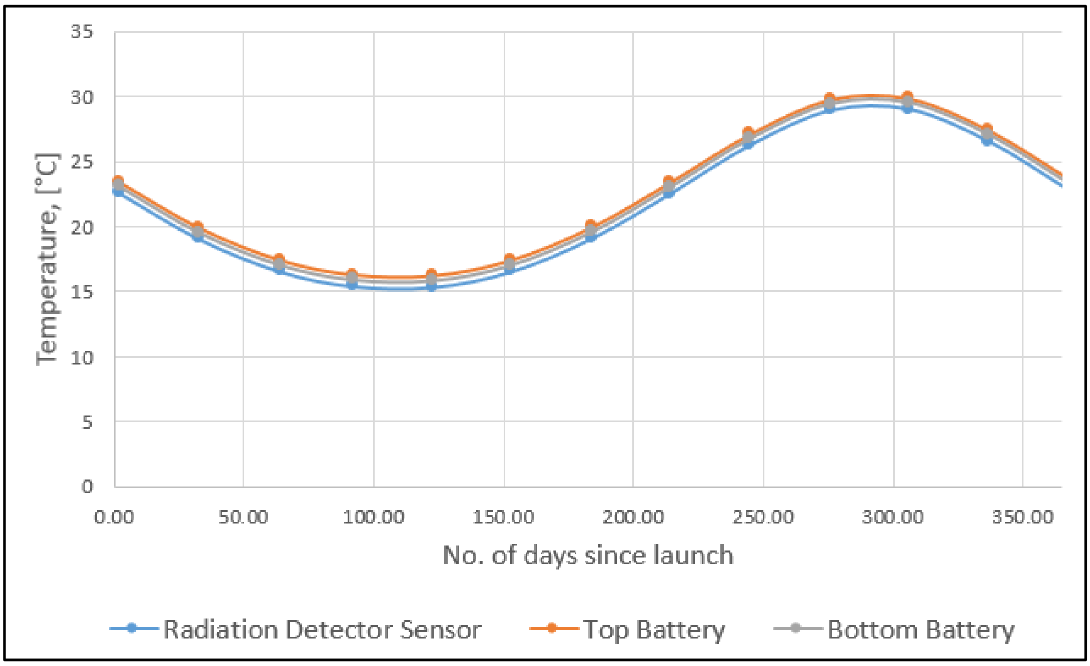

Fig.3-14 The analysis results in temperatures for one year period of time, in case of Radiation Sensor and batteries [3-3]

Table 3-13 The temperatures for the worst cold and hot case, for Radiation Sensor and batteries [3-3]

	Worst hot case (0.9 *AU*)	**Worst cold case (1.1 *AU*)**
Radiation Detector Sensor	15.36 ℃	29.02 ℃
Top Battery	16.22 ℃	29.84 ℃
Bottom Battery	15.87 ℃	29.51 ℃

The results show that all components operate within their safe temperature limits.

3.7 Telemetry data

On the flight model of Shinen2, 9 thermal sensors were attached inside the probe (Fig.3-15). After launch, Shinen2 was able to communicate with different ground stations and in the downlink data there were also temperature data. Using Sinda model, the same conditions as during the communication were simulated and the results of the thermal analysis are in good agreement with the measured data.

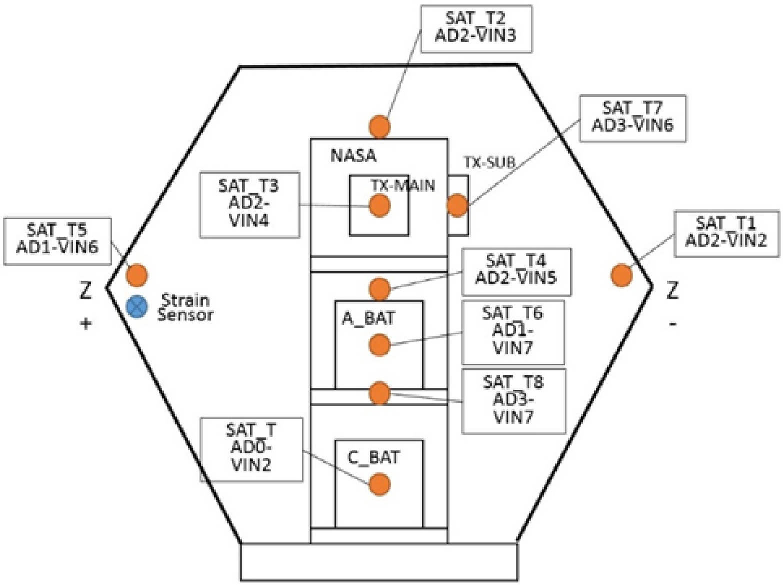

Fig.3-15 Position of the thermal sensors inside the Flight Model [3-3]

In Fig.3-16, Fig.3-17 and Fig.3-18, the instantaneous values of temperatures are represented.

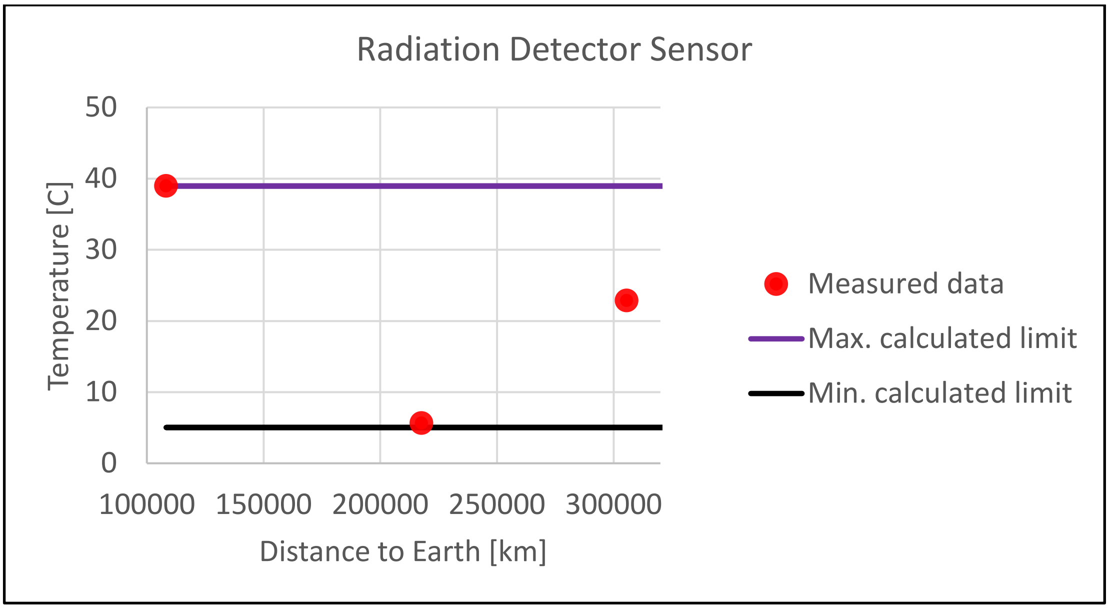

Fig.3-16 Instantaneous measured temperatures for the Radiation Detector Sensor

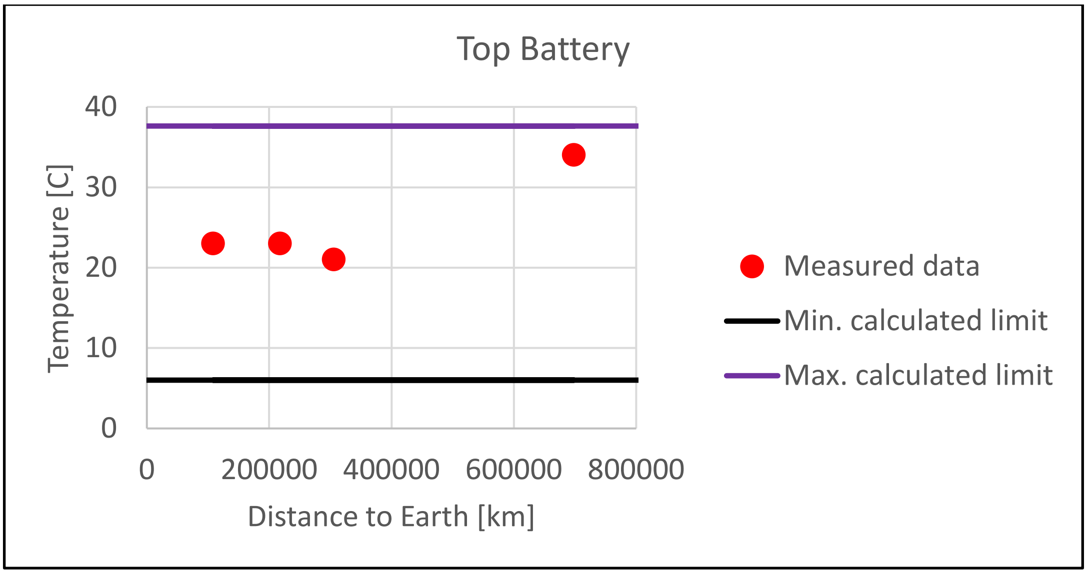

Fig.3-17 Instantaneous measured temperatures for the Top Battery

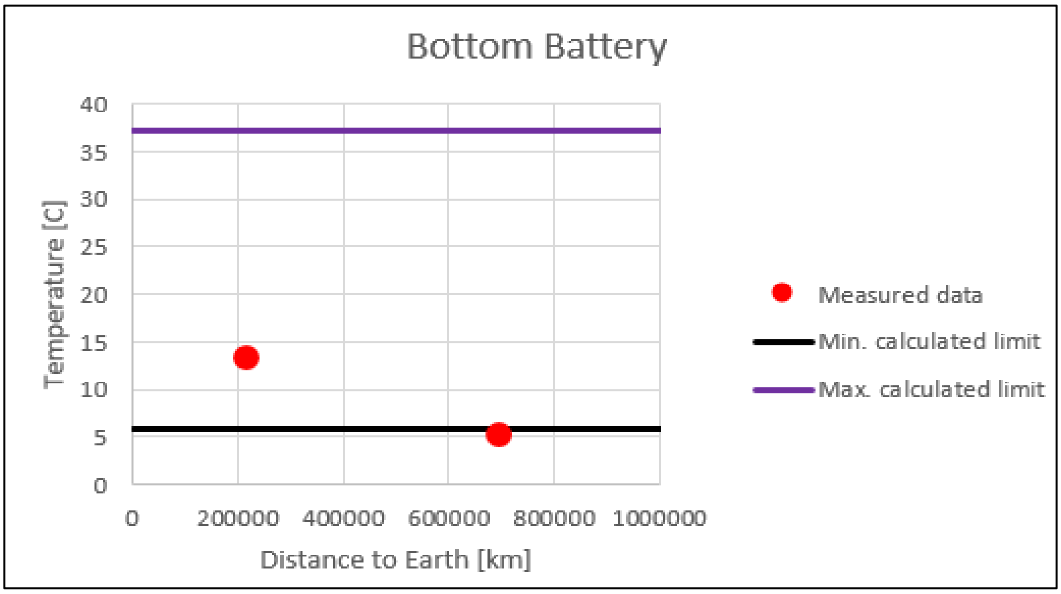

Fig.3-18 Instantaneous measured temperatures for the Bottom Battery

The Max. calculated limit and the Minimum calculated limit represent the calculated values for the maximum heat power generated, respectively for the minimum heat power generated inside Shinen2, for the time of communication (during 1 week after launch).

The results show that all components operate within their safe temperature limits. Also, the results indicate the adequacy of design methodology, which can be used for the design and analysis of similar deep space probes which will have similar mission requirements and orbital parameters.

References

[3-1] Bianca Szasz, Kei-ichi Okuyama, Yoshiharu Matsumoto, Sidi Ahmed Bendoukha, *Simple Orbit Prediction Method and its Validation for Deep Space Missions*, UNISEC Space Takumi Conference, March 2016.

[3-2] Bianca Szasz, and Keiichi Okuyama, *Thermal Design and Analysis of Shinen2, an Ultra-Small Deep Space Probe*, Conference Proceedings of the 58th Space Sciences and Technology Conference, Nagasaki, 2014.

[3-3] Bianca Szasz, Kei-ichi Okuyama, *Shinen2, an Ultra-Small Deep Space Probe: Thermal Design, Analysis and Validation*, UNISEC Space Takumi Journal, accepted for publication.

[3-4] A. Kwok, *201, Rev. B Frequency and Channel Assignments*, 810-005, Rev. E, DSN Telecommunications Link Design Handbook, DSN Document Release, California Institute of Technology, 2009.

[3-5] Tsuda, Y., Yoshikawa, M., Minamino, N., Nakazawa, S., *System Design of Hayabusa2 – Asteroid Sample Return Mission to 1999JU3*, 63rd International Astronautical Congress, IAC-12-A.3.4.5, Naples, Italy, 2012.

[3-6] Volodymyr Baturkin, *Micro-Satellites Thermal Control - Concepts and Components*, edited by Elsevier, Acta Astronautica 56, 2005, pp. 161-170.

[3-7] Oliver Montenbruck, Thomas Pfleger, *Astronomy on the Personal Computer*, Fourth Edition, Springer, 2000.

[3-8] Vladimir A. Chobotov, *Orbital Mechanics (Second Edition)*, AIAA Education Series, 1996, Reston, Virginia, USA.

[3-9] M.A. Hapgood, *Space Physics Coordinate Transformations: A User Guide*, Planet. Space Sci., Vol.40, No.5, pp.711-717, 1992.

[3-10] D.G. Simpson, *Table of Julian Day Numbers - 1950-2100*, NASA report, Science Data Processing Branch, Goddard Space Flight Center, Greenbelt, Maryland, June 2012.

[3-11] Roy, A.E., *Orbital Motion* (third ed.). Institute of Physics Publishing. ISBN 0-85274-229-0, 1988.

[3-12] The General Mission Analysis Tool (GMAT) website, URL: http://gmatcentral.org/ (2016)

[3-13] Domingos, R.C., Prado, A.F.B.A. Gomes, V.M., *Effects of the eccentricity of a perturbing third body on the orbital correction maneuvers of a spacecraft*, Mathematical Problems in Engineering, Volume 2014 (2014), Article ID 359845.

[3-14] N. Sozbir, M. Bulut, M.F. Oktem, A. Kahriman and A. Chaix, *Design of Thermal Control Subsystem for TUSAT Telecommunication Satellite*, World Academy of Science, Engineering and Technology 43, 2008.

[3-15] T. Totani, H. Ogawa, R. Inoue, T.K. Das, M. Wakita, and H. Nagata, *Thermal Design Procedure for Micro- and Nanosatellites Pointing to Earth*, American Institute of Aeronautics and Astronautics, Journal of Thermophysics and Heat Transfer, 28(3): 524-533, 2014.

IV. Ultra-light ablative materials for reentry probes

4.1 Qualification criteria for an ablator system made of LATS materials

The goal of the present research on the ablative materials is to find a suitable ablative material for future ultra-small spacecraft missions, led by a university, for which the costs and mass should be kept at minimum. The main criteria in judging the thermal performance of an ablator system is the surface recession values.

The present research presents new empirical methods to estimate the recession, the qualification test results of the light weight ablator LATS (Lightweight Ablator Series for Transfer Vehicle Systems), which will be used for the thermal shield of future university space missions, and the validation of a numerical analysis by the test results. The heat shield for these future deep space missions should withstand high heating rates and high stagnation pressures, and also should provide the necessary thermal protection to the spacecraft. The biggest advantages in using LATS materials are their low density, their superior ablation and thermal performance at severe aerothermodynamics conditions.

The ablation and thermal performances of LATS materials were qualified at the Japan Ultra High Temperature Material Center (JUTEM), the Aerospace Research and Development Directorate (ARD) of the Japan Aerospace Exploration Agency (JAXA), and Deutsches Zentrum fuer Luft- und Raumfahrt (DLR) of Germany, through the high-enthalpy heating tests in the past years. The present research addresses the recent results from the tests, new formulations to estimate the recession values (using experimental results) and the comparison between the numerical and experimental results.

It is expected that LATS material will be first used for a deep space probe which will reenter Earth and will face a heat flux of maximum 15 MW/m^2. To qualify LATS materials for this kind of space missions, they were tested for several values of heat flux and the maximum value was 15 MW/m^2.

The purpose of studying LATS materials was to measure and estimate the recession rate for given heat fluxes, flow enthalpy and duration

Also, the secondary purposes of the studies are:

- to develop a more precise empirical method for estimating recession in case of a real reentry scenario and to validate it using flight data of USERS spacecraft, having a heat shield made of conventional CFRP-based ablators;
- to analyse the side-heating which may affect the ground test results. The side-heating

---

effects must be kept at minimum for a better comparison with the unidimensional numerical analysis;

- to compare the temperature results when using a cylinder type with the case of using a mushroom type for the ablator specimen;
- to compare the experimental results with the numerical results when using an ablator code built by Ryukyus University.

4.2 New method to calculate recession and its validation using flight data

As the human race will continue to explore the space by creating new space transportation means and sending them to other planets, the enhance of atmospheric reentry study is crucial. A summary of the physical phenomena which occurs during the reentry phase of a spacecraft can be seen in Fig.4-1.

One of the most successful Japanese reentry mission was USERS mission. Its REM capsule (Fig.4-2, Fig.4-3) was launched to Earth orbit with the H2A rocket on September 10, 2002, and the atmospheric re-entry took place on May 30, 2003. The maximum heat flux was estimated to be 3.1 MW/m^2, but the real heat flux at re-entry was about 1.5 MW/m^2 [4-3].

REM capsule had a thermal shield made of heavy-weight CFRP-based ablators, composed by laminated carbon fibers layers, with a density of about 1400 kg/m^3. The thermal shield can be seen in Fig.4-4. Although the subject of the present research is lightweight ablator materials, USERS case is useful for estimating the recession rate as it was a successful mission and the flight data are available.

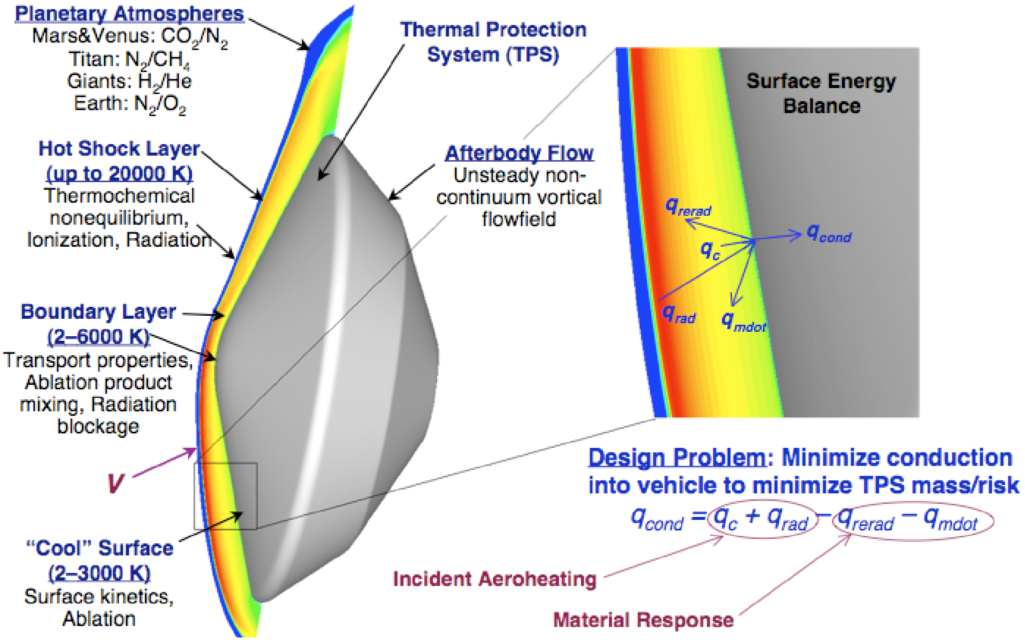

Fig.4-1 High Energy Heatshield Environments [4-4]

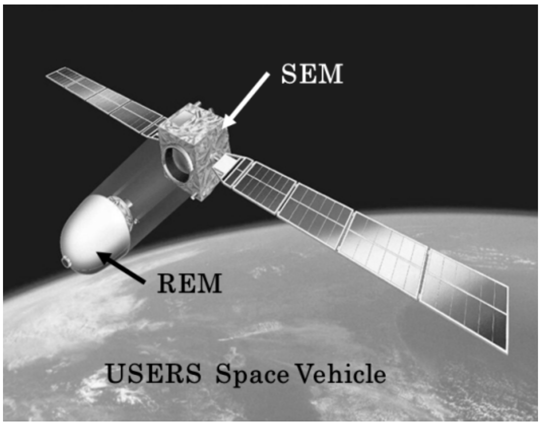

Fig.4-2 USERS space system [4-3]

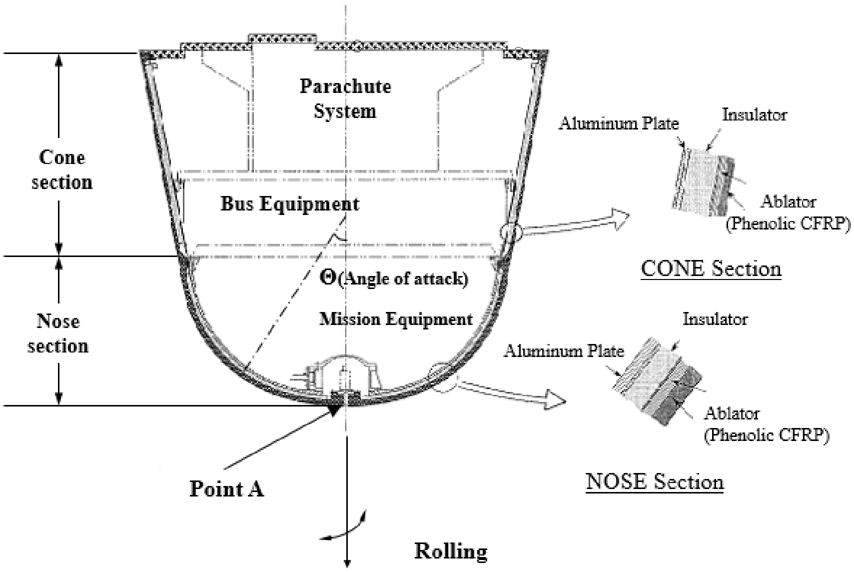

Fig. 4-3 REM capsule of USERS Spacecraft [4-3]

Fig.4-4 Recovered heatshield of USERS. The white spots near are residual paint and dried seawater. [4-5]

The surface recession measured after landing, in point A (shown in Fig.4-2), is 1.6 mm [4-5] and this value will be compared with the calculated values. The considered time range is between 1430 and 2400 seconds after separation and the stagnation pressures and wall temperatures are measured each 10 seconds. The wall temperatures are below 1500 °*K* except a period of time of 100 seconds (Fig.4-5).

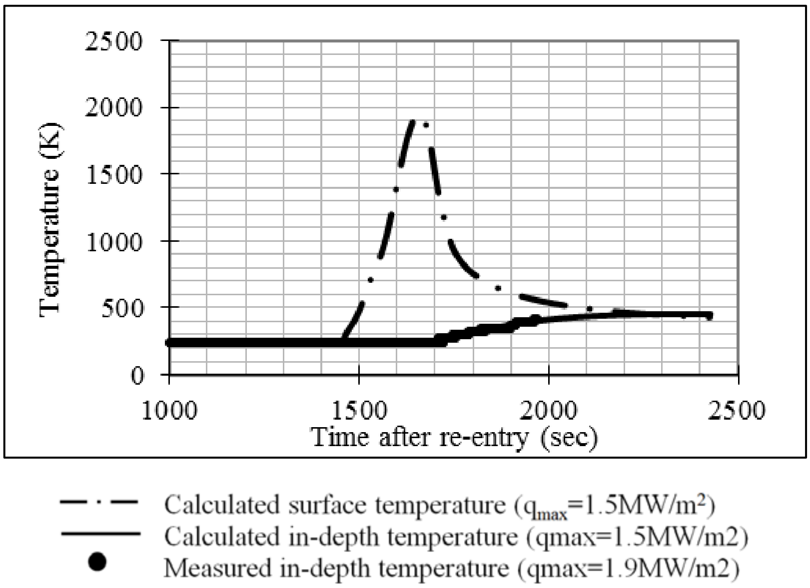

Fig.4-5 Temperature flight history of USERS [4-5]

Also, in Fig.4-6, Fig.4-7 and Fig.4-8, heat flux, dynamic pressure heating rate and enthalpy history of USERS are shown.

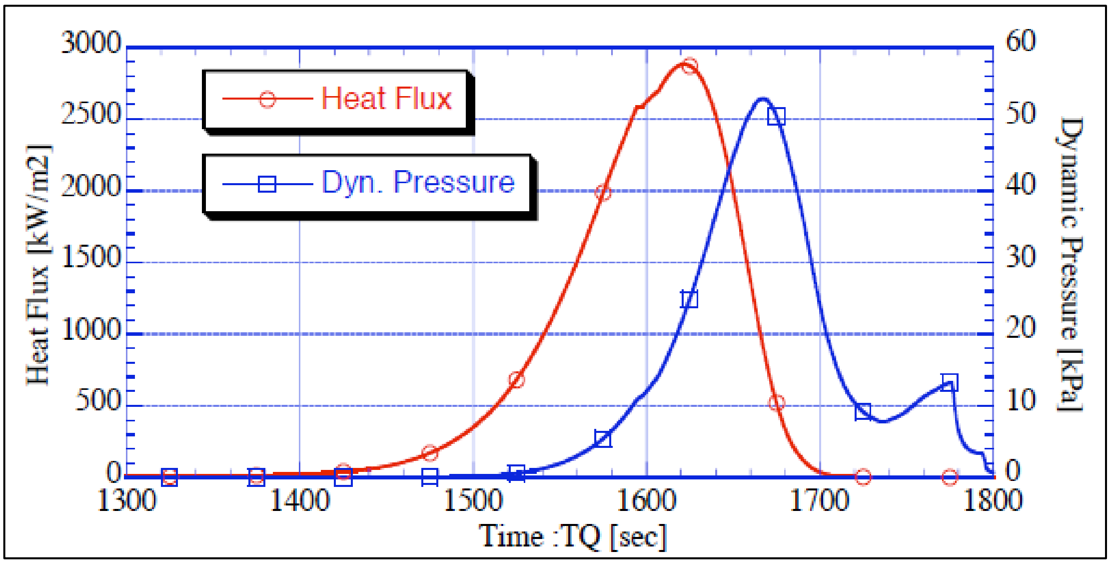

Fig.4-6 Heat Flux and Dynamic Pressure profiles of USERS. TQ [*sec*] is the time after deorbit [4-5]

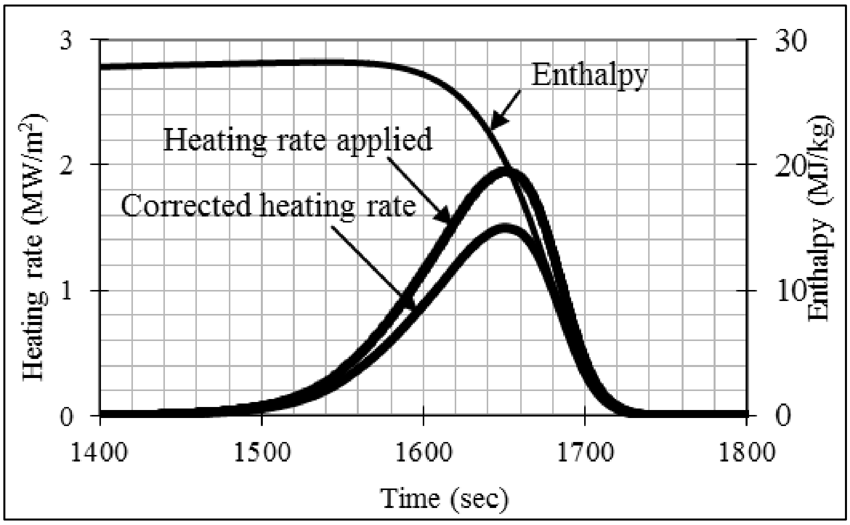

Fig.4-7 Heating rate and Enthalpy flight history of USERS [4-5]

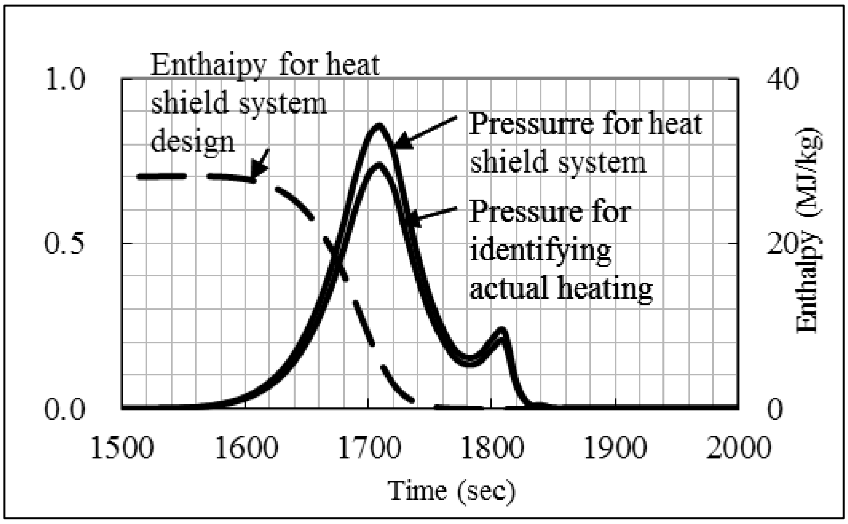

Fig.4-8 Stagnation pressure ($\times\ 10^5 Pa$) and enthalpy history of USERS [4-5]

Three methods for mass recession rate estimation are used in the present research of USERS mission: one based on Arrhenius equation for the entire time range, the second being based on Okuyama equation for the entire time range and the third one being based on a combination of both equations. More precisely, for the third method, Arrhenius equation is used for wall temperatures below 1,500 $°K$ and Okuyama equation is used for wall temperatures above 1,500 $°K$ [4-1].

According to [4-1], based on mass recession rate values, one important parameter can be calculated: surface recession which is defined as mass recession rate divided by charring density:

$$\dot{l} = \frac{\dot{m}}{\rho_{ch}} \tag{4-1}$$

Its value will be integrated in time and the final result will be compared with the measured result. Since USERS has a heavyweight ablator system, the charring density is 1180 kg/m^3 [4-1].

The following figures show the results of mass recession rate and surface recession for Arrhenius equation (Fig.4-9 and Fig.4-10), for Okuyama equation (Fig.4-11 and Fig.4-12) and for the new method based on both equations (Fig.4-13 and Fig.4-14). As pointed out in [4-1], there can be seen that the Arrhenius equation (4-1) gives large values for mass recession rate and surface recession and that the third method based on both equations gives large values in the transition place between the region where Arrhenius equation is applied and the region where Okuyama equation is applied.

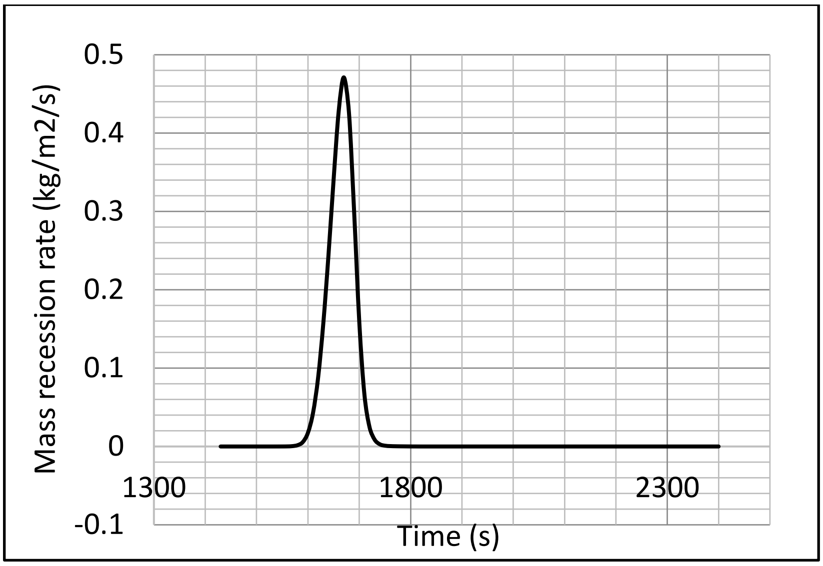

Fig.4-9 Mass recession rate in time, calculated with Arrhenius equation [4-1]

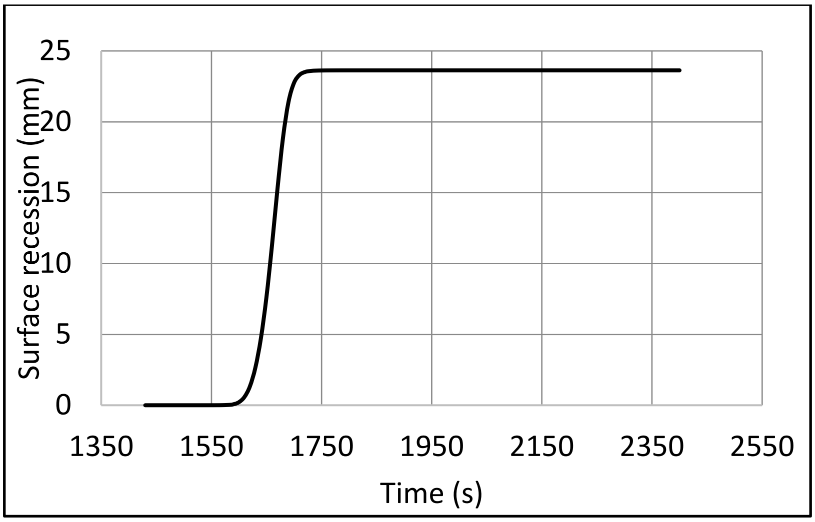

Fig.4-10 Surface recession in time, calculated with Arrhenius equation [4-1]

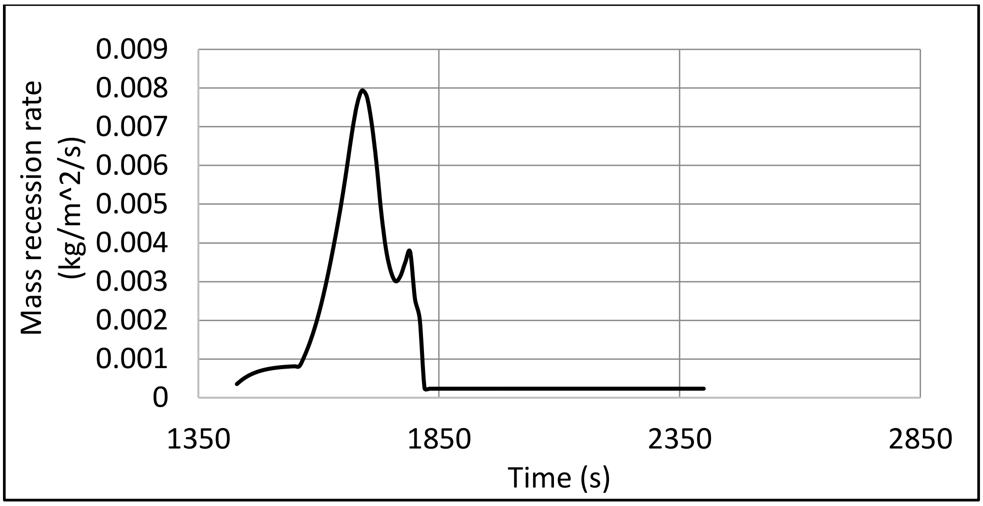

Fig.4-11 Mass recession rate in time, calculated with Okuyama equation [4-1]

In Fig.4-15 and Fig.4-16, all three methods are compared with respect to mass recession rate and surface recession. If Okuyama equation based method and the new method gives similar results, the Arrhenius equation based method gives considerably higher results, which can be explained by the fact that Arrhenius equation shouldn't be applied for the diffusion-controlled oxidation region [4-1].

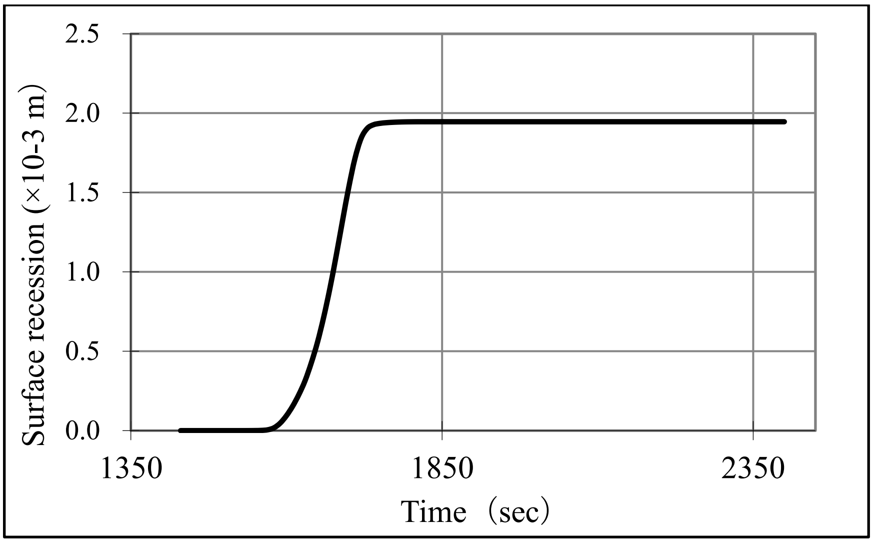

Fig.4-12 Surface recession in time, calculated with Okuyama equation ([4-1])

For validating the new method, for which Arrhenius equation was applied only in the rate-controlled oxidation region and Okuyama equation was applied in the diffusion-controlled oxidation region, a comparison with the measured data was made (Fig.4-17), the result by using the new method being very close to the measured data. If the measured data for surface recession is 1.6 *mm*, using the new method the result is 1.58 *mm*, whereas using only Okuyama equation the result was about 1.9 *mm*, giving a difference of 0.3 *mm* [4-1].

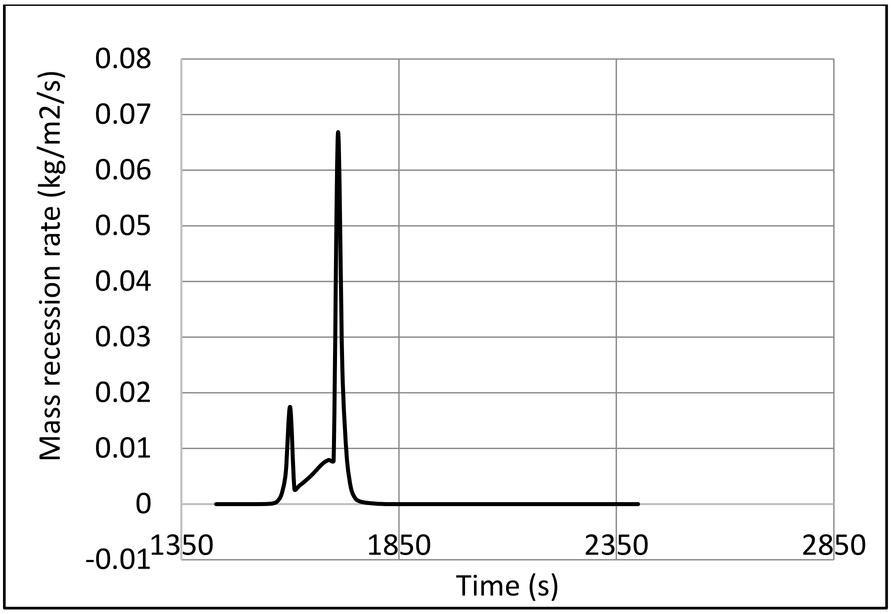

Fig.4-13 Mass recession rate in time, calculated with Arrhenius equation (for T<1500 *K*) and Okuyama equation (for T>1500 *K*) [4-1]

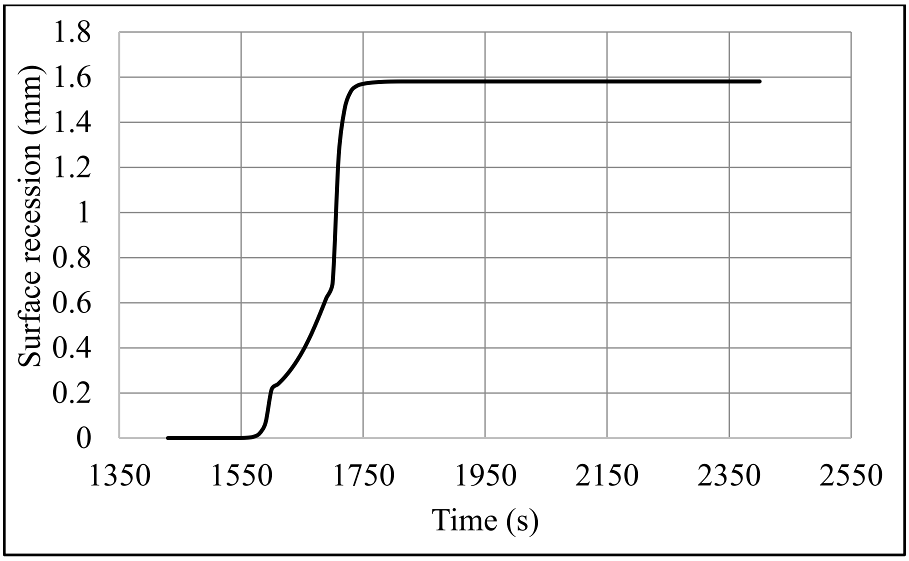

Fig.4-14 Surface recession in time, calculated with Arrhenius equation (for T<1500 *K*) and Okuyama equation (for T>1500 *K*) [4-1]

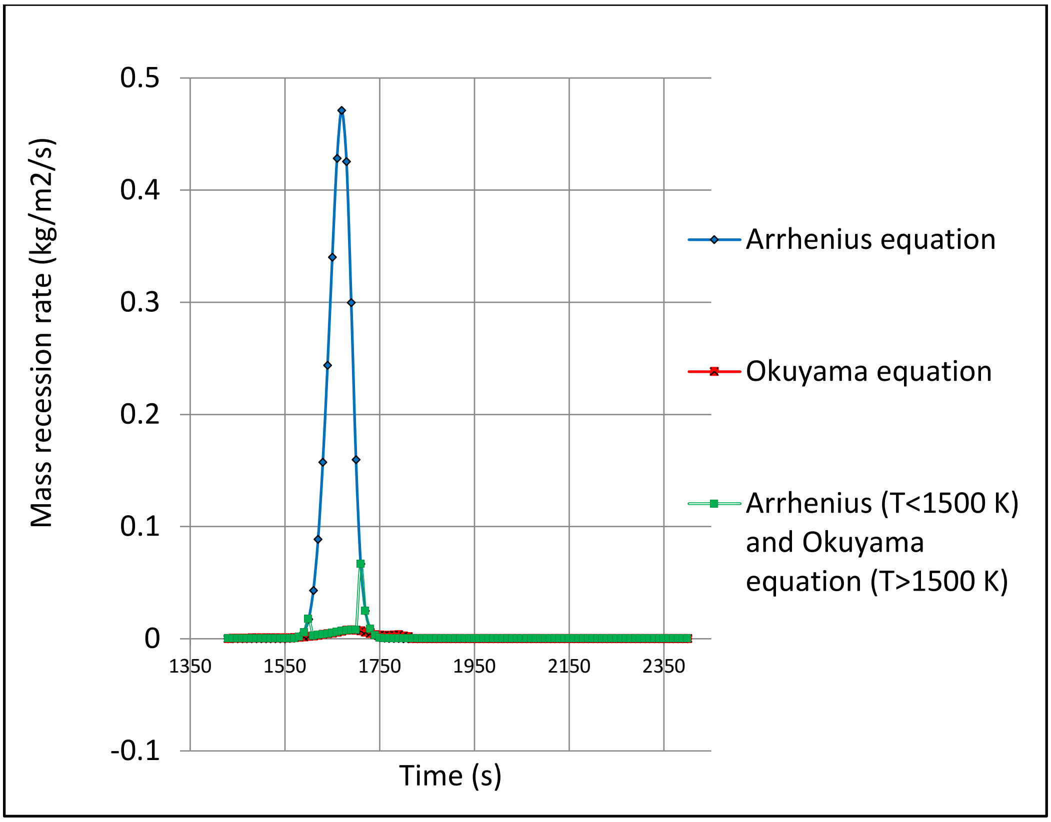

Fig.4-15 Mass recession rate calculated by 3 methods: using Arrhenius equation, Okuyama equation, respectively Arrhenius equation (for T<1500 *K*) together with Okuyama equation (for T>1500 *K*) [4-1]

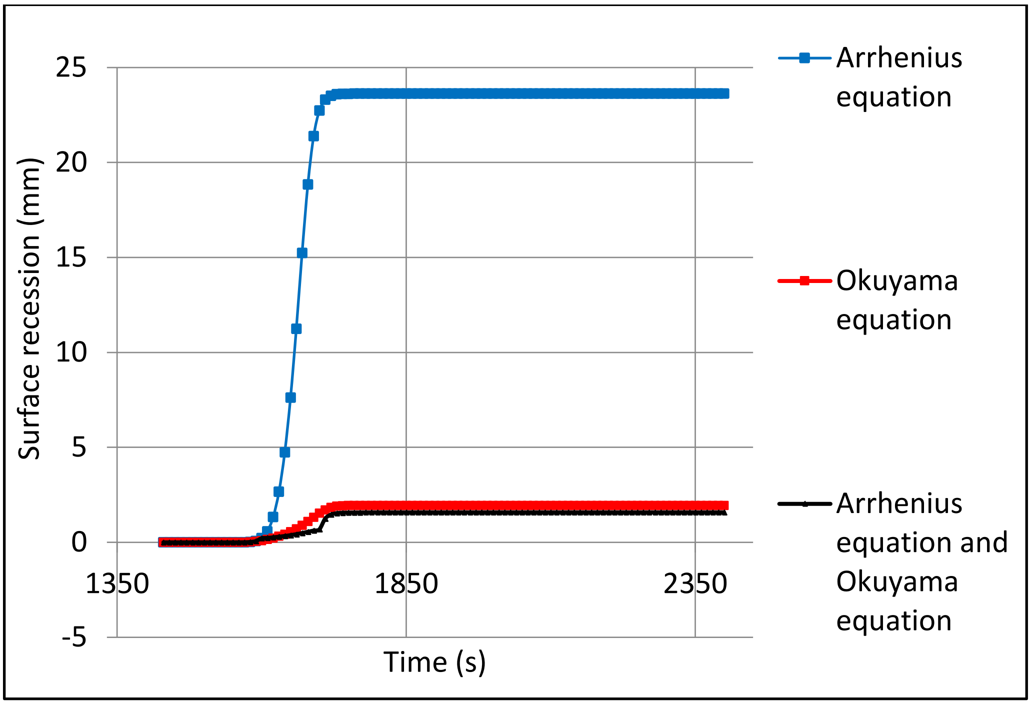

Fig.4-16 Surface recession (mm) calculated by 3 methods: using Arrhenius equation, Okuyama equation, respectively Arrhenius equation (for T<1500 *K*) together with Okuyama equation (for T>1500 *K*) [4-1]

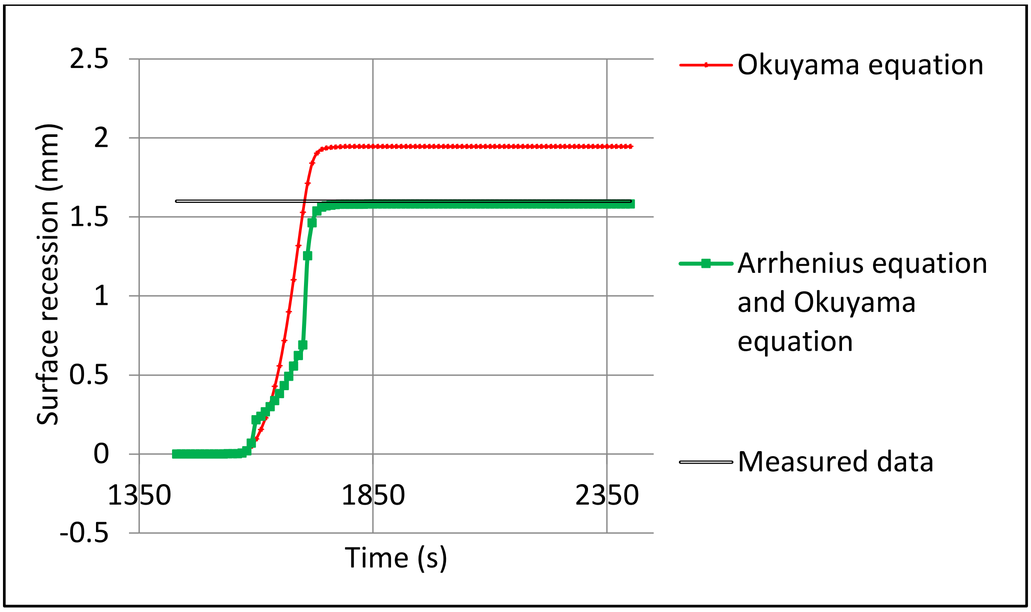

Fig.4-17 Surface recession (*mm*) calculated by using Okuyama equation, respectively Arrhenius equation (for T<1500 *K*) together with Okuyama equation (for T>1500 *K*) are compared with the measured value of 1.6 *mm* [4-1]

Based on the above findings, a new method for calculating mass recession rate and the surface recession has been developed, based on the classic methods and on the previous work of Okuyama *et al*. The new method was validated using the flight data of USERS spacecraft by giving the same value for the surface recession as the measured data [4-1]. However, further studies and validations are recommended to prove that the new method gives accurate results for more types of ablative materials.

It is worth noting that mass recession was considered independent on density. It was observed that there is a dependency between surface recession rate and density. Consequently, an empirical method for a first estimation of the surface recession rate is required to be developed, including its dependency with the density. The recession rate of ablative materials is often expressed as an empirical function of surface temperature and material properties [4-6].

4.3 High-enthalpy heating tests performed at JAXA/ISAS

To analyze the performance or thermal behavior of LATS, it is important to carry out high-enthalpy heating tests [4-2]. In developing thermal protection systems for reentry vehicles, arc-heaters are often used to simulate reentry conditions. Arcjet type arc-heaters and segmented cathode type arc-heaters are widely used. The arcjet type has the advantage that it requires almost no maintenance after several-hours operation. Therefore, arcjet type arc-heaters are convenient for basic TPS studies [4-7].

Several heating tests were performed using the arc-heating equipment at facilities in Japan and Germany, at the Japan Ultra High Temperature Material Center (JUTEM), the Aerospace

Research and Development Directorate (ARD) of the Japan Aerospace Exploration Agency (JAXA), and Deutsches Zentrum fuer Luft- und Raumfahrt (DLR) of Germany [4-2].

The tests performed for the current study of LATS materials can be classified in three groups: the tests performed for high-density ablator material (Jutem, JAXA and DLR), the tests performed for low-density ablator material (Jutem, JAXA, DLR) and the recent tests for low density ablator material performed at JAXA, in 2014-2016. The high and low-density ablators have been tested for different flow conditions in order to prove that LATS material can perform well in different environmental conditions, no matter its density.

For the first category of tests, high-density ablators (1470 kg/m^3) have been used and the main purpose was to validate the ablators for the USERS spacecraft. 42 test pieces were tested, in very different flow conditions, the stagnation pressure varying from 0.04 to 29.8 kPa and the test duration from 30 to 300 seconds [4-2].

In case of the second group, for the low-density ablators, the virgin LATS densities were of approximately 200-1500 kg/m^3 for the JUTEM, 200-700 kg/m^3 for JAXA, and 200-600 kg/m^3 for the L3K of DLR. Under this wide range of conditions, the time courses of the surface and in-depth temperatures were acquired, where the heat flux and duration were 500 kW/m^2-11.1 MW/m^2- and the heating time durations were 10-30 s, respectively. The test conditions can be seen in the Table 4-1, where by A type are denoted the test conditions at JUTEM, by B type the test conditions at JAXA and by C type the test conditions at DLR [4-3].

Table 4-1. Flow conditions for the second group of tests [4-3]

Type	Name	ρ, g/cm^3	Δt, *s*	h, *MJ/kg*	Pst, *kPa*	Heat flux, MW/m^2
A	J3-1	0.344	150	27.4	0.533	1.0
	J3-2	0.331	150	27.4	0.533	1.0
	J5-1	0.495	150	27.4	0.533	1.0
	J5-2	0.491	150	27.4	0.533	1.0
	J5-3	0.499	150	27.4	0.853	2.0
B	A3-1	0.296	60	12.8	1.9	0.97
	A3-2	0.287	60	18.8	4.6	2.0
	A5-1	0.544	60	12.8	1.9	0.98
	A5-2	0.531	110	18.8	4.6	1.97
C	D3-1	0.341	15	14.5	19.0	5.3
	D3-2	0.296	20	14.5	47.5	8.3
	D5-1	0.566	10	14.5	47.5	8.3
	D5-2	0.536	10	14.5	85.0	11.1
	D5-3	0.561	15	14.5	19.0	5.3

In case of the third group of tests (2014-2016), on which the current study is focused on, the tests were performed at JAXA Sagamihara campus, for evaluating the performance of the ultra-lightweight ablator (LATS), manufactured and assembled at Kyushu Institute of Technology [4-2].

For measuring the cold-wall heat flux rate of the high-enthalpy airflow, a flat face cylindrical copper calorimeter and a Pitot tube that stems the airflow were used for each test. The impact pressure is the difference between the total pressure (or stagnation pressure) and the static pressure. In case of the arc heating facility of JAXA Sagamihara, its dependency with the distance from the nozzle was deduced based on several measurements made in the past, by JAXA staff. In Table 4-2, the values of the distance from the nozzle, of the heat flux and of the impact pressure are given, for the tests performed in February 2015 [4-2].

Table 4-2. Values of the distance from nozzle, heat flux and impact pressure, February 2015 [4-2]

Specimens	Distance from nozzle, mm	Heat Flux, MW/m^2	Impact Pressure, kPa
A1,B1,C1,D1	100	5	12
A2,B2,C2,D2	75	7.9	25
A3,B3,C3,D3	67	11.9	32
A4,B4,C4,D4	35	13.7	62

The surface temperature is measured using an infrared thermometer (pyrometer), which is a sensor that detects the infrared radiation from the surface of the material [4-3]. The test matrix, where the flow conditions can be seen for each test, is given in Table 4-3 [4-2]. The ablators which were used in the third group of study are of the following five types [4-2]:

- Type A : density of 300 kg/m^3;
- Type B: density of 500 kg/m^3, 1st method of manufacturing;
- Type C : density of 500 kg/m^3, 2nd method of manufacturing;
- Type D: two layers - one layer of 10 mm length, with density of 300 kg/m^3 and another layer of 20 mm length, with density of 500 kg/m^3, glued together by an epoxy-based adhesive.
- Type E: two layers - one layer of 10 mm length, with density of 300 kg/m^3 and another layer of 20 mm length, with density of 500 kg/m^3, glued together by an epoxy-based adhesive.

The two methods of manufacturing, mentioned in case of B and C models refer to the fact that they were manufactured by two different teams of workers. All the models have a diameter of about 19.9 mm and the length of the test holder is 80 mm (Fig. 4-2). In order to prevent the lateral sides of the ablator specimen against the high heat, the test piece was covered with a Bakelite sleeve. Inside the specimens, the thermocouples were installed for measuring the temperatures during the test, in the direction of the heat flow (Fig. 4-3) [4-2].

The ablator specimens are subjected directly to frontal heating during each test. The Bakelite tube is covered with inorganic cloth to reduce heating of the specimen from the side.

Minimizing in this way the lateral heating, a one-dimensional analysis becomes possible and the analytical results can be compared with the test results afterwards. According to [4-6], measurements of the weight, diameter, and thickness were taken before and after each test and these measurements are used to determine the surface recession and mass loss rate for each specimen.

There are 4 models of type A (A1, A2, A3, A4), 4 models of type B (B1, B2, B3, B4), 4 models of type C (C1, C2, C3, C4), 4 models of type D (D1, D2, D3, D4) and 4 models of type E (E1, E2, E3, E4). The models with the name having the number 1 are used for a heat flux of 5 MW/m^2, those with number 2 for 8 MW/m^2, those with number 3 for 12 MW/m^2 and those with number 4 for 13.5 MW/m^2 (Table 4-3). In case of D and E models, 2 densities are presented in Table 4-3, D and E models being composed of 2 parts of different densities. The first density which is mentioned in the table corresponds to the front layer of 10 *mm* length and the second density to the second layer of 20 *mm* length [4-2]. The structure of the ablators can be seen in Fig.4-18.

Table 4-3. Test Matrix for the tests performed in February 2015, at JAXA/ISAS [4-2]

Run	Name	ρ, g/cm^3	Δt, *s*	h, *MJ/kg*	Pst, *kPa*	Heat flux, MW/m^2
1	A2 B2 C2	0.3 0.5 0.5	15 15 15	12.98 13.16 12.97	25	8
2	D2 E2	0.8; 0.5 0.3; 0.5	15 15	12.97 13.13	25	8
3	A3 B3 C3	0.3 0.5 0.5	15 15 15	13.13 13.10 13.04	32	12
4	D3 E3	0.8; 0.5 0.3; 0.5	15 15	13.19 13.12	32	12
5	A4 B4 C4	0.3 0.5 0.5	15 15 15	12.95 13.00 12.93	62	13.5
6	D4 E4	0.8; 0.5 0.3; 0.5	15 15	13.35 13.34	62	13.5
7	C1 D1	0.5 0.8; 0.5	15 15	12.93 12.88	12	5
8	A1 B1 E1	0.3 0.5 0.3; 0.5	15 15 15	12.91 12.92 13.07	12	5

As can be seen in the Table 4-3, ablators with different densities have been tested. Fig.4-19 shows a picture from the high-enthalpy heating test and Figures 4-20, 4-21 and 4-22 show the models A4 (density of 300 kg/m^3) and C4 (density of 500 kg/m^3), tested in a high heat flux flow (13.5 MW/m^2) [4-2].

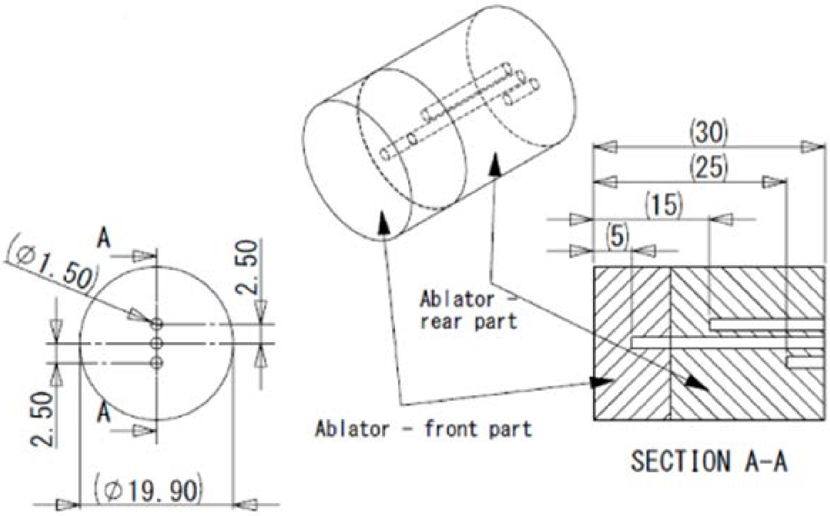

Fig. 4-18 The structure of the ablator (2 layers of 10, respectively 20 mm length for D and E models, 1 layer of 30 mm in case of A, B and C models) [4-2]

In Fig. 4-21, one can see also the char layer which was formed in the front side of the specimen. A black region (pyrolysis later) was formed between the char layer and the virgin layer [4-2].

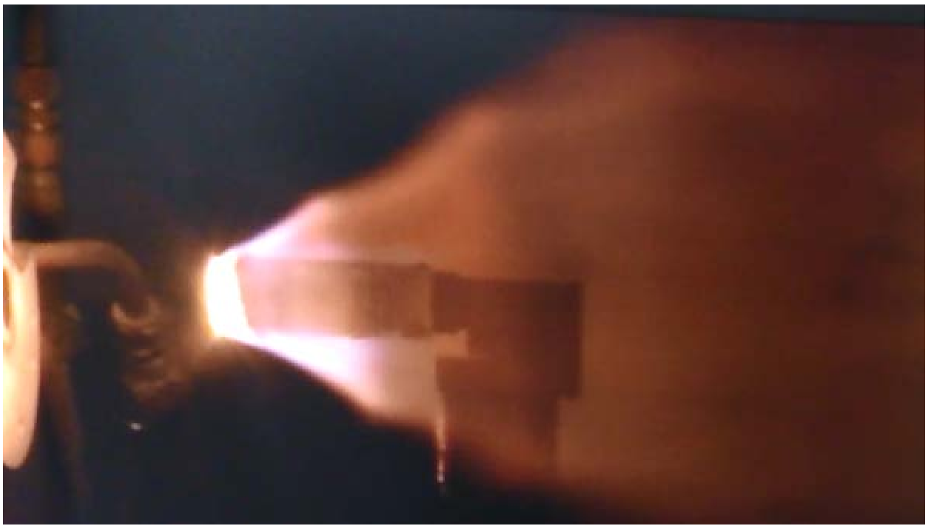

Fig. 4-19 Picture from the high-enthalpy heating tests, performed at JAXA Sagamihara campus (2015) [4-2]

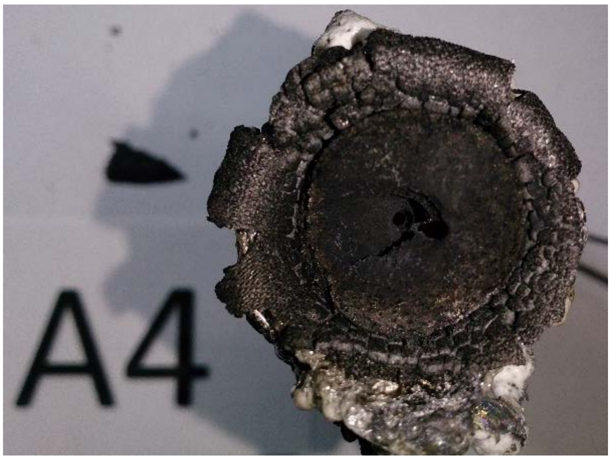

Fig. 4-20 Lowest density ablator (300 kg/m^3), after being heated with 13.5 MW/m^2 heat flux [4-2]

Thermocouples (TCs) are installed in each ablator. For A, B, and C type ablators, two thermocouples are installed for each model. For D and E ablators, three thermocouples are installed (as for E1, two TCs are installed). All TCs are installed from the rear direction along the center axis of the ablator. The surface temperature is measured using an infrared thermometer (pyrometer), which is a sensor that detects the infrared radiation from the surface of the material.

In designing the thermal protection system, the thermal behavior of the ablator for re-entry or a planetary entry of the spacecraft must be estimated [4-8]. There are several ways to study the ablative processes: by using engineering models, numerical methods (computational fluid dynamics – CFD, direct simulation Monte Carlo – DSMC, etc.), and experimental methods.

Fig. 4-21 Ablator with density of 500 kg/m^3, after being heated with 13.5 MW/m^2 heat flux [4-2]

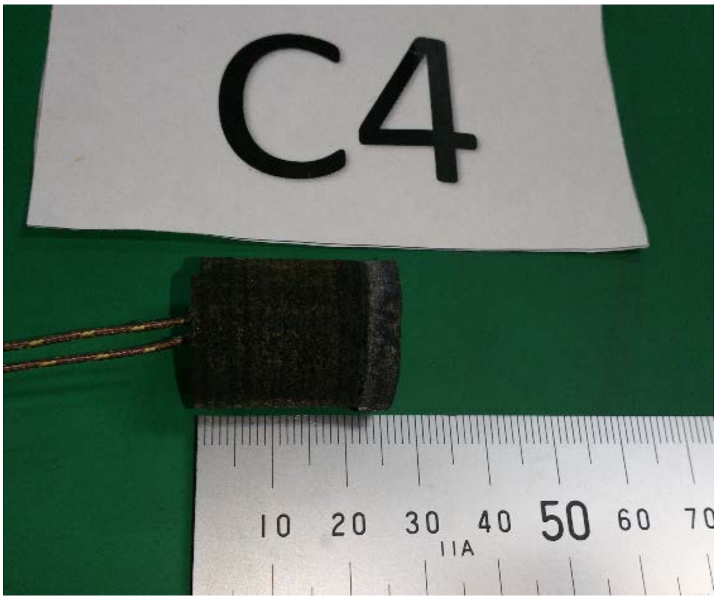

Fig. 4-22 Visualization of the char layer after the test (C4 model) [4-2]

It is difficult to simulate the re-entry environment completely with ground test facilities. For this reason, the validity of the design should be evaluated by analysis as well as tests. The validity of the thermal mathematical model used for analysis is evaluated by comparison with the ground test results based on various heating conditions. For ground tests, arc heating is mainly used. When difference arises between an analysis result and a ground test result, the thermal mathematical model must then be improved [4-9].

In order to make the ablator thin, it is desirable to reduce the effect of side heating as much as possible and to make the one-dimensional heat flow around the model as much as possible. For side heating, the temperature inside the model becomes higher than in the case of one-dimensional front heating [4-9].

With thermal test equipment, it is difficult to simulate the air density history inside the heat shield system during re-entry. In particular, the thermal conductivity (SI units: *W/m/K*) of porous materials, such as insulator and carbonized material, is greatly dependent on air density. In order to make the ablator thin, it is necessary to measure the thermal conductivity of the porous material with high accuracy [4-9].

4.4 New method for estimating the surface recession rate

Since LATS contains a resin that undergoes thermal decomposition by heating, classical methods for estimating recession cannot be applied to them. In the present research, empirical correlations for the surface recession rate were determined. A new curve-fit exponential equation was deduced for estimating the surface recession rate of the carbon-phenolic ablation in air, by taking into consideration its dependency with the surface temperature and density, using the measured data from the high-enthalpy heating facilities of the German Aerospace

Center (DLR, Germany), Japan Ultra High Temperature Material Center (Jutem, Japan) and Japan Aerospace Exploration Agency (JAXA, Japan) [4-2].

By using an empirical estimation of the surface recession rate, considering different heat fluxes and densities, the decision on the thickness of the ablator can be made quickly [4-2].

As noted in [4-2], the last results of the tests performed at JAXA Sagamihara in 2015 fit very well with the results of the older tests, made in the past, at Jutem, JAXA and DLR, regarding the relation between the surface temperature and the heat flux, which can be seen in Fig. 4-23. The temperatures values show that the LATS specimens heated under the specified conditions of Table 4-3 reached approximately 2000 – 3500 *K* at the surface, most of these temperatures being in the diffusion-controlled oxidation region (1500 – 3000 *K*).

A linear dependency between the measured mass loss rate and $\sqrt{P_{st}/R_B}$ can be established for the diffusion controlled oxidation region. For the previous tests, the slope of the linear function was found to be $2.0 \times 10^{-4}\ \sqrt{kg}/m$ for low density LATS materials [4-7]. Comparing the results of the last tests at JAXA Sagamihara with the previous tests (Fig. 4-24 and Fig.4-25), the dependency can still be established using the new test results from 2015, and the found slope has the same value of $2.0 \times 10^{-4}\ \sqrt{kg}/m$.

In case of the surface recession rate, an empirical method could be established, taking into consideration its dependency with the density. In Fig. 4-26, there can be seen the relationship between the product of surface recession rate and density with the surface temperature for different tests performed with high and low-density LATS materials and, in Fig. 4-27, an exponential dependency can be clearly seen. *Ldot* is the symbol for the surface recession rate, measured in m/s and *ρ(char)* is the char density, measured in kg/m^3 [4-2].

The new equation that can be written for estimating the surface recession rate is the following:

$$Ldot = 0.0872 \times (e^{0.0021 \times T}/\rho(char)) \tag{4-2}$$

where *Ldot* is the surface recession rate, *e* is the base of the natural logarithm, *T* is the surface temperature and *ρ(char)* is the char density of the ablator. As mentioned also in [4-2], the surface recession has an exponential dependency with the surface temperature and an indirect proportionality with the density, having low values for high-density LATS materials and high values for low density LATS materials.

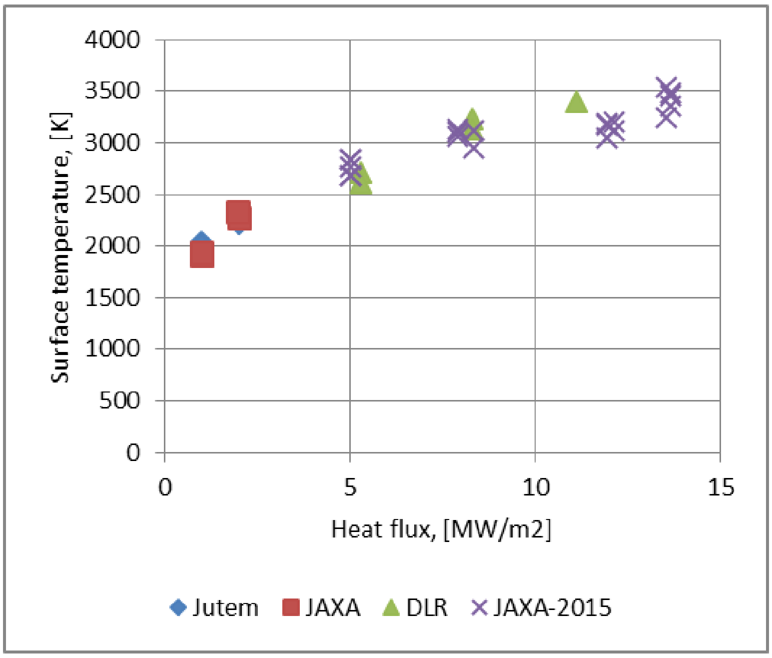

Fig. 4-23 Dependency of Surface Temperature with the Heat Flux for low-density LATS materials [4-2]

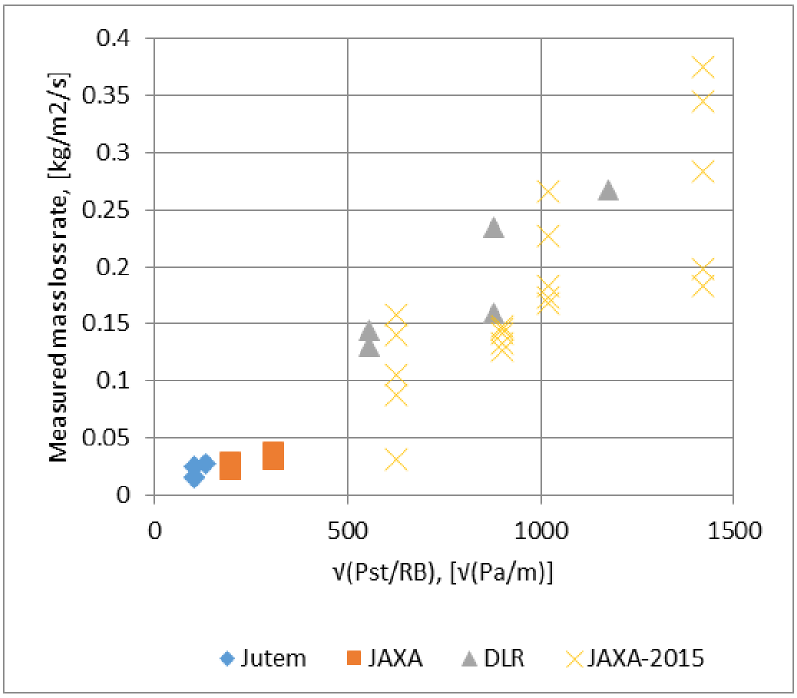

Fig. 4-24 Relationship between total mass loss rate and $\sqrt{P_{st}/R_B}$ of low-density LATS materials: distribution for different tests performed at Jutem, JAXA and DLR [4-2]

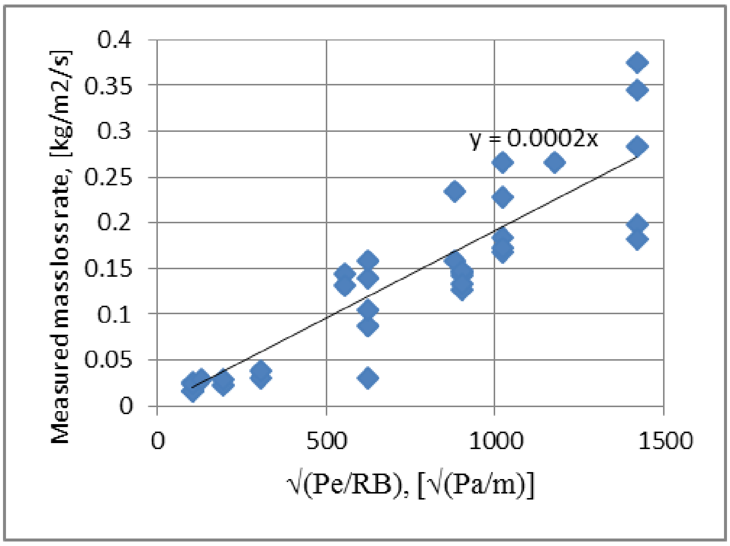

Fig. 4-25 Relationship between total mass loss rate and $\sqrt{P_{st}/R_B}$ of low-density LATS materials: linear dependency

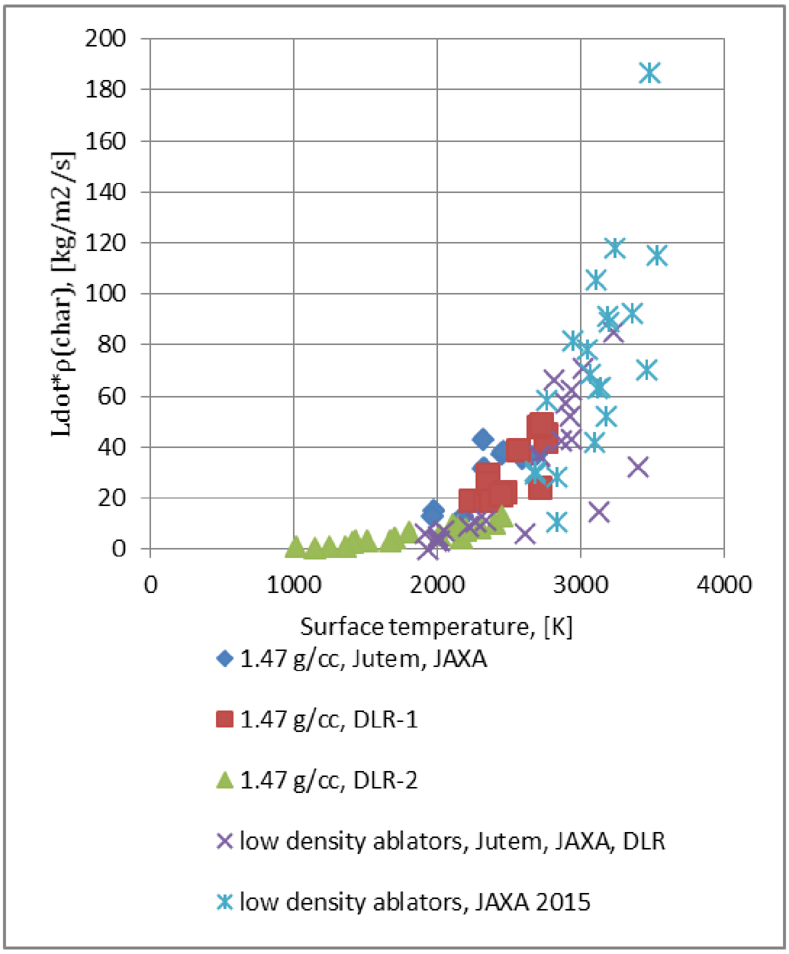

Fig. 4-26 Relationship between $Ldot \times \rho(char)$ and the surface temperature in case of high and low density LATS materials: distribution for different tests performed at Jutem, JAXA and DLR [4-2]

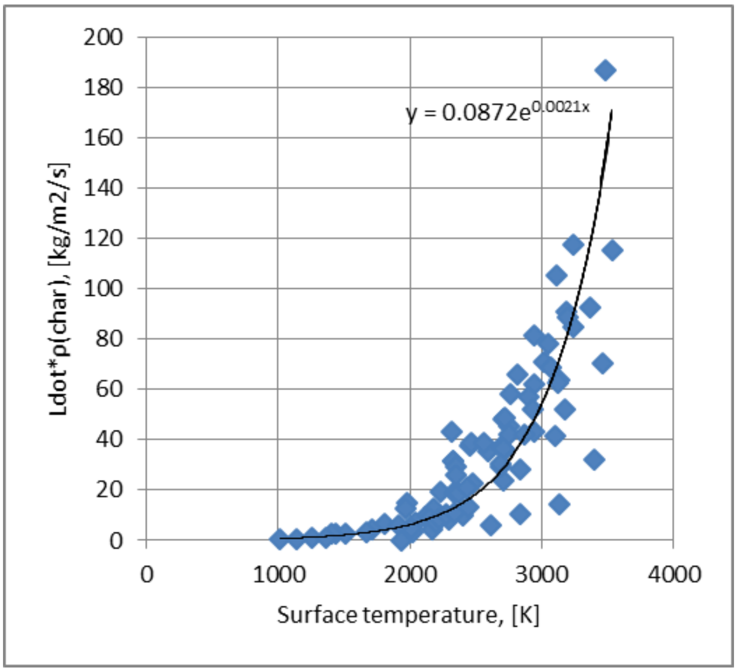

Fig. 4-27 Relationship between $Ldot \times \rho(char)$ and the surface temperature in case of high and low density LATS materials: the exponential dependency [4-2]

4.5 Main test results from the high-enthalpy tests for LATS materials

4.5.1 Test results of September 2015 campaign

Another study with LATS materials was performed in September 2015, for the Australian reentry vehicle (MERS) for which LATS materials will function as heat shield materials. In case of MERS spacecraft, it will have Aluminum parts installed behind the thermal shield, for a better protection of the payload (micro-gravity experimental module).

The purpose of these tests is to check the temperatures inside the ablator for 12 MW/m^2 (reentry heat flux) and also the temperatures behind the Aluminum structure (big Aluminum part for A models and small Aluminum part for B model). Also, the recession phenomenon is studied. Two of the models had solar cells mounted in front of the models A1 and A2. Another purpose of the tests was to evaluate the side heating effects by using models made only by Bakelite.

There are 7 models of type A (A1, A2, A3, A4, A5, A6, A7), 7 models of type B (B1, B2, B3, B4, B5, B6, B7), 3 models of type C (C1, C2, C3). The model A represents a more realistic model of the MERS's thermal shield, the model B is used for a better comparison with the 1-dimensional ablation analysis, the models C are tested in order to analyze the side-heating effects.

The A and B models are represented in the Fig.4-28 and Fig.4-29.

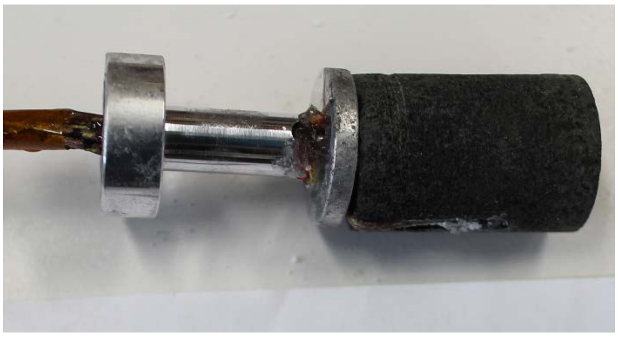

Fig.4-28 A model

Fig.4-29 B model

The test conditions are represented in the Table 4-4.

The temperatures history for an A model can be seen in the Fig.4-30. The first thermocouple, TC1, was installed at about 10 mm from the surface, the second thermocouple, TC2, at 20 mm from the surface and the third and fourth thermocouples, TC3 and TC4, at 30 mm from the surface.

A jump in temperatures can be seen for the front thermocouples (TCs). Regarding the TC signals, it might be because of the water evaporation (at around 100 degrees Celsius). The phase transition of the water inside the ablator influences the heat transfer.

One of the goals of the arc heating tests was to measure the temperatures around the Aluminum body. The averaged values for the temperatures are given in the Table 4-5.

Table 4-4 Test conditions for September 2015

Run	**Models**	**Δt (s)**	**Heat flux (MW/m^2)**	**No. of TCs**	**ρ (g/cm^3)**	**Solar cells**
1	C1, C2, C3	15	8	4 for each model	-	X
2	A5, B5	15	8	8 for A and 4 for B	0.7	X
3	A6, B6	15	8	8 for A and 4 for B	0.7	X
4	A7, B7	15	8	8 for A and 4 for B	0.5	X
5	A1, B1	15	12	8 for A and 4 for B	0.7	○
6	A2, B2	15	12	8 for A and 4 for B	0.7	○
7	A3, B3	15	12	8 for A and 4 for B	0.5	X
8	A4, B4	15	12	8 for A and 4 for B	0.7	X

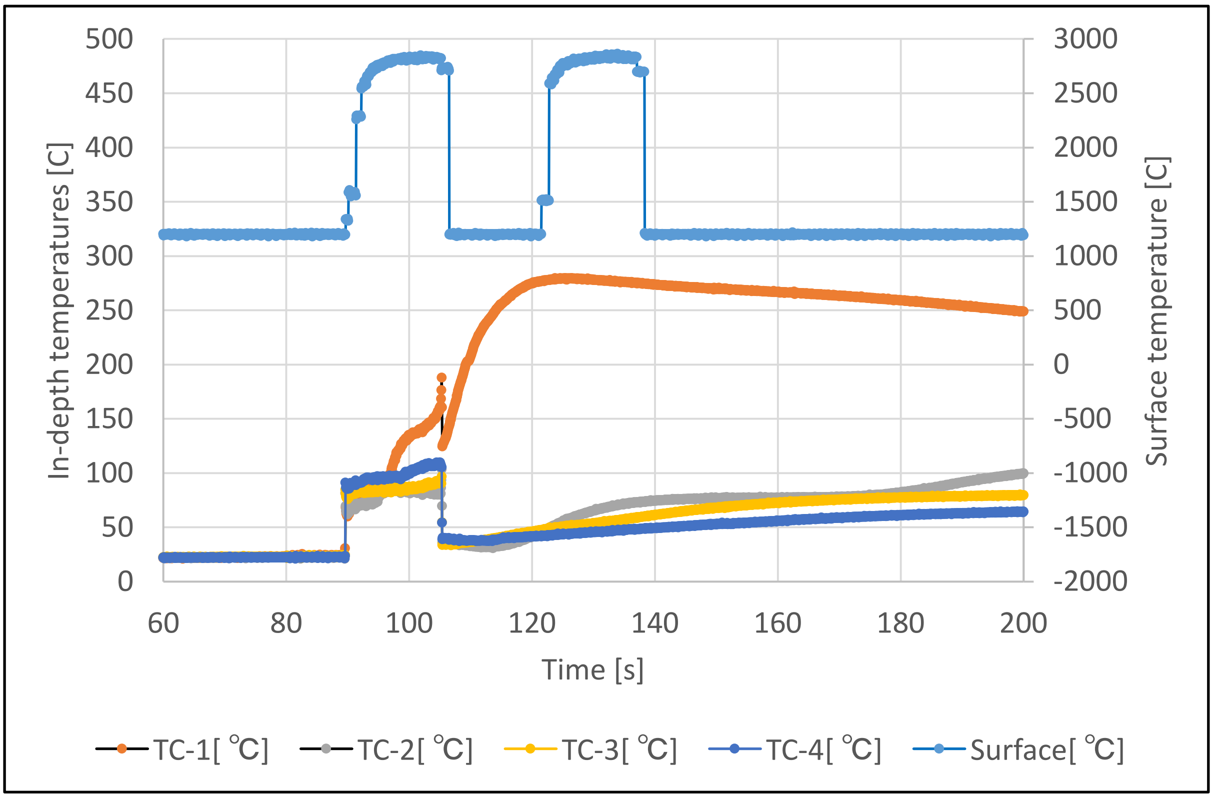

Fig.4-30 Temperature history for A1 model

Table 4-5 Average temperatures around Aluminum part

Average temperature at the bottom of the ablator	Average temperature around Aluminum body	Average temperature at the bottom of Aluminum part
99.22	94.24	91.93

Regarding the study of the side-heating effect, C models were used and they were made entirely by Bakelite material (Fig.4-31).

Fig.4-31 C model

In case of C models, 4 thermocouples were installed for each model, positioned at a distance from the surface of 10, 20 and 30 *mm* for C1, C2, respectively C3. The results in temperatures can be seen in the Table 4-6 and also the temperatures history for C1 model are shown in Fig.4-32. The temperatures near the lateral side are visible higher than the ones in the center and this is due to the side heating effects.

Table 4-6 Average temperatures inside C models

	Distance from the surface (*mm*)	Temperature in the center of Bakelite (°C)	Temperature (°C), in the middle of Bakelite, 7 *mm* from the wall	Temperature (°C), on the lateral side of Bakelite, at 2 *mm* from the wall
C1-9/15	10	152.63	169.41	210.09
C2-9/15	20	128.23	126.15	167.64
C3-9/15	30	97.30	93.80	106.60

Another study performed during the arc heating tests of September 2015 was to see the behavior of the ablator when it has solar cells mounted on the front surface (Fig.4-33).

The temperature history, for a model with solar cells (A2), is shown in the Fig.4-34. The model was tested at 15 MW/m^2, 15 seconds and the ablator had a density of 720 kg/m^3. The first thermocouple, TC1, was installed at 10 mm from the surface, the second and the third, TC2 and TC3, were installed at 20 mm from the surface, the fourth, TC4, at 30 mm from the surface and the other thermocouples were installed around the Aluminum body.

The solar cells were melted during the test and has disappeared completely. One interesting observation was that the pyrolysis gas was ejected suddenly when the solar cells melted and this lead to a sudden increase in temperatures at 1 cm from the surface in the moment of melting of the solar cell.

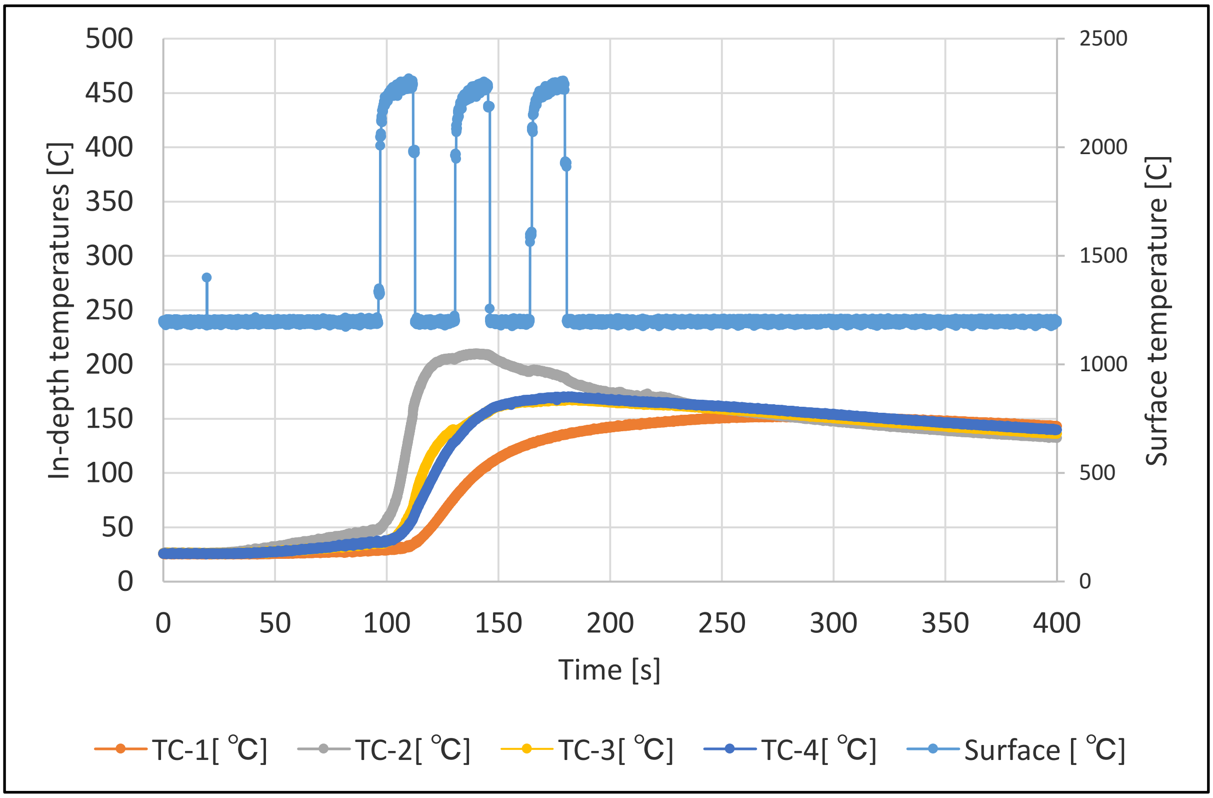

Fig.4-32 Temperatures history for C model

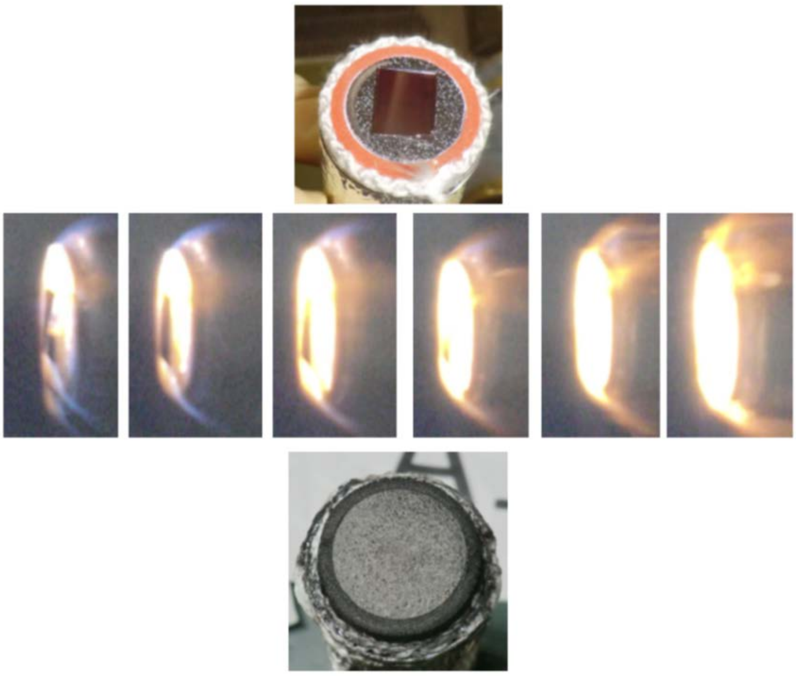

Fig.4-33 Ablator model with solar cell mounted on its front surface

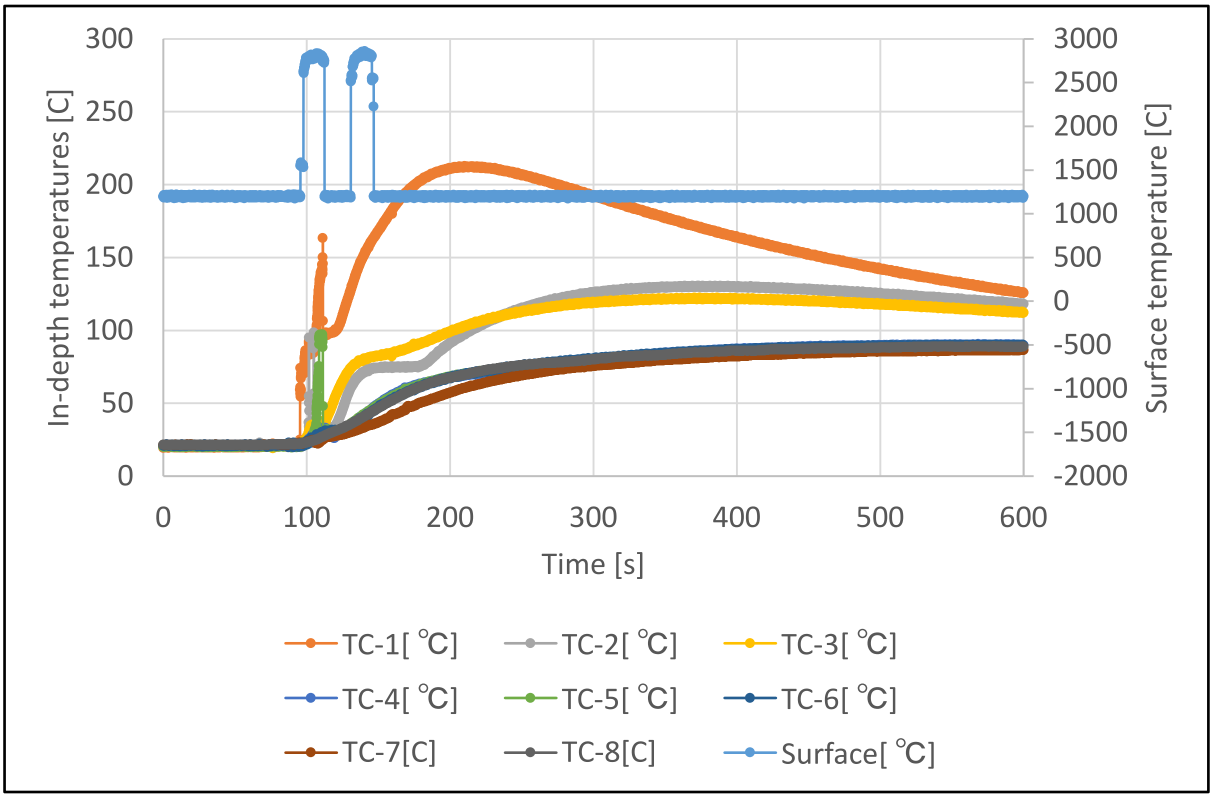

Fig.4-34 Temperature history for A2

4.5.2 Test results of March 2016 campaign

The main objectives of the tests performed on March 2016 were: 1) to test ceramic coating; 2) to compare the results between the case of using specimens with ring (mushroom type) and the case without ring (or cylinder type).

8 test pieces were tested for the study of ceramic coating: 2 without coating (models A1 and A2), 2 with x type of ceramic coating (models A3 and A4), 2 with y type of ceramic coating (models A5 and A6) and 2 with z type of ceramic coating (models A7 and A8).

Each of the test model had 2 thermocouples installed inside them: the first thermocouple at a distance between 7.9 to 11.3 mm from the surface and the second thermocouple at a distance between 13.1 to 16.2 mm from the surface.

The outline of the tests for A models can be seen in Table 4-7. The A models have high density (between 1430 and 1520 kg/m^3) and were tested for very low heat flux (less than 1 MW/m^2). The heat flux couldn't have been measured due to the setting of ISAS facility (the distance from the nozzle was too big, 200 mm, and the calorimeter equipped with sensor to read the heat flux couldn't have been used). A1, A3, A5, A7 models were tested together in the first run and A2, A4, A6, A8 were tested in the second run, A1 being almost identical with A2, A3 with A4, A5 with A6 and A7 with A8. For the first run, the test duration was about 60 seconds and for the second run the duration was 2 seconds. Because the duration was high for the first run (60 seconds), the surface coating disappeared in most of the cases. For the second run (low time duration of 2 seconds), the differences between the surface aspect before the test and after the test were minimal. A detailed analysis of the surface aspects will be done by Tocalo company.

Table 4-7 Outline of the tests for A models

Model	Type of coating	Density g/cm^3	Heat flux MW/m^2	Duration (s)	Distance between TC1 and surface (mm)	Distance between TC2 and surface (mm)
A1	No coating	1.43	<1	60	7.9	
A2	No coating	1.43	<1	2	11.2	13.5
A3	X type coating	1.44	<1	60	11.3	13.1
A4	X type coating	1.44	<1	2	10.0	16.2
A5	Y type coating	1.43	<1	60	10.1	15.9
A6	Y type coating	1.44	<1	2	9.4	20.3
A7	Z type coating	1.52	<1	60	8.4	15.4
A8	Z type coating	1.48	<1	2	8.3	15.5

Regarding the thermal behavior of the test models, in Fig.4-35. One can see a comparison between the temperature history of the first TC for A1, A3, A5 and A7 models. In Fig.4-36, the temperature history of the second TC is presented, for A5 and A7 models (the second TCs of A1 and A3 were accidentally removed, during assembly before the tests). In case of A2, A4, A6, A8, the time was too short (2 seconds) for a relevant study of the temperature history.

Analyzing the thermal behavior of the test models from Fig.4-35 and 4-36, it can be seen that the model without coating (A1) had a higher internal temperature than the models with coating and the difference was more than 100 degrees Celsius. Also, comparing the model with Y type coating (A5) with the one with Z type coating (A7), it can be seen that the model with Z type coating behaved better, having a lower in-depth temperature, but this difference can be also due to the higher density of Z type coating model.

At the high enthalpy tests performed at ISAS in March 2016, 2 different shapes of ablator have been used: cylinder and mushroom shape. The structure of the ablators of mushroom type can be seen in Fig.4-37 and the structure of cylinder type in Fig.4-38.

B1, C1 and D1 models had a mushroom shape and B2, C2 and D2 models had a cylinder shape. The outline of these specimens can be seen in Table 4-8, where d represents the distance in mm from the surface of the thermocouples. 3 thermocouples were installed in each model.

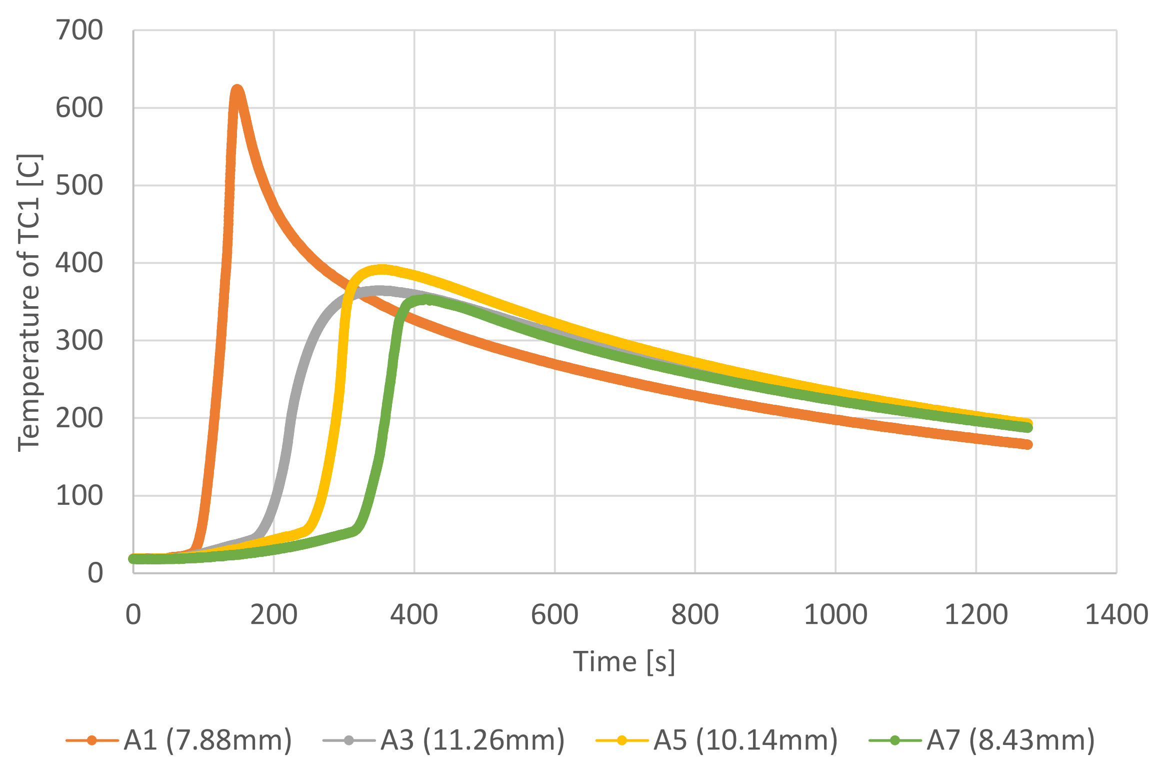

Fig. 4-35 Temperature history for TC1 of A1, A3, A5 and A7 models

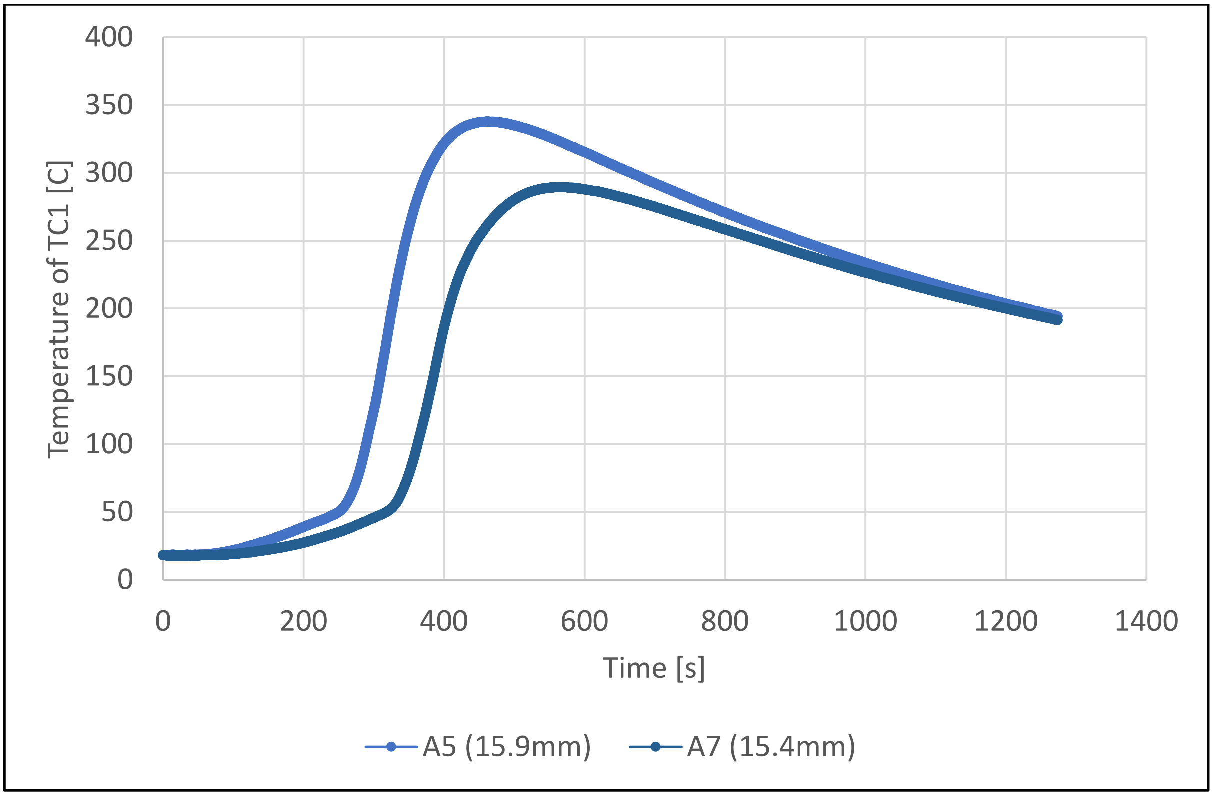

Fig. 4-36 Temperature history for TC2 of A5 and A7 models

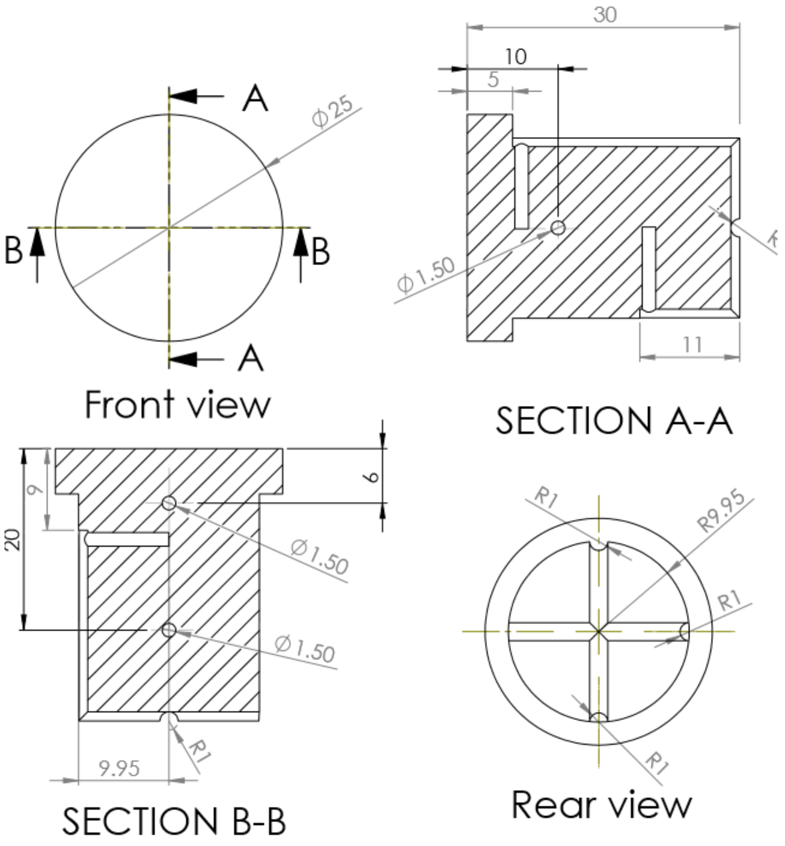

Fig.4-37 Mushroom type of the ablator specimen

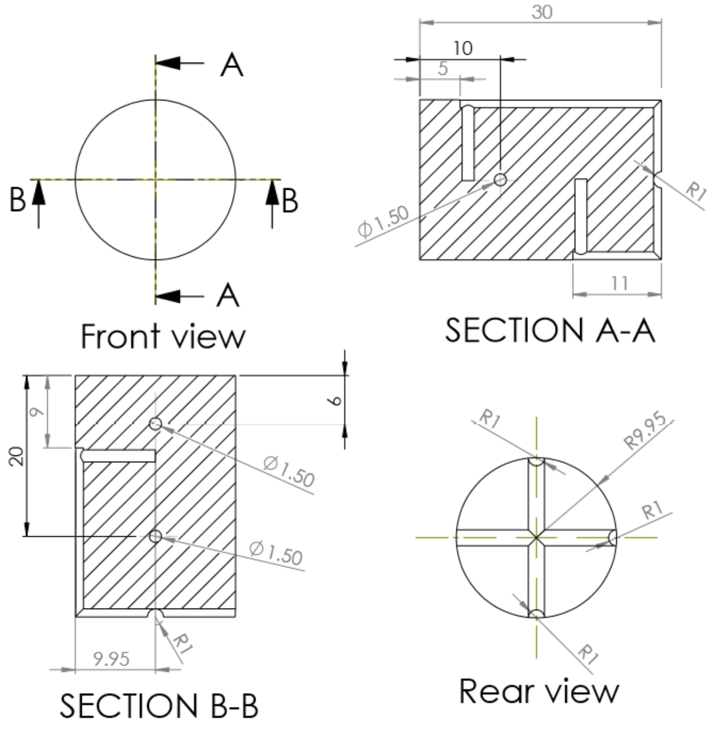

Fig.4-38 Cylinder type of the ablator specimen

Table 4-8 Outline of B, C and D models

Model	Type	Density g/cm^3	Heat flux MW/m^2	Duration (s)	d (mm) for TC1	d (mm) for TC2	d (mm) for TC3
B1	mushroom	0.36	7.5	30	8.5	12.3	20.7
B2	cylinder	0.44	7.5	30	7.9	8.2	19.1
C1	mushroom	0.54	7.5	30	6.7	9.6	19.7
C2	cylinder	0.55	7.8	30	4.9	8.9	18.7
D1	mushroom	0.76	7.5	30	6.1	10.1	17.3
D2	cylinder	0.75	7.8	30	6.3	9.8	20.7

Since B1 and B2 have a difference in density of about 0.08 g/cm^3, they will not be compared with each other. Also, their first TCs are located at a different distance from the surface than C and D models.

The differences in thermal response between C1, respectively D1 (mushroom type) and C2, respectively D2 (cylinder type) can be seen in Fig.4-39 and Fig.4-40 (temperature history only for TC3, because TC1 and TC2 read very high temperatures and gave erroneous data). There can be seen that for the mushroom type, the temperatures are higher, which is unexpected. Many factors can affect the temperature measurements. Some of these factors can be the gap between the ablator ring and the Bakelite in case of the mushroom type or the gap between the ablator and the Bakelite. More studies are recommended. Also, a numerical simulation should be done and the numerical results for the temperatures should be compared with the experimental results of both types (mushroom and cylinder types).

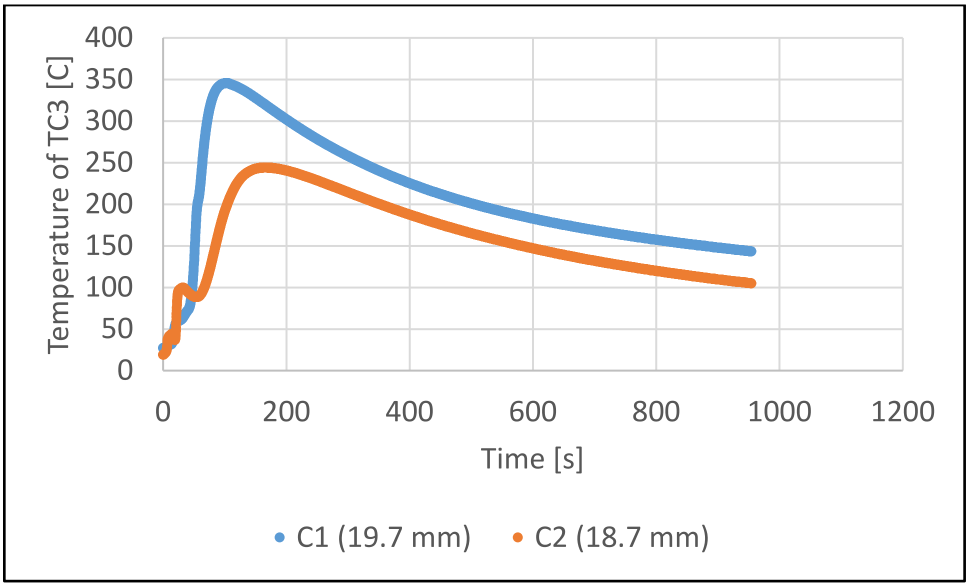

Fig.4-39 Temperature history for TC3 of C1 model (mushroom type) and C2 model (cylinder type)

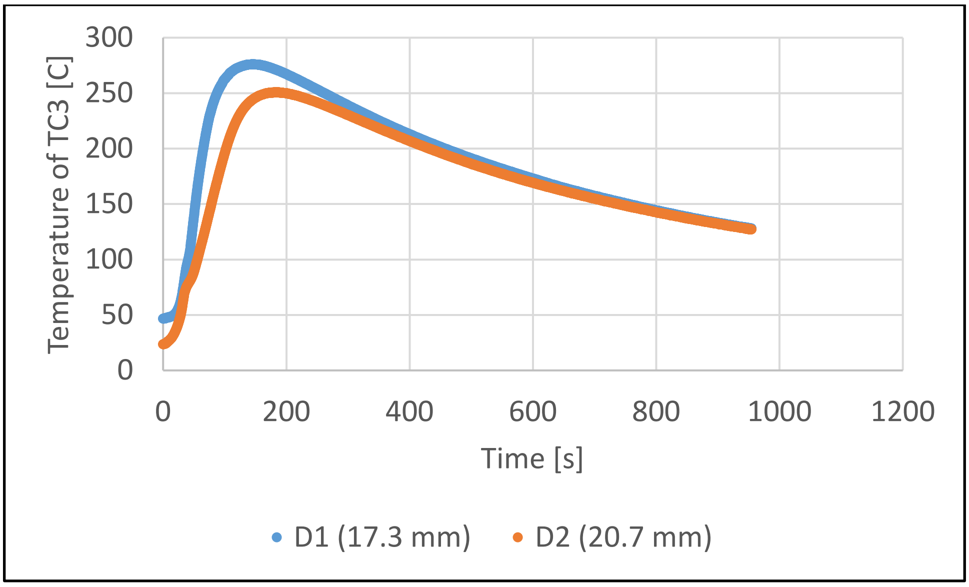

Fig.4-40 Temperature history for TC3 of D1 model (mushroom type) and D2 model (cylinder type)

4.5.3 Test results of June 2016 campaign

The main objectives of the tests performed on June 2016 were: 1) to study the Re-entry blackout transmission signal during the arc heating tests; 2) to study the thermal performances of the LATS material (2D and 3D); 3) to study the thermal performances of the PEEK material; 4) To compare the results between 3D, 2D LATS, PEEK material and the hybrid models. The present study concentrates on the last three objectives.

The types of ablators used in the June 2016 campaign are presented in the Fig.4-41 and the test conditions in Table 4-9.

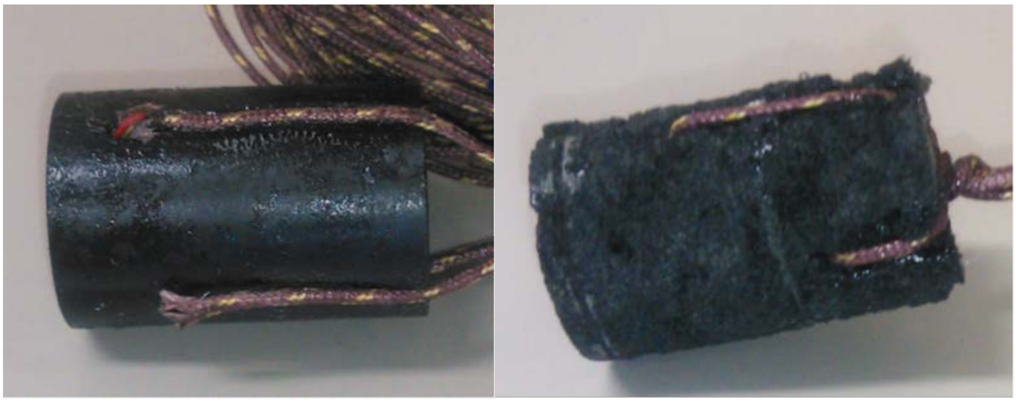

(a) PEEK (D models)

(b) 3D LATS (E models, F3 model)

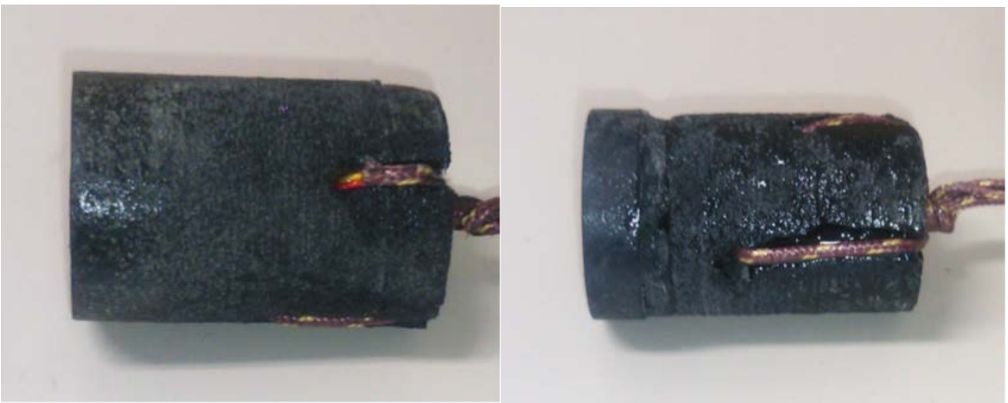

(c) 2D LATS (F4 model)

(d) PEEK+3D LATS (C models)

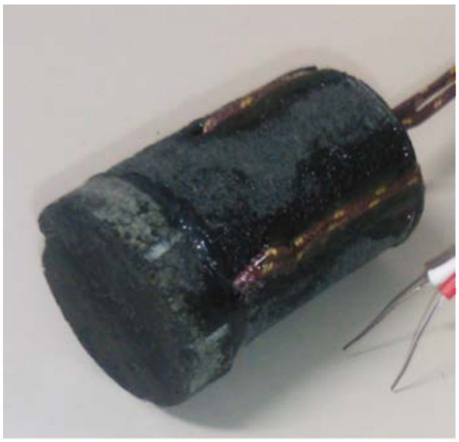

(e) 3D+2D LATS (F1 model)

Fig.4-41 The ablator specimens used in the June 2016 campaign

Table 4-9 The test conditions for the June 2016 campaign

Model	**Material**	**Density of the first layer (g/cc)**	**Density of the second layer (g/cc)**	**Heat flux (MW/m2)**	**Heating time (s)**
C1	PEEK+3D	1.410255	0.656635	4.5	32.2
C2	PEEK+3D	1.411404	0.710386	9.8	31.4
C3	PEEK+3D	1.410463	0.758238	15.75	22.2
C4	PEEK+3D	1.419684	0.620843	4.6	62.2
C5	PEEK+3D	1.41518	0.739856	8.1	32.2
C6	PEEK+3D	1.414236	0.737572	15.75	12.2
D1	PEEK	1.410116		4.5	32.2
D2	PEEK	1.410864		9.8	61.2
D3	PEEK	1.411178		15.75	42.6
D4	PEEK	1.407264		4.6	62.2
D5	PEEK	1.409332		8.1	61.2
D6	PEEK	1.410237		15.75	11.4
E1	3D	0.521106		4.5	32
E2	3D	0.421179		9.8	24.4
E3	3D	0.495469		15.75	11
E4	3D	0.63784		4.6	31.8
E5	3D	0.601717		8.1	21.6
E6	3D	0.705515		15.75	11.4
F1	3D+2D	0.903609	0.584034	15.38	11.8
F3	3D	0.666647		15.38	12.8
F4	2D	0.725483		15.38	12.8

The maximum values of the measured temperatures during the test, for the surface and the thermocouples installed inside the specimens are shown in Table 4-10.

The functions between the surface and mass recession rates with the $\sqrt{P/RB}$ and the heat flux are given in the Fig. 4-42 to Fig.4-47.

Table 4-10 The temperature results in maximum values, from the June 2016 campaign

Model	Surface temperature (C)	Temperature at 5-10 mm (C)	Temperature at 10-15 mm (C)	Temperature at 15-20 mm (C)	Temperature at 20-25 mm (C)
C1	2481.219	695.4	45.5	28	
C2	2615.014		111	39.5	
C3	2843.8		405.1	61.5	33.9
C4	2500.498		744.7		96
C5	2650.839		89.7	66.4	31.3
C6	2683.326		56.4		26.4
D1	2416.816	408.3		40.8	39.7
D2	2685.725			365.1	
D3	2752.605				144.6
D4	2540.269	1297.6		186.2	111.2
D5	2626.839			135.8	83
D6	2778.838	76.9	35.2	30.1	29.2
E1	2317.751		920.3		99.4
E2	2727.767			1039.8	
E3	2718.734				
E4	2244.938		631.8		120.4
E5	2477.47		646.8	96.7	
E6	2859.828	108.7		163.7	109.9
F1	2890.51	1244.5	110.2	87.4	
F3	2727.1	1243.3	73.1		
F4	2661.791	1226.4	87.9	28.7	

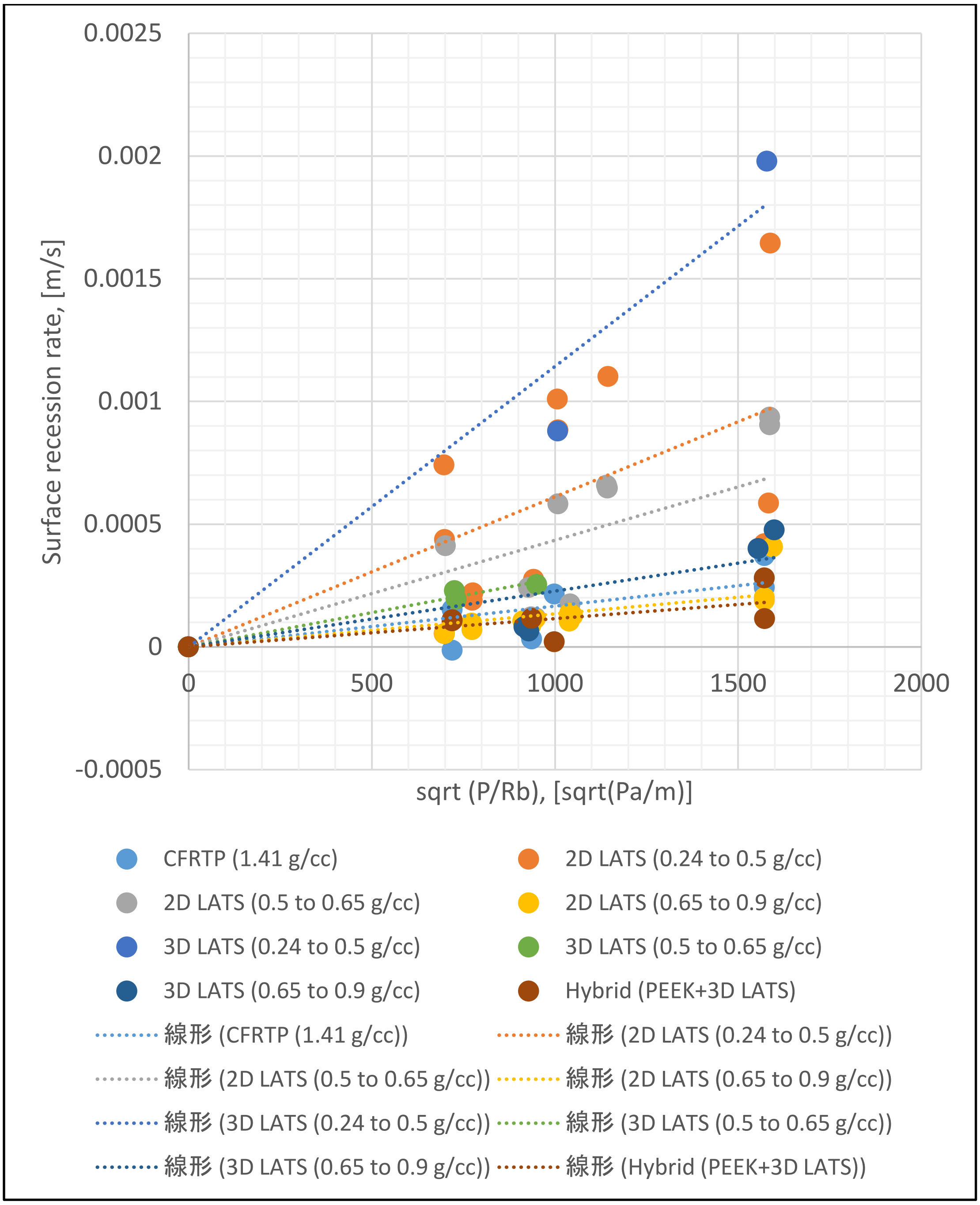

Fig. 4-42 Dependency of surface recession rate with $\sqrt{P_e/RB}$ for CFRTP, 2D LATS and 3D LATS

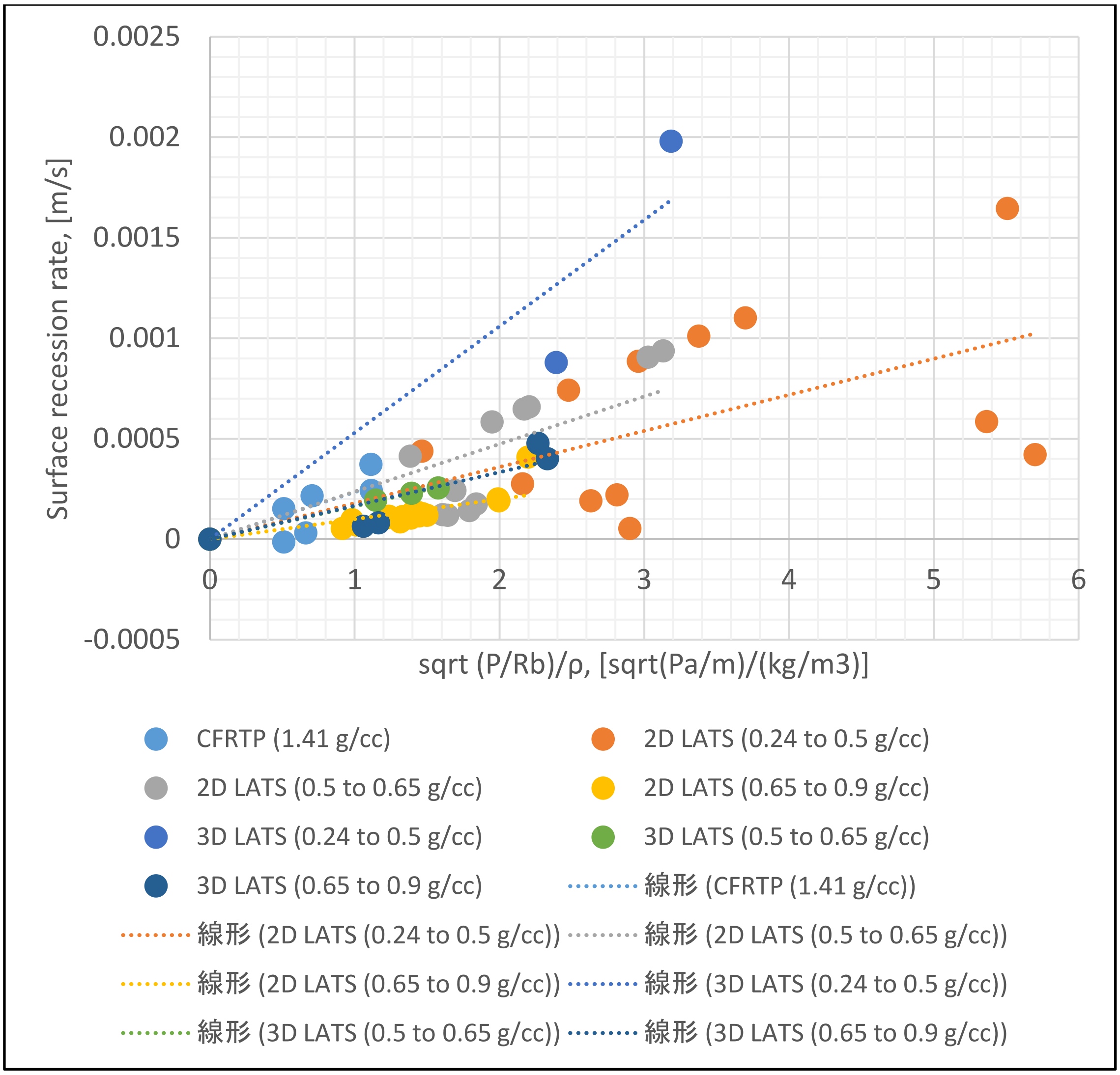

Fig. 4-43 Dependency of surface recession rate with $\sqrt{P_e/RB}\,/\rho$ for CFRTP, 2D LATS and 3D LATS

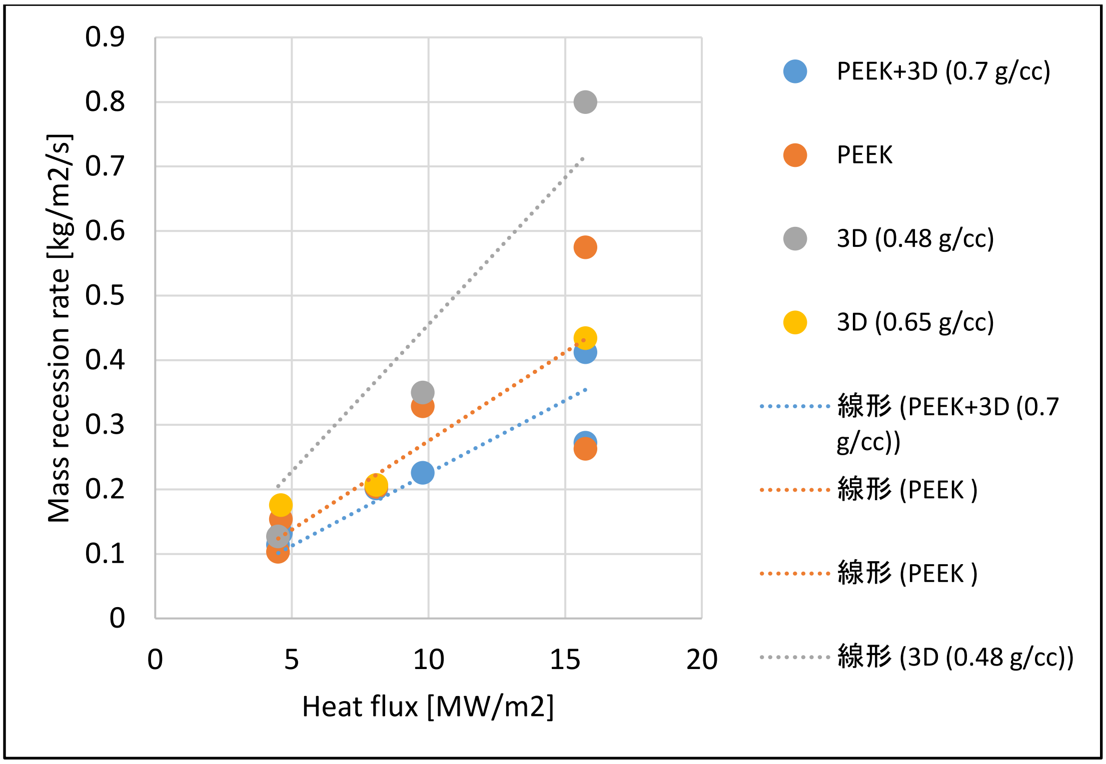

Fig. 4-44 Dependency of mass recession rate with $\sqrt{P_e/RB}$ for CFRTP, 2D LATS and 3D LATS

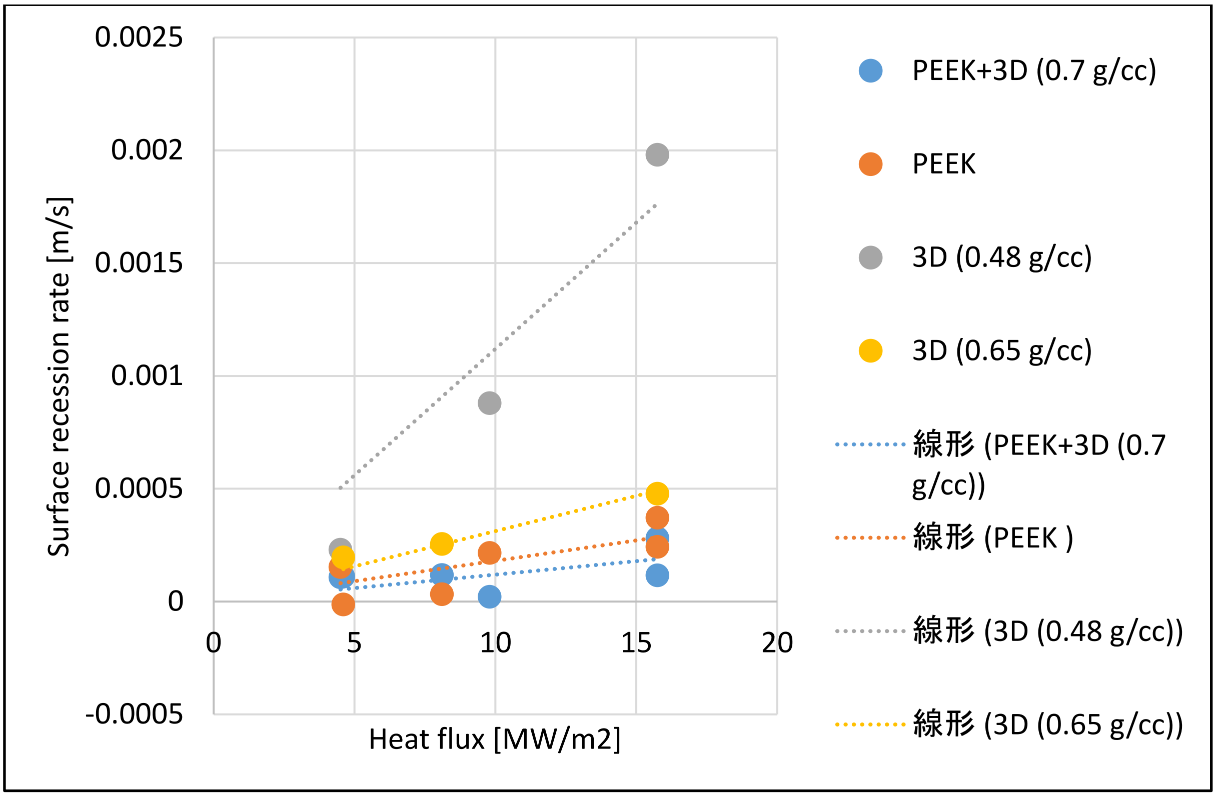

Fig. 4-45 Dependency of surface recession rate with the heat flux for PEEK+3D, PEEK and 3D LATS

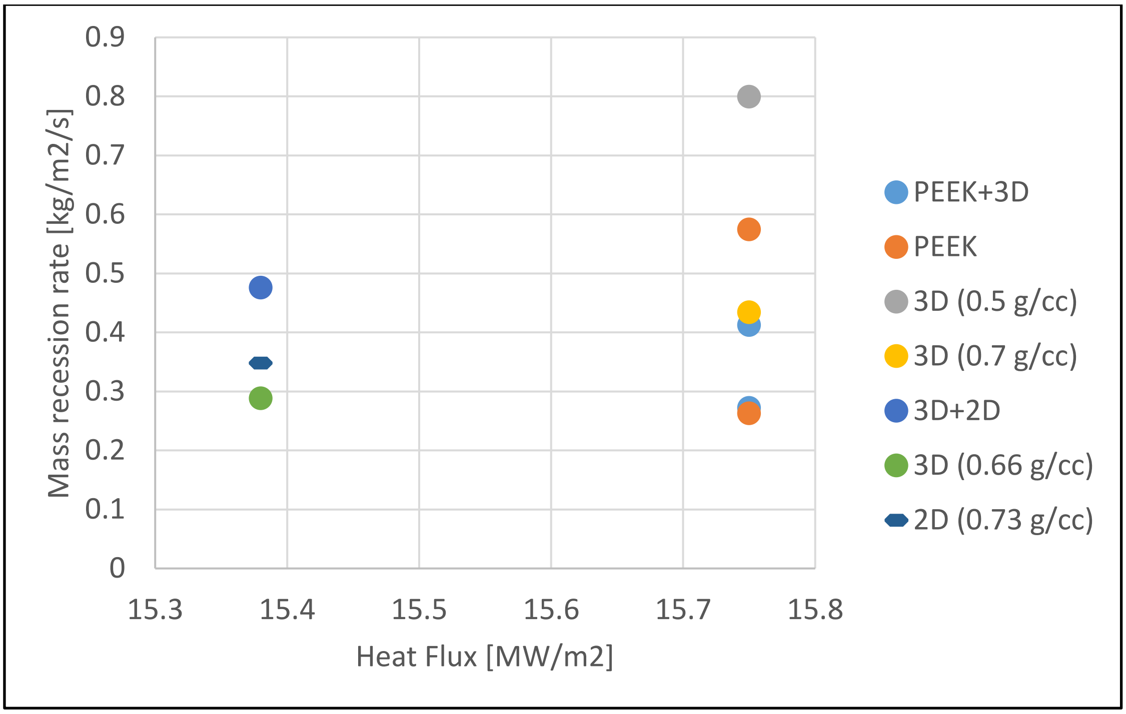

Fig. 4-46 Dependency of mass recession rate with the heat flux for PEEK+3D, PEEK, 3D+2D, 3D and 2D LATS

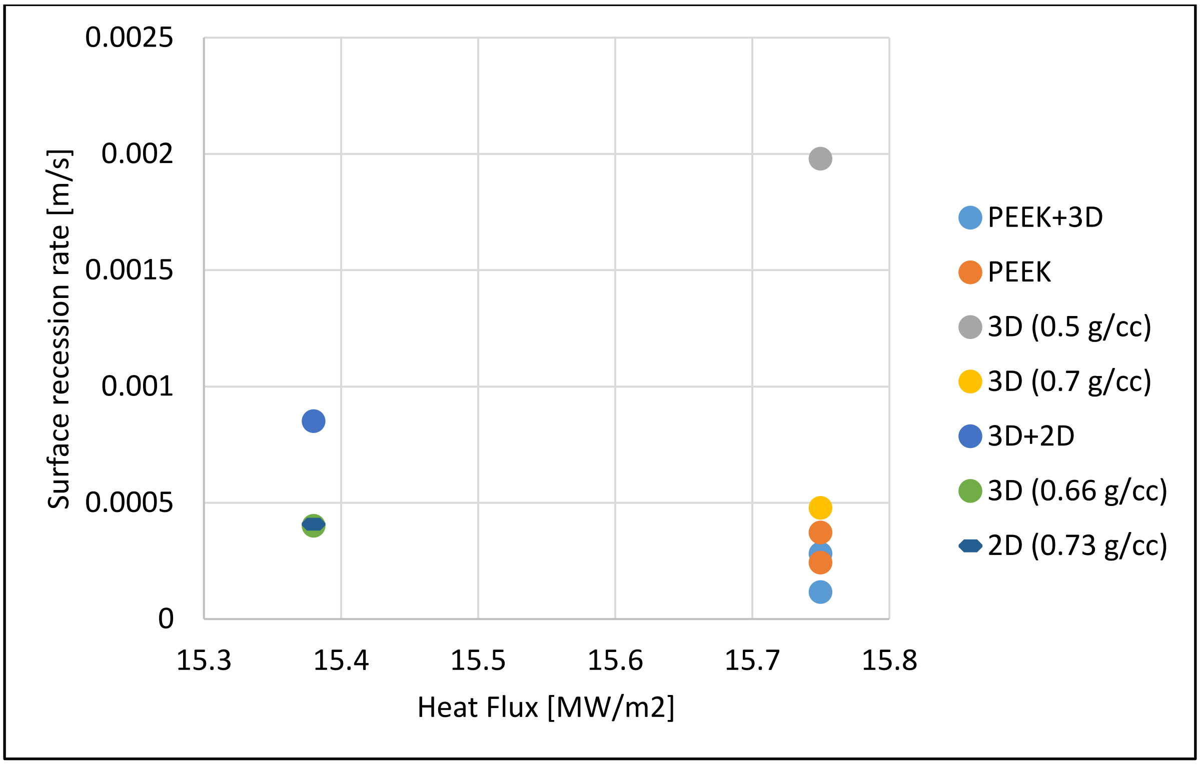

Fig. 4-47 Dependency of surface recession rate with the heat flux for PEEK+3D, PEEK, 3D+2D, 3D and 2D LATS

It can be observed that the lowest recession rates and in-depth temperatures are those of PEEK and PEEK+3D ablators (D and C models) and their values are similar. Regarding 3D and 2D LATS, they have similar recession rates; the hybrid model (3D+2D) has lower recession rate than 3D or 2D. Also, as expected, the in-depth temperatures of low density-ablators are higher than those of high density-ablators.

4.6 Numerical analysis model of ablation phenomenon and its validation

In the process of designing a thermal protection system made by ablative materials, it is important to have a reliable numerical procedure to compute the recession or in-depth temperatures history [4-1].

In the present subchapter, the experimental results from the high enthalpy heating tests performed at JAXA, Sagamihara campus are compared with the numerical results, obtained using an ablation code developed at Ryukyus University, Japan. The comparison will provide a better understanding regarding the accuracy of the ablation code and the results confirm that the CFRP-based Ablator LATS behaves well when heated in a high-enthalpy flow [4-10].

The mathematical model for the charring ablation is described in [4-11]. Some of the basic assumptions are [4-11]:

(a) the heating is one-dimensional and unsteady;

(b) One layer or two layers ablator model can be modeled;

(c) The pyrolysis gas generated in the ablator is ejected through the surface, without remaining inside the ablator.

(d) After being released, the pyrolysis gas is chemically inert with respect to the gas in the boundary layer.

(e) the char layer of ablator is assumed to be composed only by carbon, and the surface recession depends only on the oxidation and sublimation.

In the code, several basic equations are implemented. One of them is the in-depth energy equation of the ablator which is expressed in [4-12,4-13,4-14,4-15]:

$$\rho C_p \left(\frac{\partial T}{\partial t}\right)_x = \frac{\partial}{\partial x}\left(k\frac{\partial T}{\partial x}\right)_t + \Delta h_{pyro}\left(\frac{\partial \rho}{\partial t}\right)_y + \dot{S}\rho C_p\left(\frac{\partial T}{\partial x}\right)_t + \dot{m}_g\left(\frac{\partial h_g}{\partial x}\right)_t \tag{4-3}$$

In the equation above, x is the coordinate with the origin fixed to the surface which moves due to the surface recession, y is the coordinate with the origin fixed to the ablator surface before heating, ρ is the density (kg/m^3), T is the temperature (*K*), k is the thermal conductivity (*W/m/K*), C_p is the specific heat (*J/kg/K*), t is the time (*s*), Δh_{pyro} is the heat of pyrolysis per produced gas of unit mass (*J/kg*), $\dot{S}$ is the surface recession rate (*m/s*), $\dot{m}_g$ is the gas flow rate ($kg/m^2/s$) (mass flux) and h_g is the enthalpy of the pyrolysis gas (*J/kg*). k and C_p is calculated by [4-11]:

$$k = k_v\omega + (1-\omega)k_{ch}; \quad \omega = (\rho - \rho_{ch})/(\rho_v - \rho_{ch}) \tag{4-4}$$

$$\rho C_p = \omega\rho_v C_{pv} + (1-\omega)\rho_{ch}C_{pch} \tag{4-5}$$

where , ρ_v, ρ_{ch} is the virgin and char density, k_v, k_{ch} is the thermal conductivity of the virgin and char materials, and C_{pv}, C_{pch} is the specific heat of the virgin and char materials, respectively [4-11].

Another equations are the equation of mass conservation and the Arrhenius type expression for the decomposition rate:

$$\left(\frac{\partial \dot{m}_g}{\partial y}\right)_t = \left(\frac{\partial \rho}{\partial t}\right)_y \tag{4-6}$$

$$\left(\frac{\partial \rho}{\partial t}\right)_y = -\sum_{k=1}^{N} A_k f_k(\rho_v - \rho_{ch})\left(\frac{\rho-\rho_{ch}}{\rho_v-\rho_{ch}}\right)^{\mu_k} exp\left(-\frac{B_k}{T}\right) \tag{4-7}$$

where μ_k is the reaction order, f_k is the collision frequency (1/s), A_k is the weighting factor, B_k is the activation temperature (*K*). These values are assumed to be constant [4-11].

The energy balance at the ablator surface gives the surface boundary condition [4-15]:

$$\dot{q}_{net} = \dot{q}_{cw}(1 - h_w/h_r)\phi_{blow} - \varepsilon\sigma\left({T_w}^4 - {T_\infty}^4\right) - \dot{m}_{ab}(h_w - h_u) \tag{4-8}$$

In the equation above, $\dot{q}_{net}$ is the net heat flux conducted into the ablator (W/m^2), h_w is the enthalpy of the gas adjacent to the surface, $\dot{q}_{cw}$ is the cold wall convective heat flux (W/m^2), h_r is the recovery enthalpy of the flow, ϕ_{blow} is the blowing correction factor, σ is the Stefan-Boltzmann constant ($5.670 \times 10^{-8}\frac{W}{m^2}/K^4$), ε is the emissivity, T_w is the temperature of the char surface (*K*), T_∞ is the temperature of the surroundings (considered 300 *K*), $\dot{m}_{ab}(= \rho_{ch}\dot{S})$ is the mass flux due to the thermochemical ablation of the char ($\frac{kg}{m^2}/s$), and h_u is the enthalpy of the char at the surface (*J/kg*) [4-11].

The one-dimensional transient charring ablation model for the analysis is shown in Fig.4-41, in which thermal models of one-layer and two-layer types are used. The precise description of this code is shown in [4-8] and [4-16]. As pointed out in [4-10], on the back surface of the model, radiation exchange is assumed. The calculation was carried out mainly with the time increment of 0.005 *s*. The number of nodes was 60 for one-layer ablator, 20 for the 1st layer and 40 for the 2nd layer of the two-layers ablator.

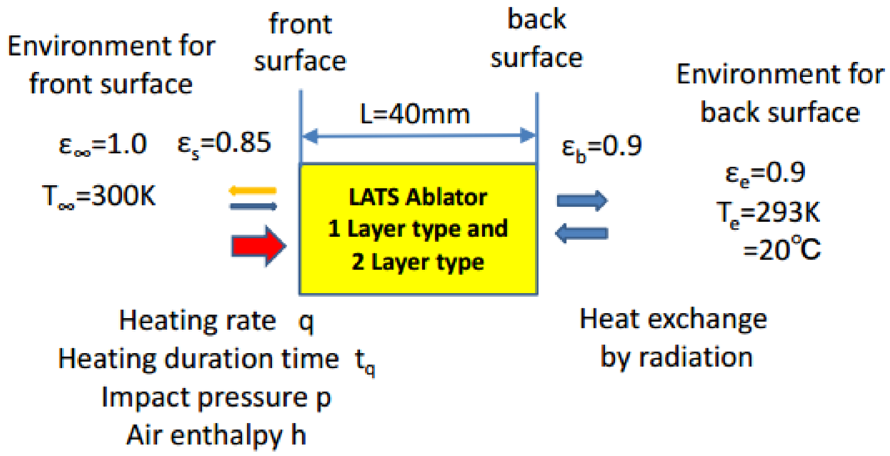

Fig.4-48 Thermal model for ablation analysis of the LATS ablator [4-10]

The surface temperature Ts was evaluated within the time of heating. Calculation was continued until the time of t=600 *s* (t=0 *s* corresponds to the start time of the heating), where the maximum temperature was obtained within the time range of 0 to 600 *s*. In some cases (D1, E1-1, E1-2, D2 and D4-1), the calculation was continued until the time of 800 seconds. The surface recession and the mass loss were evaluated at the time of 600 seconds. The calculation was carried out for each test case, and the in-depth temperature which corresponds to that of the target TC was tuned, from which the tuning coefficients were determined. Rectangular heating conditions are assumed [4-10].

Material properties of the LATS ablator are constructed based on the measured data of materials and literature data of [4-8] and [4-16]. The char density ρ(ch) is calculated by ρ(ch)=0.7×ρ(v), where ρ(v) is the virgin density. In the present paper, the tuning coefficients C1 and C2 were determined so that the calculated maximum temperature agrees with that measured by a thermocouple (TC) installed the farthest from the front surface since it gives the most accurate measured value of temperature [4-10]. TC1 is installed at 5 mm from the surface, TC2 at about 15 mm from the surface and TC3 at about 25 mm from the surface.

After running the code, the results of surface temperature, in-depth temperatures, surface recession, and mass loss for each ablator model were obtained and they were compared with the measured data. In Fig.4-49, Fig.4-50 and Fig.4-51, the comparison between the experimental and the measured results can be seen [4-10].

According to [4-10], when the distance of the target TC from the front surface is larger, the errors of the measured temperature are smaller and the tuning coefficients become larger. It seems that the reason for this tendency is due to the fact that the TC installed along the central axis of the ablator, where heat flows to the rear direction and the measured temperature is decreased from the real value. Because of this, TC farthest from the front surface (TC2 for one-layer type, and TC3 for two layer type) was mainly selected as a target TC for tuning the coefficients. In case of the surface recession, the measured values were smaller than the calculated values. One of the reasons might be the difference in the calculated and measured temperatures. However, a better agreement between calculated and measured results could be seen for the mass loss and mass loss per area.

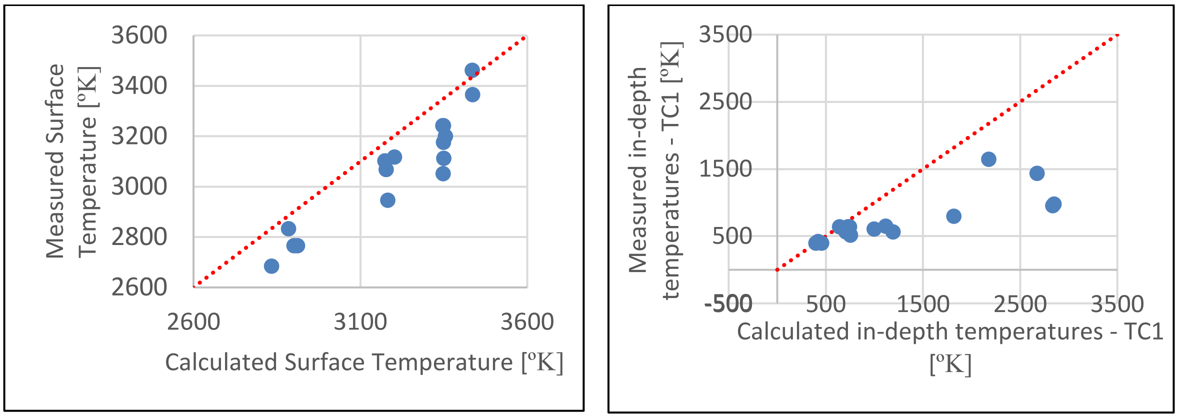

a) Surface Temperature

b) In-depth temperature TC1

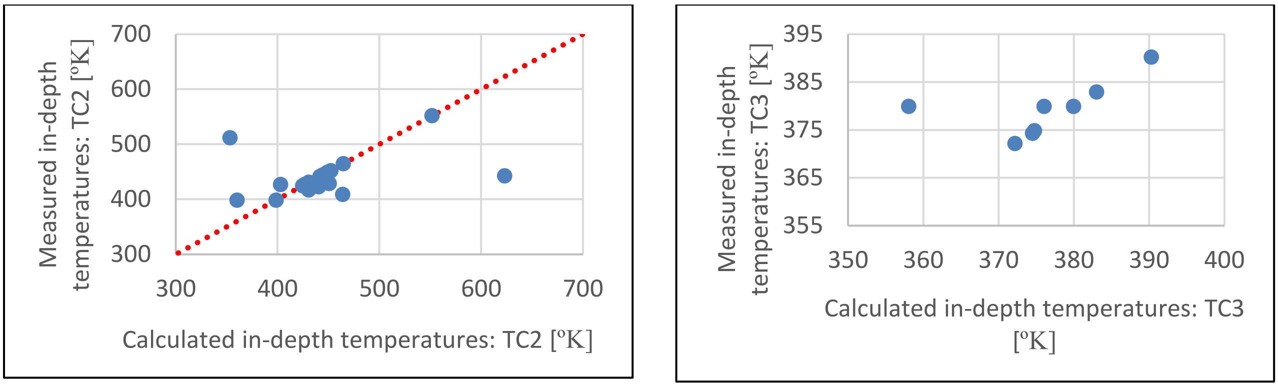

c) In-depth Temperature TC2

d) In-depth Temperature TC3

Fig.4-49 Comparison between calculated and measured temperature results [4-17]

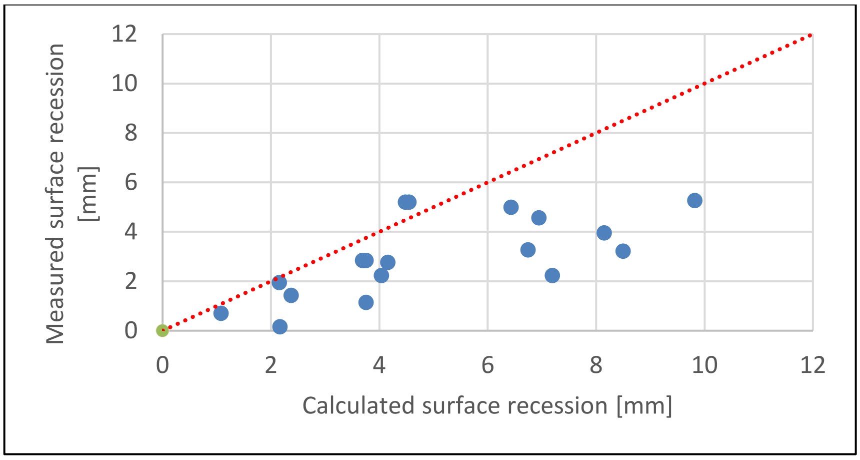

Fig.4-50 Calculated and measured Surface Recession [*mm*] [4-17]

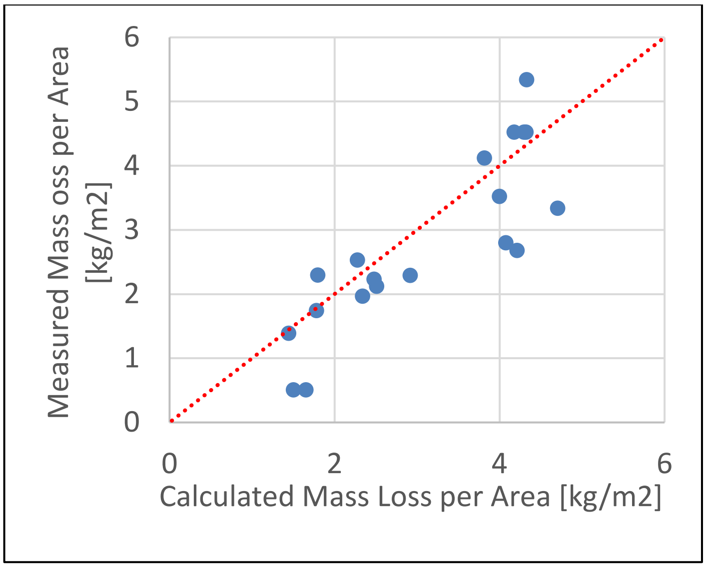

Fig.4-51 Calculated and Measured Mass Loss and Mass Loss per Area [4-17]

REFERENCES

[4-1] Bianca Szasz, Keiichi Okuyama, A New Method for Estimating the Mass Recession Rate for Ablator Systems, International Science Index, Vol:8, No:11, 2014, e-ISSN: 1307-6892, pp. 1246-1250.

[4-2] Bianca Szasz, Kei-ichi Okuyama, Sumio Kato, Takayuki Shimoda, Empirical Study of the Lightweight Ablator Series for Transfer Vehicle Systems (LATS), Transaction of JSASS, Aerospace Technology Japan, scheduled for publication.

[4-3] Tetsuya Yamada, Seiji Matsuda, Keiichi Okuyama, Nobuaki Ishii, Lessons Learned from the Recovered Heatshield of the USERS REV Capsule, Proceedings of IAF 2005, IAC-05-2.6.11.

[4-4] Robin A.S. Beck, Ablative Thermal Protection Systems Fundamentals, NASA Ames Research Center, International Planetary Probe Workshop 10, California, U.S., 2013.

[4-5] N.H. Kemp, Surface recession rate of an ablating polymer, AIAA Journal, Vol.6, No.9 (1968), pp. 1790-1791. Doi: 10.2514/3. 4870.

[4-6] Makoto Matsui, Kimiya Komurasaki, and Yoshihiro Arakawa, Characterization of Arcjet Type Arc-Heater Plumes, AIAA-2002-2242, 33rd Plasmadynamics and Lasers Conference, 20-23 May 2002, Maui, Hawaii.

[4-7] Keiichi Okuyama, Sumio Kato and Hiroaki Ohya, Thermochemical Performance of a Lightweight Charring Carbon Fiber Reinforced Plastic, Trans. Japan Soc. Aero. Space Sci., Vol.56, No.3, pp. 159-169, 2013.

[4-8] Sumio Kato, Keiichi Okuyama, Kenta Gibo, Takuma Miyagi, Toshiyuki Suzuki, Kazuhisa Fujita, Takeharu Sakai, Seiji Nishio and Akihiro Watanabe, Thermal Response

Simulation of Ultra Light Weight Phenolic Carbon Ablator by the Use of the Ablation Analysis Code, Trans. JSASS Aerospace Tech. Japan, Vol. 10, No. ists28, pp. Pe_31-Pe_39, 2012.

[4-9] Keiichi Okuyama, Sumio Kato, Yoshitsugu Kanno, Masahiro Uto, Ryuji Sakata, Kazumori Hama, Tetsuya Yamada, Yoshifumi Inatani, Masaru Zako, A Lightweight Heat Shield System using a Phenol CFRP Material, 2003 ESASP 521-3030.

[4-10] Sumio Kato, Ablation Analysis Report of Ultra-Lightweight Ablator (LATS), University of Ryukyus, Report No.: RK-2015-02.

[4-11] Sumio Kato, Keiichi Okuyama, Kenta Gibo, Takuma Miyagi, Toshiyuki Suzuki, Kazuhisa Fujita, Takeharu Sakai, Seiji Nishio and Akihiro Watanabe, Thermal Response Simulation of Ultra Light Weight Phenolic Carbon Ablator by the Use of the Ablation Analysis Code, Trans. JSASS Aerospace Tech. Japan, Vol. 10, No. ists28, pp. Pe_31-Pe_39, 2012.

[4-12] Kato, S., Okuyama, K., Nisio, S., Sakata, R., Hama, K. and Inatani, Y.: Numerical Analysis of Charring Ablation for Ablative Materials of Re-Entry Capsules, Journal of the Japan Society for Aeronautical and Space Sciences, 50, No.582 (2002), pp. 255-263.(in Japanese).

[4-13] Moyer, C. B. and Rinadal, R. A.: An Analysis of Coupled Chemically Reacting Boundary Layer and Charring Ablator, Part Ⅱ, Finite Difference Solution for the In-Depth Response of Charring Materials Considering Surface Chemical and Energy Balances, NASA CR-1061, 1967.

[4-14] Chen, Y.-K. and Milos, F. S.: Ablation and Thermal Response Program for Spacecraft Heatshield Analysis, Journal of Spacecraft and Rockets, 36, No. 3 (1999), pp. 475-483.

[4-15] Potts, R, L: Application of Integral Methods to Ablation Charring Erosion, A Review, Journal of Spacecraft and Rockets, 32, No.2, March-April (1995), pp. 200-209.

[4-16] Sumio Kato, T. Kishimoto, S. Matsuda, K. Okuyama, A. Watanabe, and N. Shimada, Study of the Effects of Density, Thickness and Heat Load on Heat Shielding Performance of Phenolic Carbon Ablators Using a One-Dimensional Ablation Analysis Code, Transactions of JSASS Aerospace Technology Japan, Vol.12, No. ists29 (2014), pp.Po_2_29-Po_2_38.

[4-17] Bianca Szasz, Kei-ichi Okuyama, Sumio Kato, Takayuki Shimoda, Sean Lee Tuttle, Study of the Heat Shield Characteristics of a Lightweight Charring CFRP-based Ablator, Annual Convention of the Japan Society of Mechanical Engineers, September 2015.

V. Conclusions

Deep space exploration has one of its motivations in the human endeavor to explore the resources of the Solar System, while the space exploration programs motivate young people to study in science and engineering. Recently, the size and cost of the satellites missions have been reduced and nowadays many universities have the capability to build small satellites and spacecraft. The micro spacecraft technologies can enhance space travel reliability through better designs. Also, through the small deep space probes missions which collect space flight data and return it to Earth, the thermal protection systems for human missions can be validated.

Some of the biggest challenges related to these missions are the harsh thermal environment of deep space and the atmospheric re-entry. The aim of this research was to address the two aspects, the one related to the harsh thermal environment of outer space, for which the study case will be represented by Shinen2 deep space mission, and the one related to atmospheric re-entry, focused on the validation of the ablative materials called LATS (Light-weight Ablator Series for Transport Vehicle Systems). The both studies are contributing in enhancing the knowledge and in developing new technologies related to a future small spacecraft mission, led by universities.

Regarding the thermal system of Shinen2 space probe, the following conclusions can be drawn:

- The thermal analysis of Shinen2 was successfully validated by performing thermal vacuum tests and the analysis model gave similar results with the temperature data measured in flight;
- The validated thermal analysis model indicates that the internal equipment will survive the thermal environment in deep space, between 0.9 *AU* and 1.1 *AU*;
- The passive thermal protection method using the simple solution of white paint outside and black paint inside was proven as being appropriate for an ultra-small deep space probe and this method can be used for other future ultra-small deep space probes.

To estimate the thermal environment, an orbit analysis method was developed. The main conclusions regarding the orbit prediction are the following:

- Orbit analysis is a very important part in designing a deep space mission. The thermal design and communication mission depend on it.
- A simple orbit prediction method was used for calculating the trajectory of Shinen2 (ignoring all the perturbing accelerations).
- The simple prediction method results were compared to those obtained using GMAT software.
- The compatibility between the results of orbit calculation (the differences are of about 10E+5 *km*) proves that the simple orbit calculation method can be used for the deep space missions, led by universities, where the cost of the resources must be kept at minimum;

- The simple prediction method can be used for estimating the thermal environment along the orbit, but for the purpose of communication, a more complex software as is GMAT software with its advanced orbit modelling techniques is preferable.

Regarding the reentry study using LATS ablative materials, several heating tests were performed using the arc-heating equipment at facilities in Japan and Germany, at the Japan Ultra High Temperature Material Center (JUTEM), the Aerospace Research and Development Directorate (ARD) of the Japan Aerospace Exploration Agency (JAXA), and Deutsches Zentrum fuer Luft- und Raumfahrt (DLR) of Germany. Based on the results of the tests, it can be concluded that the LATS can well function as a heat shield material even under a high-enthalpy flow. Also, one of the advantages of using LATS materials is the simplicity of the resin impregnation process, because the dried bulk density can be easily controlled.

Ablation being a very complex phenomenon, its analysis can be extremely difficult. Therefore, simple engineering methods, based on empirical results, could be extremely useful in the first estimation of the ablator recession in high enthalpy flows. As demonstrated in previous studies, a linear dependency between the measured mass loss rate and $\sqrt{P_{st}/R_B}$ can be established. The slope of the linear function was found to be $2.0 \times 10^{-4}\ \sqrt{kg/m}$ for low density LATS materials. This value was confirmed by the more recent tests in 2015, at JAXA Sagamihara.

In case of the surface recession rate, it was proved to be dependent with density, having an exponential dependency with the surface temperature and an indirect proportionality with the char density. The new empirical formula could be very useful in estimating the thickness of the ablative thermal shield of the reentry spacecraft. However, the empirical correlations should be backed-up in the future with the analytical models which allows extrapolation to conditions beyond ground test data base.

In this research, the experimental results were compared with the numerical results obtained using an one-dimensional ablation code, developed at Ryukyus University, in this way the ablator code been validated.

Also, one innovative study of the present research is the use of PEEK CFRTP ablator. It was observed that PEEK ablators have very low recession rates and low in-depth temperatures.

Below a summary of the findings related to atmospheric re-entry is given:

- The ablation phenomenon depends strongly on the temperature range;
- The classic methods for estimating the surface recession gives inaccurate results in case of CFRP materials;
- The new method for calculating the surface recession has been validated by comparing the results with the in-flight data;
- A higher density ablative material LATS behaved better than a low density one when heated with high enthalpy flow;
- The linear dependency (θ) for the calculation of mass recession rate was proved to have the same slope for the previous tests in 2015 as in the tests performed in the past;
- The surface recession rate was proven to be dependent on density and a new empirical

formula for its calculation was established;

- The empirical correlation should be backed-up in the future with analytical models;
- It was proven that PEEK CFRTP ablators have high thermal efficiency when exposed to high enthalpy heat flux and they can be used together with LATS ablators as a hybrid model.

The main findings of the present research are that the passive thermal control was proven reliable in deep space and LATS and PEEK CFRTP ablative materials were proven to have high thermal efficiency and they can well function as heat shield materials even under a high-enthalpy flow. Based on the findings, it can be concluded that a basic technology for a deep space exploration mission led by university, including an atmospheric re-entry phase (Earth or other planet's atmosphere) and using an ultra-small space probe, was developed.

References

[1-1] Bianca Szasz and Keiichi Okuyama, *Thermal Design and Analysis of SHINEN2, an Ultra-Small Deep Space Probe*, Proceedings of The 58th Space Sciences and Technology Conference, Nagasaki, Japan, 2014.

[1-2] Bianca Szasz, Kei-ichi Okuyama, Sumio Kato, Takayuki Shimoda, *Empirical Study of the Lightweight Ablator Series for Transfer Vehicle Systems (LATS)*, Transaction of JSASS, Aerospace Technology Japan, accepted for publication.

[1-3] Bianca Szasz, Kei-ichi Okuyama, *A New Method for Estimating the Mass Recession Rate for Ablator Systems*, Proceedings of The XII International Conference on Thermophysics and Heat Transfer (ICTHT 2014), London, United Kingdom.

[1-4] E. Brian Pritchard, *Mars: Past, Present, and Future*, Progress in Astronautics and Aeronautics, Volume 145, American Institute of Aeronautics and Astronautics, Washington, U.S.A., 1992.

[1-5] *India becomes first Asian nation to reach Mars orbit, joins elite global space club*, The Washington Post. 24 September 2014. Retrieved 24 September 2014.

[1-6] *India's spacecraft reaches Mars orbit ... and history*, CNN. 24 September 2014. Retrieved 24 September 2014.

[1-7] Harris, Gardiner (24 September 2014), *On a Shoestring, India Sends Orbiter to Mars on Its First Try,* New York Times. Retrieved 25 September 2014.

[1-8] Bhatt, Abhinav (5 November 2013), *India's 450-crore mission to Mars to begin today: 10 facts*, NDTV. Retrieved 13 October 2014.

[1-9] Molczan, Ted (9 November 2011), *Phobos-Grunt – serious problem reported*, SeeSat-L. Retrieved 9 November 2011.

[1-10] NASA Website, *Micro Spacecraft to Pave the Way for Future Space Exploration*, URL: http://www.nasa.gov/centers/ames/research/exploringtheuniverse/blackbox.html (2016).

[1-11] Nakasuka, S., *From Education to Practical Use of Nano-satellites – Japanese University Challenge towards Low Cost Space Utilization*, 8th IAA Symposium on Small Satellite for Earth Observation, Berlin, Germany, 2011.

[1-12] Ryu Funase, Hiroyuki Koizumi, Shinichi Nakasuka, Yasuhiro Kawakatsu, Yosuke Fukushima, Atsushi Tomiki, Yuta Kobayashi, Junichi Nakatsuka, Makoto Mita, Daisuke Kobayashi, Taku Nonomura, *50kg-class Deep Space Exploration Technology Demonstration Micro-spacecraft PROCYON*, SSC14-VI-3.

[1-13] David G. Gilmore, *Satellite Thermal Control Handbook*, The Aerospace Corporation Press, California, U.S.A, 1994.

[1-14] Humberto Araujo Machado, *Simulation of Ablation in a Composite Thermal Protection System via an Interface Tracking Method*, Journal of Aerospace Technology and Management, vol. 04, No.3, July-September, 2012, pp. 331-340, Instituto de Aeronautica e Espaço, Sao Paulo, Brasil.

[1-15] Rogan, J.E. and Hurwicz, H., 1973, *High-temperature Thermal Protection Systems*, in Handbook of Heat Transfer, edited by Rohsenow, W.M., Hartnett J.P., McGraw-Hill, New York, section 19.

[1-16] Silva, D.V.F.M.R., 2001, *Estimative of Thermal Properties of Ablative Materials*, M.Sc. Dissertation, Federal University of Rio de Janeiro – UFRJ, Rio de Janeiro, Brazil, 108 p.

[1-17] Keiichi Okuyama, Sumio Kato and Hiroaki Ohya, *Thermochemical Performance of a Lightweight Charring Carbon Fiber Reinforced Plastic*, Trans. Japan Soc. Aero. Space Sci., Vol.56, No.3, pp. 159-169, 2013.

[2-1] Bianca Szasz, Keiichi Okuyama, *A New Method for Estimating the Mass Recession Rate for Ablator Systems*, International Science Index, Vol.8, No.:11, 2014, London, UK.

[2-2] Bianca Szasz, Kei-ichi Okuyama, Sumio Kato, Takayuki Shimoda, *Empirical Study of the Lightweight Ablator Series for Transfer Vehicle Systems (LATS)*, Transaction of JSASS, Aerospace Technology Japan, scheduled for publication;

[2-3] Garzon, M., *Development and Analysis of the Thermal Design for the Osiris 3U Cubesat*. Pennsylvania: The Pennsylvania State University, 2012.

[2-4] Lee-Her, H., Ming-Shong, C., & Jih-Run, T., *Thermal Control Design and Analysis for Picosatellite Yamsat*, Transaction of the Aeronautical and Astronautical Society of the Reoublic of China, Vol 35, 227-233, 2003.

[2-5] Karam, R., *Satellite thermal Control for Systems Engineers*. Virginia, American Institute of Aeronautics, 1998.

[2-6] David G. Gilmore, *Satellite Thermal Control Handbook*, The Aerospace Corporation Press, California, U.S.A, 1994.

[2-7] The Japan Carbon Fiber Manufacturers Association website, *Carbon Fiber*, URL: http://www.carbonfiber.gr.jp/english/index.html , 2016.

[2-8] Central Carbon Fiber website, *CFRTS & CFRTP*, URL: http://www.centralcarbonfiber.com/cfrts_cfrtp/index.html (July 2016).

[2-9] Taro Nakamura, Yi Wan, Haowen Wei, Isamu Ohsawa, Jun Takahashi, *"Investigation of sandwich panel made by CFRTS and CFRTP*," 13th Japan International Sampe Symposium and Exhibition, December 2015.

[2-10] Kazuto Tanaka, Ryuma Sukena, Syota Mizuno and Tsutao Katayama, "*Roll forming of CFRTP Prepreg and Evolution of its Mechanical Property"*, The Science and Engineering Review of Doshisha University, Vol.55, No.3, October 2014.

[2-11] S. Pimenta, S.T. Pinho, *"Recycling carbon fiber reinforced polymers for structural applications: Technology review and market outlook,"* Waste Management, vol.31, pp.378-392, 2011.

[2-12] S. Pimenta, S.T. Pinho, "*The effect of recycling on the mechanical response of carbon fibers and their composites,*" Composite Structures, vol.94, pp.3669-3684, 2012.

[2-13] Hiroaki Takei, Michelle Salvia, Alain Vautrin, Akira Tonegawa and Yoshitake Nishi, *"Effects of Electron Beam Irradiation on Elasticity of CFRTP (CF/PEEK),"* Materials Transactions, Vol.52, No.4 (2011), pp.734 to 739.

[2-14] Jun Takahashi and Takashi Ishikawa, *"Current Japanese Activity in CFRTP for Industrial Application*", Leuven and TexComp -11 Conference, 16-20 September 2013, Leuven.

[2-15] Jun Takahashi, Kiyoshi Uzawa and Tsuyoshi Matsuo, "*Development of CFRTP for Mass Produced Automobile,*" The University of Tokyo, CDW-15, Kanazawa, Japan, October 18-19, 2010.

[2-16] M. Makihara: *Plastics 53 (2002)* 119-122.

[2-17] M. Kuehnel, A. Schuster, A. Buchheim, T. Gergross and M. Kupke, *"Automated Near-Net-Shape Preforming of Carbon Fiber Reinforced Thermoplastics (CFRTP)",* ICS of the JEC Europe 2014, Paris, March 11-13.

[2-18] Keiichi Okuyama, Sumio Kato, Yoshitsugu Kanno, Masahiro Uto, Ryuji Sakata, Kazumori Hama, Tetsuya Yamada, Yoshifumi Inatani, Masaru Zako, *A Lightweight Heat Shield System using a Phenol CFRP Material*, 2003 ESASP 521-3030.

[2-19] Makoto Matsui, Kimiya Komurasaki, and Yoshihiro Arakawa, *Characterization of Arcjet Type Arc-Heater Plumes*, AIAA-2002-2242, 33rd Plasmadynamics and Lasers Conference, 20-23 May 2002, Maui, Hawaii.

[2-20] Keiichi Okuyama, Sumio Kato and Tetsuya Yamada: *Thermo-chemical recession characteristics of CFRP in an earth atmospheric reentry environment*, TANSO, 2005, No.219, pp. 232-237.

[2-21] Keiichi Okuyama, Sumio Kato and Hiroaki Ohya: *Thermochemical Performance of a Lightweight Charring Carbon Fiber Reinforced Plastic*, Trans. Japan Soc. Aero. Space Sci., Vol.56, No.3, pp. 159-169, 2013.

[2-22] Humberto Araujo Machado, *Simulation of Ablation in a Composite Thermal Protection System via an Interface Tracking Method*, URL: http://www.jatm.com.br/papers/vol4_n3/JATMv4n3_p331-340_Simulation_of_Ablation_in_a_Composite_Thermal_Protection_System_via_an_Interface_Tracking_Method.pdf .

[2-23] Tran, H.K., Johnson, C.E., Rasky, D.J., Hui, F.C.L., Hsu, M., Chen, T., Chen, Y.K., Paragas, D. and Kobayashi, L.: *Phenolic Impregnated Carbon Ablators (PICA) for Discovery Missions*, NASA Technical Memorandum 110440, 1997, pp. 1-69.

[2-24] Yoseph Bar-Cohen, *High Temperature Materials and Mechanisms*, CRC Press, Taylor & Francis Group, LLC, 2014, International Standard Book Number-13:978-1-4665-6645-3.

[2-25] M. Stackpoole *et al.*, *Post-Flight Evaluation of Stardust Sample Return Capsule Forebody Heatshield Material*, AIAA 2008-1202.

[2-26] Huy K. Tran, Christine E. Johnson, Daniel J. Rasky, Frank C.L. Hui, Ming-Ta Hsu, Timothy Chen, Y.K. Chen, Daniel Paragas, and Loreen Kobayashi, *Phenolic Impregnated Carbon Ablators (PICA) as Thermal Protection Systems for Discovery Missions*, NASA Technical Memorandum 110440, 1997.

[2-27] DSC Beginners Guide, URL: https://www.perkinelmer.com/CMSResources/Images/44-74542GDE_DSCBeginnersGuide.pdf.

[2-28] TA-DSC, URL: http://www.hic.ch.ntu.edu.tw/TA/TA-DSC-TR-PRIN.pdf

[2-29] Ethiraj Venkatapathy and James Reuther, NASA Crew Exploration Vehicle, *Thermal Protection System, Lessons Learned*, 6th International Planetary Probe Workshop, June 26th, 2008.

[2-30] William M. Congdon, *Development of Design and Production Processes for Block-Ablator Heatshields with Preliminary Test Results*, ARA Ablatives Laboratory, URL: https://solarsystem.nasa.gov/docs/p477.pdf (July 2016).

[2-31] Sumio Kato, Keiichi Okuyama, Kenta Gibo, Takuma Miyagi, Toshiyuki Suzuki, Kazuhisa Fujita, Takeharu Sakai, Seiji Nishio and Akihiro Watanabe, *Thermal Response Simulation of Ultra Light Weight Phenolic Carbon Ablator by the Use of the Ablation Analysis Code,* Trans. JSASS Aerospace Tech. Japan, Vol. 10, No. ists28, pp. Pe_31-Pe_39, 2012.

[2-32] J. Lachaud, T.E. Magin, I. Cozmuta, and N.N. Mansour, *A Short Review of Ablative-Material Response Models and Simulation Tools*, NASA Archive, URL: http://ntrs.nasa.gov/archive/nasa/casi.ntrs.nasa.gov/20110014340.pdf .

[2-33] Jean Lachaud, Ioana Cozmuta, and Nagi N. Mansour, *Ablation of PICA-like Materials. Surface or Volume Phenomenon?*, Proceedings of the 6th International Planetary Probe Workshop, Atlanta, June 2008.

[2-34] Tiantian Yin, Zhongwei Zhang, Xiaofeng Li, Xiang Feng, Zhihai Feng, Yu Wang, Linghui He, Xinglong Gong, *Modelling ablative behaviour and thermal response of carbon/carbon composites*, Journal of Computational Materials Science 95 (2014) 35-40, Elsevier, 2014.

[2-35] Jesse W. Metzger, *Response of Galileo Aft Cover Components to Laser Radiation*, Paper No. 82-0853, 3rd AIAA/ASME Joint Thermophysics, Fluids, Plasma & Heat Transfer Conference, 1982.

[2-36] Robert L. Potts, *Analysis of an Integral Method for Computing Reentry Vehicle Heat Conduction in Systems Level Computer Codes*, Science Applications, Inc., El Segundo, California.

[2-37] Daniele Bianchi, Alessandro Turchi, F. Nasuti, M. Onofri, *CFD Ablation Predictions with Coupled GSI Modeling for Charring and non-Charring Materials*, 5th Ablation Workshop, Lexington, Kentucky, U.S.A., February 28 – March 1, 2012, available at http://uknowledge.uky.edu/ablation/2012/Coupling/3/ .

[3-1] Bianca Szasz, Kei-ichi Okuyama, Yoshiharu Matsumoto, Sidi Ahmed Bendoukha, *Simple Orbit Prediction Method and its Validation for Deep Space Missions*, UNISEC Space Takumi Journal, in review.

[3-2] Bianca Szasz, and Keiichi Okuyama, *Thermal Design and Analysis of Shinen2, an Ultra-Small Deep Space Probe*, Conference Proceedings of the 58th Space Sciences and Technology Conference, Nagasaki, 2014.

[3-3] Bianca Szasz, Kei-ichi Okuyama, *Shinen2, an Ultra-Small Deep Space Probe: Thermal Design, Analysis and Validation*, UNISEC Space Takumi Journal, accepted for publication.

[3-4] A. Kwok, *201, Rev. B Frequency and Channel Assignments*, 810-005, Rev. E, DSN Telecommunications Link Design Handbook, DSN Document Release, California Institute of Technology, 2009.

[3-5] Tsuda, Y., Yoshikawa, M., Minamino, N., Nakazawa, S., *System Design of Hayabusa2 – Asteroid Sample Return Mission to 1999JU3*, 63rd International Astronautical Congress, IAC-12-A.3.4.5, Naples, Italy, 2012.

[3-6] Volodymyr Baturkin, *Micro-Satellites Thermal Control – Concepts and Components*, edited by Elsevier, Acta Astronautica 56, 2005, pp. 161-170.

[3-7] Volodymyr Baturkin, *Micro-Satellites Thermal Control – Concepts and Components*, edited by Elsevier, Acta Astronautica 56, 2005, pp. 161-170.

[3-8] Oliver Montenbruck, Thomas Pfleger, *Astronomy on the Personal Computer*, Fourth Edition, Springer, 2000.

[3-9] Vladimir A. Chobotov, *Orbital Mechanics (Second Edition)*, AIAA Education Series, 1996, Reston, Virginia, USA.

[3-10] M.A. Hapgood, *Space Physics Coordinate Transformations: A User Guide*, Planet. Space Sci., Vol.40, No.5, pp.711-717, 1992.

[3-11] D.G. Simpson, *Table of Julian Day Numbers - 1950-2100*, NASA report, Science Data Processing Branch, Goddard Space Flight Center, Greenbelt, Maryland, June 2012.

[3-12] Lee-Her Hu, Ming-Shong Chang, and Jih-Run Tsai, *Thermal Control Design and Analysis for a Picosatellite-YamSat*, edited by Transactions of the Aeronautical and Astronautical Society of the Republic of China, Vol.35, No.3, pp.227-233 (2003).

[3-13] *MSC Software*, http://www.mscsoftware.com/product/sinda , 2015.

[3-14] Roy, A.E., *Orbital Motion* (third ed.). Institute of Physics Publishing. ISBN 0-85274-229-0, 1988.

[3-15] S. S. Fernandes and W. A. Golfetto, *Numerical and analytical study of optimal low-thrust limited-power transfers between close circular coplanar orbits*, Mathematical Problems in Engineering, vol. 2007, Article ID 59372, 23 pages, 2007.

[3-16] S. S. Fernandes and F. D. C. Carvalho, *A first-order analytical theory for optimal low-thrust limited-power transfers between arbitrary elliptical coplanar orbits*, Mathematical Problems in Engineering, vol. 2008, Article ID 525930, 30 pages, 2008.

[3-17] C. R. H. Solórzano and A. F. B. A. Prado, *A comparison of averaged and full models to study the third-body perturbation*, The Scientific World Journal, vol. 2013, Article ID 136528, 16 pages, 2013.

[3-18] N. Sozbir, M. Bulut, M.F. Oktem, A. Kahriman and A. Chaix, *Design of Thermal Control Subsystem for TUSAT Telecommunication Satellite*, World Academy of Science, Engineering and Technology 43, 2008.

[3-19] T. Totani, H. Ogawa, R. Inoue, T.K. Das, M. Wakita, and H. Nagata, *Thermal Design Procedure for Micro- and Nanosatellites Pointing to Earth*, American Institute of Aeronautics and Astronautics, Journal of Thermophysics and Heat Transfer, 28(3): 524-533, 2014.

[4-1] Bianca Szasz, Keiichi Okuyama, *A New Method for Estimating the Mass Recession Rate for Ablator Systems*, International Science Index, Vol:8, No:11, 2014, e-ISSN: 1307-6892, pp. 1246-1250.

[4-2] Bianca Szasz, Kei-ichi Okuyama, Sumio Kato, Takayuki Shimoda, *Empirical Study of the Lightweight Ablator Series for Transfer Vehicle Systems (LATS)*, Transaction of JSASS, Aerospace Technology Japan, scheduled for publication.

[4-3] Robin A.S. Beck, *Ablative Thermal Protection Systems Fundamentals*, NASA Ames Research Center, International Planetary Probe Workshop 10, California, U.S., 2013.

[4-4] Keiichi Okuyama, Sumio Kato and Hiroaki Ohya, *Thermochemical Performance of a Lightweight Charring Carbon Fiber Reinforced Plastic*, Trans. Japan Soc. Aero. Space Sci., Vol.56, No.3, pp. 159-169, 2013.

[4-5] Robert L. Potts, *Application of Integral Methods to Ablation Charring Erosion*, A Review, Journal of Spacecraft and Rockets, Vol.32, No.2, March-April 1995.

[4-6] Tetsuya Yamada, Seiji Matsuda, Keiichi Okuyama, Nobuaki Ishii, *Lessons Learned from the Recovered Heatshield of the USERS REV Capsule*, Proceedings of IAF 2005, IAC-05-2.6.11.

[4-7] N.H. Kemp, *Surface recession rate of an ablating polymer*, AIAA Journal, Vol.6, No.9 (1968), pp. 1790-1791. Doi: 10.2514/3. 4870.

[4-8] Makoto Matsui, Kimiya Komurasaki, and Yoshihiro Arakawa, *Characterization of Arcjet Type Arc-Heater Plumes*, AIAA-2002-2242, 33rd Plasmadynamics and Lasers Conference, 20-23 May 2002, Maui, Hawaii.

[4-9] Sumio Kato, Keiichi Okuyama, Kenta Gibo, Takuma Miyagi, Toshiyuki Suzuki, Kazuhisa Fujita, Takeharu Sakai, Seiji Nishio and Akihiro Watanabe, *Thermal Response*

Simulation of Ultra Light Weight Phenolic Carbon Ablator by the Use of the Ablation Analysis Code, Trans. JSASS Aerospace Tech. Japan, Vol. 10, No. ists28, pp. Pe_31-Pe_39, 2012.

[4-10] Keiichi Okuyama, Sumio Kato, Yoshitsugu Kanno, Masahiro Uto, Ryuji Sakata, Kazumori Hama, Tetsuya Yamada, Yoshifumi Inatani, Masaru Zako, *A Lightweight Heat Shield System using a Phenol CFRP Material*, 2003 ESASP 521-3030.

[4-11] Sumio Kato, *Ablation Analysis Report of Ultra-Lightweight Ablator (LATS)*, University of Ryukyus, Report No.: RK-2015-02.

[4-12] Sumio Kato, Keiichi Okuyama, Kenta Gibo, Takuma Miyagi, Toshiyuki Suzuki, Kazuhisa Fujita, Takeharu Sakai, Seiji Nishio and Akihiro Watanabe, *Thermal Response Simulation of Ultra Light Weight Phenolic Carbon Ablator by the Use of the Ablation Analysis Code*, Trans. JSASS Aerospace Tech. Japan, Vol. 10, No. ists28, pp. Pe_31-Pe_39, 2012.

[4-13] Kato, S., Okuyama, K., Nisio, S., Sakata, R., Hama, K. and Inatani, Y.: *Numerical Analysis of Charring Ablation for Ablative Materials of Re-Entry Capsules, Journal of the Japan Society for Aeronautical and Space Sciences*, 50, No.582 (2002), pp. 255-263.(in Japanese).

[4-14] Moyer, C. B. and Rinadal, R. A.: *An Analysis of Coupled Chemically Reacting Boundary Layer and Charring Ablator, Part II*, Finite Difference Solution for the In-Depth Response of Charring Materials Considering Surface Chemical and Energy Balances, NASA CR-1061, 1967.

[4-15] Chen, Y.-K. and Milos, F. S.: *Ablation and Thermal Response Program for Spacecraft Heatshield Analysis*, Journal of Spacecraft and Rockets, 36, No. 3 (1999), pp. 475-483.

[4-16] Potts, R, L: *Application of Integral Methods to Ablation Charring Erosion*, A Review, Journal of Spacecraft and Rockets, 32, No.2, March-April (1995), pp. 200-209.

[4-17] Sumio Kato, T. Kishimoto, S. Matsuda, K. Okuyama, A. Watanabe, and N. Shimada, Study of the Effects of Density, *Thickness and Heat Load on Heat Shielding Performance of Phenolic Carbon Ablators Using a One-Dimensional Ablation Analysis Code*, Transactions of JSASS Aerospace Technology Japan, Vol.12, No. ists29 (2014), pp.Po_2_29-Po_2_38.

Acknowledgments

First and foremost, I would like to thank my advisor, Professor Kei-ichi Okuyama. It has been an honour to be his Ph.D. student, at Kyushu Institute of Technology and I appreciate all his help in making my Ph.D. program a very productive and rewarding experience. The enthusiasm and the immense dedication he has for his research was very motivational for me. I am also thankful for the great example he has been for me as a very friendly person and a very hard-working scientist. I had the chance to meet him for the first time at the German Aerospace Center and I am deeply grateful that he advised me to apply for the Ph.D program in Japan. Due to this opportunity, I was able to live in Japan for 3 years, this time having been a tremendous professional and life experience which I will always remember with great pleasure.

Also, I would like to deeply thank Professor Mengu Cho for initiating the collaboration with the United Nations Office for Outer-Space Affairs and for establishing the Post-graduate study on Nano-Satellite Technologies (PNST) Fellowship Programme at Kyushu Institute of Technology, program which I am part of. I would like to express my appreciations to Professor Mengu Cho, Professor Akahoshi Yasuhiro, Professor Komori Mochimitsu and Professor Kazuhiro Toyoda for being great examples of very professional, hard-working and highly knowledgeable scientists. I would like to thank them for being in the committee for evaluation of my Ph.D thesis and also to thank them for giving me precious advices related to my Ph.D research.

I am also grateful towards Doctor Shimoda, from the Japan Aerospace Exploration Agency/ISAS, who guided me in my experimental work, at the arc-heating facilities of the space agency. Thanks to him, my work went very smoothly and the days were brighter. Also, I appreciate very much the help I received there from Mr. Nagai and his team who always stood by me and helped me tremendously. Also, I am deeply grateful to Professor Kato from University of the Ryukyus for his precious advices regarding my experimental work and for being a great example of a brilliant researcher. Moreover, I want to thank Professor Nishio for his hard work and dedication in the Shinen2 project and Professor Sean Tuttle from University of New South Wales Australia for his help in planning and performing the arc heating tests at the Japan Aerospace Exploration Agency/ISAS.

I would like to express a special gratitude towards Professor Premkumar Saganti from the Prairie View A&M University, U.S., and Mr. Doug Holland, from the NASA Johnson Space Center, for their great contributions in Shinen2 project and for the great insights I received from our discussions. Especially, I am grateful for the visit of Professor Saganti to our research laboratory at Kyushu Institute of Technology, for his kindness which he expressed towards me and my colleagues.

The members of Okuyama laboratory (Bui Nam Duong, Sidi Ahmed Bendoukha, Kevin Marriete, Kuroiwa, Yoshio, Iwanaga, Mashima, Fuji, Miyoshi, Yamanouchi, Matsumoto and

all the others) and many other students from other laboratories have been great friends and colleagues and I am grateful for the great time we spent together, for our amazing trips and for all the great memories.

Lastly, but most importantly, I would like to thank my family for all their love and all their emotional support they gave me in all of my endeavours.

Bianca Szasz

Kyushu Institute of Technology, Japan

July 2016